UNIVERSITÄT ZU LÜBECK

From the Institute of Anatomy of the University of Lübeck

Director: Prof. Dr. med. Jürgen Westermann

"Distribution and Interaction of Pulmonary Phagocytes in the Murine Lung under Steady-State Conditions and after Allergen Challenge"

Dissertation

for Fulfillment of Requirements

for the Doctoral Degree of the University of Lübeck

- from the Department of Natural Sciences -

Submitted by

Franziska Marie Hoffmann

from Hamburg

Lübeck 2017

First referee: Prof. Dr. med. Peter König

Second referee: Prof. Dr. rer. nat. Frank Petersen

Date of oral examination: 02.06.2017

Approved for printing: Lübeck, 06.06.2017

Content

Abbreviations

-/-	knock out
°C	degree Celsius
3D	three-dimensional
α-SMA	alpha smooth muscle actin
Ab	antibody
AHR	airway hyperresponsiveness
AM	alveolar macrophage
APC	allophycocyanin
APC	antigen presenting cell
AW	airway
BAL	bronchoalveolar lavage
Batf3	basic leucine zipper ATF-like transcription factor 3
BM	bone marrow
BSA	bovine serum albumin
C5aR1	complement C5a receptor 1
CCL	CC-chemokine ligand
CCR	CC-chemokine receptor
CD	cluster of differentiation
(c)DC	(conventional) dendritic cell
CDP	common DC progenitor
CLSM	confocal laser scanning microscopy
cMOP	common monocyte progenitor
CMP	common myeloid progenitor
CSF	colony-stimulating factor
Cy	cyanine
DNA	deoxyribonucleic acid
e.g.	for example
EDTA	ethylenediaminetetraacetic acid
FACS	fluorescence-activated cell sorting
FBS	fetal bovine serum
FcR	Fc receptor
fig.	figure

FITC	fluorescein-isothiocyanat
Flt3L	FMS-like tyrosine kinase 3 ligand
FMO	fluorescence minus one
g	gram
g	earth's gravitational acceleration
GM-CSF	granulocyte-macrophage colony-stimulating factor
h	hours
HDM	house dust mite extract
hi	high
HSC	hematopoietic stemm cell
i.p.	intra-peritoneal
i.t.	intra-tracheal
IA	intra-acinar artery
IgE	immunglobulin E
IgG	immunglobulin G
IHC	immunohistochemistry
IL	interleukin
ILC	innate lymphoid cell
IM	interstitial macrophage
IMLC	interstitial macrophage-like cell
int	intermediate
IRF	rnterferon regulatory factor
l	liter
lo	low
LPS	lipopolysaccharide
LV	lymph vessel
MDP	macrophage DC progenitor
MHC	major histo-compatibility complex
µg	microgram
min	minute
µl	microliter
ml	milliliter
mm	milimeter
Mo	monocyte
moDC	monocyte-derived DC

MoMΦ	monocyte-derived macrophage
n.s.	not significant
OVA	ovalbumin
PA	pulmonary artery
PBS	phosphate buffered saline
PCLS	precision cut lung slices
pDC	plasmacytoid dendritic cell
PE	phycoerythrine
PerCP	peridinin-chlorophyll
PFA	paraformaldehyde
PRR	pattern recognition receptor
RBC	red blood cell
RNA	ribonucleic acid
RT	room temperature
s.a.	see above
SEM	standard error of the mean
Siglec	sialic acid-binding immunoglobulin-type lectins
SPF	specific pathogen free
tab.	table
TBS	TRIS-buffered saline
TNF	tumor necrosis factor
T_{reg}	regulatory T cell
V	vein
wt	wildtype

1 Zusammenfassung

Das allergische Asthma ist eine chronisch-entzündliche Krankheit mit steigender Prävalenz in den westlichen Industriestaaten. Die exakten Mechanismen der Krankheitsentstehung konnten bisher nicht aufgedeckt werden, man geht aber davon aus, dass die Inhalation harmloser Antigene, wie z.B. Pflanzenpollen oder den Exkrementen der Hausstaubmilbe, fälschlicherweise eine Entzündungsreaktion auslöst.

Nach der Inhalation dieser Partikel stellen pulmonale Phagozyten, insbesondere Dendritische Zellen (DCs) und Makrophagen, die erste Station des Abwehrmechanismus der Lunge dar. Diese Zellen sezernieren verschiedene Botenstoffe, welche in suszeptiblen Individuen die Entstehung einer Entzündungsreaktion, inklusive der typischen Symptome (Niesen, Husten, Atemnot), begünstigen. Man geht davon aus, dass pulmonale Phagozyten, bestehend aus verschiedenen Subpopulationen von DCs, Makrophagen und Monozyten, verschiedene Funktionen während der Induktion der Immunantwort erfüllen. Dabei agieren einige Populationen proinflammatorisch während andere eine anti-inflammatorsiche Immunantwort begünstigen. Da die mögliche Zellfunktion maßgeblich von der Zelllokalisation beeinflusst wird, es aber bisher keinen umfassenden Überblick über die Lokalisation pulmonaler Phagozyten gibt, ist das Ziel dieser Studie einen Überblick bezüglich der Lokalisierung und Quantität in der naiven Lunge zu schaffen. Weiterhin sollen Unterschiede zwischen der naiven Lunge und der Lunge in einem frühen Entzündungsstadium analysiert werden.

Mittels multipler Immunfluoreszens wurde ein Panel mit vier Farben entwickelt, welches die Identifizierung von $CD11b^+$ DCs, $CD103^+$ konventionellen (c)DCs, Interstitiellen Makrophagen (IM) und Alveolarmakrophagen (AM), mittels Immunhistochemie anhand der unterschiedlichen Expression der Oberflächenmoleküle CD11c, MHCII, CD11b und CD103, erlaubt. Erwartungsgemäß wurden AMs ausschließlich im alveolaren Lumen gefunden. Im Gegensatz dazu waren $CD11b^+$ DCs und $CD103^+$ cDCs epithelnah an Atemwegen und weiterhin um Pulmonalarterien, Venen und intra azinäre Arterien lokalisiert. Interessanterweise wurde eine Zellpopulation gefunden, die dem Phänotyp nach IMs entspricht, allerdings starke Abweichungen zu der für IMs beschriebenen Lokalisation aufweist. Diese Zellen werden nachfolgend als IM ähnliche Zellen (IMLCs) bezeichnet, welche in häufigem Zellkontakt zu $CD103^+$ cDCs an Atemwegen gefunden wurden. Diese Kontakte traten mit niedrigerer Frequenz ebenfalls an Blutgefäßen auf. Eine Analyse des Markerproteins CD64 ergab, dass diese IMLCs einen monozytären Ursprung besitzen. Unerwarteterweise zeigte diese Analyse

ebenfalls, dass etwa 50% der $CD11b^+$ DCs in der naiven Lunge eine monozytäre Herkunft aufweisen. Dieses Ergebnis steht im Widerspruch zu einer vorherigen Studie basierend auf Durchflusszytometrie. Da ähnliche Unstimmigkeiten bezüglich der Zellquantifizierung mittels Durchflusszytometrie bereits zuvor berichtet wurden, stellt sich die Frage, ob die Expression der Oberflächenmoleküle während der Zellaufbereitung für die Durchflusszytometrie verändert werden kann.

Im nächsten Schritt sollten die Bedingungen der naiven Lunge mit dem frühen Entzündungsstadium verglichen werden. Hierbei zeigte sich keine Veränderung bezüglich der Zelllokalisation. Allerdings kam es zu einem signifikanten Anstieg von $CD11b^+$ DCs basierend auf der Rekrutierung von inflammatorischen $CD11b^+$ monozytären (mo)DCs. Gleichzeitig wurde eine Verminderung der IMLC:$CD103^+$ cDC Kontakte an Atemwegen und Blutgefäßen beobachtet. Basierend auf der Tatsache, dass zeitgleich ein Anstieg von $CD11b^+$ moDCs und eine Abnahme von IMLCs beobachtet wurde, kann spekuliert werden, ob IMLCs als Vorläuferzellen für $CD11b^+$ moDCs agieren. Diese Annahme stützt sich auf die Tatsache, dass beide Zelltypen nur in der Expression von CD11c divergieren.

Im letzten Teil dieser Arbeit wurde die Präsenz von CCR7 in der Lunge untersucht, um das migratorische Potential pulmonaler Phagozyten zu untersuchen. Hierbei stellte sich heraus, dass die CCR7 Expression auf $CD11b^+$ DCs und $CD103^+$ cDCs beschränkt ist, während keine migratorischen Makrophagen oder Monozyten identifiziert werden konnten.

Diese Studie fasst die Gegebenheiten in der naiven Lunge, bezüglich Lokalisation und Quantität von pulmonalen Phagozyten, zusammen. Darüber hinaus konnte ein neuartiger Zellkontakt zwischen IMLC und $CD103^+$ cDC identifiziert werden. Dieser Zellkontakt könnte an der Induktion einer Toleranzreaktion beteiligt sein, welches bereits für zwei ähnliche Zelltypen im Darm beschrieben wurde [1]. Diese Hypothese wird weiterhin durch die Tatsache gestützt, dass bereits eine IL-10 Expression für Zellen, die einen IM Phänotyp aufweisen, gezeigt wurde [2]. Ein weiterer wichtiger Aspekt dieser Arbeit ist der Vergleich von Immunhistochemie und Durchflusszytometrie bezüglich der Zellquantifizierung, basierend auf der Widersprüchlichkeit publizierter Zellfrequenzen. Dieses stellt einen wichtigen Punkt für die Vergleichbarkeit verschiedener Studien dar. Die Lösung dieses Problems ist unumgänglich und eine Kombination beider Methoden in nachfolgenden Studien erlaubt neue Möglichkeiten für die Untersuchung der dem Asthma zugrundeliegenden Krankheitsmechanismen.

2 Summary

Allergic asthma has become a common chronic inflammatory disease with increasing prevalence in the western civilization. Today, the exact mechanisms of asthma development are not fully understood, but it is believed that the inability of inducing tolerance towards harmless inhaled antigen (e.g. plant pollen, house dust mite) is responsible for the inflammatory response.

After inhalation of airborne particles pulmonary phagocytes, mainly dendritic cells (DCs) and macrophages, act in the first place of the defense mechanism by the immune system. These cells secrete different soluble substances, which trigger the induction of the inflammatory response, resulting in the common symptoms wheezing, coughing, and airway hyperresponsiveness in susceptible individuals. The subsets of pulmonary phagocytes including different subsets of DCs, macrophages, and monocytes are believed to fulfill specific tasks within the disease whereas some cells act proinflammatory and other anti-inflammatory. Since possible cell function is directly linked to cell localization but no comprehensive overview for pulmonary phagocytes is available so far this study aimed to shed light on the steady-state circumstances regarding cell localization and cell quantity in the murine lung. In addition, the steady-state will be compared to an early inflammation.

Using a four-color panel for immunohistochemistry it was possible to identify cluster of differentiation (CD)11b$^+$ DCs, CD103$^+$ conventional (c)DCs, interstitial macrophages (IMs), and alveolar macrophages (AMs) simultaneously based on their different expression patterns of the markers CD11c, major histo-compatibility complex (MHC)II, CD11b, and Langerin. As expected AMs were exclusively found in the alveolar lumen. In contrast, CD11b$^+$ DCs and CD103$^+$ cDCs were located inside the lung tissue close to the airway epithelium. In addition, both subsets were situated around veins, pulmonary arteries, and around intra-acinar arteries. Interestingly, a cell population matching the IM phenotype was often found in close cell contact to CD103$^+$ cDCs around airways and to a lesser extend also around blood vessels. Because IMs were originally described to be located in the alveolar interstitium apart from airways and blood vessels this IM matching cell population was called IM-like cell (IMLC) in this study. The analysis of CD64 revealed that those IMLCs derive from a monocytic origin. Unexpectedly, it turned out that also approximately 50% of the CD11b$^+$ DC population at steady-state derives from a monocytic background which was contradictory to a former study based on flow cytometry. Since similar differences in cell frequencies were also reported before this raises the question whether surface markers can be altered during the cell preparation for flow cytometry.

In the next step, the steady-state was compared to early inflammation. While localization itself was not changed, HDM treatment resulted in a significant increase of $CD11b^+$ DCs based on the recruitment of inflammatory $CD11b^+$ monocytic-derived (mo)DCs to the lung. At the same time there was a decrease in IMLCs resulting in a loss of $CD103^+$ cDC:IMLC contacts at airways and vessels. Since inflammatory $CD11b^+$ moDCs increase while there is a simultaneous decrease of IMLCs and both cell types only differ in their CD11c expression it can be speculated whether IMLCs might act as lung-resident precursors for inflammatory moDCs.

In the last part the expression of CCR7 was examined to determine possible locations for cell activation. Immunohistochemistry for CCR7 revealed that its expression is restricted to $CD11b^+$ DCs and $CD103^+$ cDCs and no $CCR7^+$ macrophages or monocytes were detected.

This study summarizes the steady state circumstances regarding phagocytes numbers and localization. In addition, a novel cell contact between $CD103^+$ cDCs and IMLCs was discovered which might be involved in tolerance induction since a similar interaction resulting in tolerance has been reported for the gut [1]. Congruent with this hypothesis IL-10 expression by cells matching the IM phenotype has already been shown in the lung [2]. Further this study addresses different results regarding cell frequencies obtained by immunohistochemistry and flow cytometry, which is an important issue for the comparability of different studies. The solution of this inconsistency and the suitable combination of flow cytometry and immunohistochemistry in following studies would provide new possibilities to unravel mechanisms supporting the development of allergic inflammation in susceptible individuals.

3 Introduction

This study will focus on the characterization of pulmonary phagocytes including identification, quantification, localization, and migratory properties at steady-state. In addition, the steady-state will be compared to the inflamed lung in a house dust mite extract (HDM)-mediated mouse model of early allergic airway inflammation. For a better understanding the introduction will describe the respiratory system and give an overview about the onset of allergic asthma, which represents a common allergic disease in the western civilization with increasing prevalence. Further, the current knowledge about the different pulmonary subsets and their involvement in the development of an inappropriate inflammatory immune response towards harmless environmental allergens during allergic sensitization will be summarized.

3.1 The Respiratory System in the Context of an Allergic Airway Inflammation

While breathing, the lung is in constant contact to the environment. Every day the distal airways, including bronchioles and alveoli, which possess a surface area of 90-130 m^2 in a healthy human lung are in contact to around 8,000 to 9,000 liters of air [3-5]. Considering the large amount of inhaled air, it is obvious, that the lung is exposed to various airborne particles and air pollutants every day. After inhalation, a smaller portion of inhaled particles will be removed from the airways by coughing or wheezing. However, mucociliary clearance serves as the main mechanism to remove inhaled pathogens (e.g. bacteria) or harmless particles (e.g. plant pollen) [6]. Mucus is produced by pulmonary secretory cells and is covering the surface of the airways. During mucociliary clearance the majority of inhaled particles are sticking to the mucus and will be transported out of the lung by ciliary-driven mucus transport to the upper airways [7-9]. Only a minor fraction of particles will reach the lung tissue. Those particles are engulfed by pulmonary phagocytes in order to induce an appropriate immune response resulting in tolerance towards harmless substances. However, sometimes the immune system fails to induce a tolerogenic response towards these stimuli resulting in an allergic airway response.

3.1.1 The Respiratory System

The lung is one of the most important organs, since it provides oxygen to the body. Inhaled air passes the upper airways (pharynx and nose), the larynx, and is forwarded through lower airways (trachea, bronchioles) to the bronchioli until it reaches the alveoli, where the gas exchange takes place.

The human lung is separated into the right lung consisting of *lobus superior*, *lobus medius*, and *lobus inferior*, and the smaller left lung containing *lobus superior* and *lobus inferior*. The trachea branches into the two main bronchi which again split into two or three lobe bronchi, respectively. The intrapulmonary branching pattern of the human lung is dichotomous and comprises about 17 generations [10]. These bronchi split up to smaller bronchi until they become *bronchioli terminales* constituting the final step of the air conducting bronchial tree. By definition, bronchi contain cartilage rings and mucus-secreting glands while those structures are not present in bronchioli. Further downstream, respiratory bronchioles, alveolar ducts and alveoli, that emerge from the *bronchioli terminali*, are forming the *terminal respiratory unit* also called the *acinus* [11, 12]. The respiratory bronchial tree starts at the *bronchioli respiratorii* leading towards the *ductuli alveolares*. *Ductuli alveolares* on their part are branching into *sacculi alveolares* representing a bulge that is the terminal point of several alveoli [13-15].

In addition to the complex structure of airways, the lung contains a dense network of blood vessels, which ensures the gas exchange. Blood vessels enter and leave the lung at the same location as bronchi, the *hilum pulmonis*. While pulmonary arteries lie side by side with the airways pulmonary veins are autonomous structures that are anatomically distant from pulmonary arteries and their adjacent airways [11, 12]. The gas exchange occurs in the alveolar region at the borders between oxygen harboring alveoli and blood vessels. Both compartments share most of their surface areas [4]. Pulmonary capillaries are thin-walled tubes forming an air-blood barrier with the single layered alveolar epithelium to enable the exchange of oxygen and carbon dioxide via diffusion [11, 12].

3.1.2 Allergic Asthma

Bronchial asthma, a chronic inflammatory disease of the lower airways, has become a common disease affecting about 300 million people worldwide with a mortality rate of 250,000 each year with increasing prevalence [16-18]. Clinical manifestations of this inflammatory disorder

are difficulties in breathing caused by airway hyperresponsiveness (AHR), overproduction of mucus, coughing, and wheezing [17]. The disease can be differentiated into allergic and non-allergic forms. While allergic asthma is caused by the inhalation of allergens like feces of house dust mite, plant pollen, or animal dander in susceptible persons, the non-allergic form is triggered by physical stimuli like cigarette smoke, diesel exhausts, physical effort, or respiratory infections. However, a clear distinction of these types is often impossible, since factors responsible for non-allergic asthma can also exacerbate the features of allergic asthma [17, 19].

Due to the increasing prevalence of severe allergic asthma researchers are focusing on possible treatments and the mechanisms behind the disease. From the immunological point of view allergic asthma is a disorder involving both the innate and the adaptive immune system resulting in an inappropriate Th2/Th17 response to harmless environmental antigens [20]. During the allergic response activated DCs that have taken up allergen migrate towards the lung draining lymph nodes where they activate naïve T cells. The activated T helper cells then leave the lymph nodes and migrate towards the site of inflammation where they accumulate close to the airway wall resulting in the release of proinflammatory cytokines including interleukin (IL)-4, IL-5, IL-13 and tumor necrosis factor (TNF)-α [21]. These cytokines are directly involved in inducing characteristic features of asthma by inducing immunoglobulin (Ig)E synthesis (IL-4), eosinophilic infiltration (IL-5), goblet cell metaplasia (IL-4, IL-13) and proliferation of airway smooth muscle cells (IL-13) [22].

3.1.3 The Mouse as a Model Organism for Allergic Asthma

Because lung structure is approximately the same for most mammalian species [23-27] human diseases might be transferred to animal models for examination of mechanisms and possible treatments. Nevertheless, there are some differences regarding the lung anatomy of human and mouse. The most obvious difference between human and murine lung beside the size is the arrangement of the single lobes. In contrast to the human lung, the mouse lung contains only a single left lobe and four right lobes (*lobus cranialis*, *lobus medialis*, *lobus caudalis*, and *lobus accessorius*). In addition, there are no cartilage rings present around airways inside the lobes. Inside the airways, the epithelial structure shows some striking differences between human and mouse since humans have different types and higher numbers of mucus secreting glands and cells compared to mice [27].

Despite those differences, the mouse, used as the common laboratory species, develops similar features of allergic airway inflammation after sensitization with an allergen. Early mouse models used ovalbumin (OVA) with aluminum hydroxide as adjuvant to induce the allergic inflammation, because mice do not spontaneously develop asthma when given the antigen alone. However, more recent studies mainly use more physiologic allergens like HDM, aspergillus, or even a combination of different natural allergens for the sensitization without addition of adjuvants [28, 29]. After sensitization and final treatment with the selected allergen acting as a trigger signal for an acute inflammation the effects of the typical Th2 response can be measured. Of note, the selection of a suitable mouse strain is essential for the experimental success since different strains respond differently to allergic sensitization. BALB/c mice are the most common animals used for asthma research, while C57BL/6 mice were thought to be resistant to allergic sensitization since they do not develop AHR [30]. However, more recent studies suggested that depending on the sensitization protocol C57BL/6 mice also develop the common asthma features [31, 32].

As described, the mouse as a model organism does not perfectly reflect the exact mechanisms occurring in human asthma, but it is an adequate model to investigate basal mechanisms under standardized conditions in a complex organism that might be transferable to the human and finally lead to a better treatment or even prevention of the disease.

3.1.4 Allergic Sensitization

Allergic asthma is a disease based on an inappropriate Th2/Th17 response of the adaptive immune system after inhalation of harmless natural substances in susceptible individuals [20]. After inhalation of those particles (e.g. plant pollen, animal dander, house dust mite) most of the particles will be removed from the lung by mucociliary clearance but partially it will reach the airway epithelium. The epithelium is not only a physical barrier but harbors different pattern recognition receptors (PRR), in particular Toll-like receptors (TLR) [33, 34], that can be activated by the protease activity of some allergens [35-40].

As a consequence of its disturbed homeostasis, the epithelium releases different alarmin substances, including cytokines such as IL-33, uric acid, high-mobility group box 1, and adenosine triphosphate. Further triggers for the activation of the immune system are the secretion of IL-1α, IL-25, thymic stromal lymphopoietin (TSLP), granulocyte-macrophage colony-stimulating factor (GM-CSF, CSF-2) and chemokines like CC-chemokine ligand 2

(CCL2) [36]. Those substances then initiate the recruitment and activation of innate immune cells including type 2 innate lymphoid cells (ILCs), macrophages, and pulmonary DCs [41]. Among these cells DCs probably play the most important role during the onset of the inflammatory response since they are thought to take up huge amount of antigen, process it, and present it via their MHCII to naïve T cells, which then differentiate into effector T cells [42]. DCs are thereby able to bridge between innate and adaptive immune system. During effector phase of allergic asthma DCs are important sources of CCL17 and CCL22. Effector T cells are then attracted to the site of inflammation by these chemokines [43].
In general, an inflammatory Th2 response is induced by the immune system to fight against a helminth infection, while a Th17 response is used to fight bacterial infections. It still needs to be revealed whether or to which extend DCs interact with other innate immune cells during activation and recruitment of T cells and maintenance of inflammation. Further, the release of IL-4, IL-5, and IL-13, mainly from T cells, contributes to the development of the typical characteristics of asthma including AHR, goblet cell metaplasia, IgE syntheses, and eosinophilia [22]. In addition, type 2 conditions are characterized by IgE secretion of B cells that can bind to FcR-expressing innate cells such as mast cells. The Th17 response promotes neutrophil infiltration which might influence activation and function of innate cells [44, 45]. Taken together, both T cell responses are characterized by the secretion of soluble mediators from innate and adaptive effector cells, that can mediate the common features as goblet cell metaplasia and AHR [22, 45-48].

DCs possess the ability to bridge the innate and adaptive immune system by their ability to activate naïve T cells. During the last years, different subsets of pulmonary DCs have been identified. Every single subset possesses different localizations and functions although there are still gaps and debates caused by contradictory findings [49-54]. Further, other studies showed important functions for other types of pulmonary phagocytes including alveolar macrophages (AMs) and interstitial macrophages (IMs) during allergic asthma [2, 55-58]. Taken together the gross mechanism of allergic airway sensitization has already been discovered, but there are still open questions regarding the differentiation of pulmonary phagocytes and their specific functions during sensitization and also the chronic phase of allergic asthma. The specialized functions of the different phagocyte populations will be addressed in the next chapter.

3.2 Pulmonary Phagocytes in the Context of Allergic Asthma

3.2.1 Pulmonary Phagocytes

Initially, pulmonary phagocytes were described as a homogenous population of $MHCII^+$ cells [59-62]. Today, it is known that the lung comprises a complex compartment of lung phagocytes including DCs, macrophages, and monocytes each with different subsets. From these phagocytes DCs are set as the most important antigen uptaking cell type since, in contrast to monocytes and macrophages, they are able to activate naïve T cells [63].

3.2.2 Diversity of Pulmonary Phagocytes

Today it is well appreciated that the compartment of pulmonary phagocytes consists of at least four types of DCs, two different macrophage populations, and two types of monocytes. At steady-state, using their surface marker profiles, DCs can be separated into cluster of differentiation (CD)$11b^+$ conventional (c)DCs, $CD103^+$/$Langerin^+$ cDCs (later referred to as $CD103^+$ cDCs) and plasmacytoid (p)DCs. Under inflammatory conditions a population of monocyte-derived (mo)DCs is recruited to the lung. Pulmonary macrophages can be divided into AMs and IMs. In addition, monocytes can be divided into classical $Ly6C^{hi}$ and non-classical $Ly6C^{lo}$ monocytes [64, 65]. Although DCs are the only phagocytes that are able to activate T cells [63], also the other phagocytes are able to influence the immune response. As suggested by the term phagocyte all subsets are able to ingest antigen and secrete messenger substances to modify the immune response.

Since most of these subsets express similar surface markers, distinction can be rather difficult and various markers have to be taken into account [66]. The most common markers to distinguish cDCs and macrophages are CD11c, CD11b, CD103, MHCII, sialic acid-binding immunoglobulin-type lectins (Siglec)-F, and CD64. Based on the individual gating strategy some studies have used additional markers for the identification of pulmonary phagocytes. [51, 52, 67-69], which complicates the comparison between different studies. As a result of this heterogeneity, different absolute and relative numbers for DC subsets and sometimes even different functions have been reported in different studies using flow cytometry although the same antibody clones were used. [51, 52, 66-74].

3.2.3 Origin of Pulmonary Phagocytes

In addition to the analysis of surface markers cellular origin is useful to distinguish the different phagocytic populations and their specific functions, especially because surface marker expression is similar and sometimes even overlapping for some populations e.g. $CD11b^+$ cDCs and $CD11b^+$ moDCs. The origin of pulmonary phagocytes is summarized in figure 1.

$CD103^+$, $CD11b^+$ Conventional DCs, and Plasmacytoid DCs

The generation of cDCs and pDCs starts in the bone marrow where hematopoietic stem cells differentiate into a macrophage DC progenitor (MDP) [75]. This MDP then gives either rise to the common DC progenitor (CDP) [72, 76] or a common monocyte progenitor (cMoP) [77]. Though, it remains unclear whether CDPs might also evolve without the intermediate MDP step [78]. Subsequently, CPDs differentiate into pre-DCs, the common progenitor of pDCs and cDCs [79, 80]. While pre-DCs maturing to cDCs directly leave the bone marrow, pDCs differentiate from the CDP into a mature pDC before leaving the bone marrow towards other organs [81]. The differentiation of pre-DCs into the different cDC subsets is not fully understood by now, but existing data shows development of $CD103^+$ cDCs to be dependent on basic leucine zipper ATF-like transcription factor 3 (BATF3) [82, 83], interferon regulatory factor (IRF)8, and Id2 [84], while $CD11b^+$ cDCs mainly depend on the expression of IRF4 [85]. Although pre-DCs are thought to enter the lung and cells phenotypically resembling these cells were found in the lung, differentiation to DCs has not been shown yet *in situ* [3, 84, 86].

However, the differentiation of $CD11b^+$ cDCs is less understood compared to $CD103^+$ cDCs. This is caused by the similarity of $CD11b^+$ cDCs and $CD11b^+$ resident moDCs resulting in easy confusion of both population even at steady-state. Besides, it remains unclear whether peripheral and lymphoid $CD11b^+$ cDCs have the same origin [74, 87-91].

Generation of cDCs and pDCs from precursors includes many more cytokines and transcriptional factors as pointed out here and was recently reviewed in Hoffmann *et al.* [66]. There is still an ongoing debate about the origin of pulmonary DCs in particular regarding the $CD11b^+$ compartment. Although it was indicated that $CD64^+$ moDCs are only recruited to the lung under inflammatory conditions [51] there are several studies pointing towards a mixed population also at steady-state. Nakano *et al.* [52] described the presence of a heterogenous population in the lung using CD14 and complement C5a receptor 1 (C5aR1)/CD88. The same

group underpinned this hypothesis by the detection of different expression levels of CC-chemokine receptor 7 (CCR7) in both populations [73]. A heterogeneity of $CD11b^+$ DCs was also found using lineage tracking for DNGR-1, a bona fide marker of mouse cDC precursors about half of the $CD11b^+$ DC population was not traced [92].

Monocytes and Monocyte-Derived DCs

As already mentioned, the cMop raises in the bone marrow from MDP, that in turn develops out of hematopoietic stem cells [77]. The cMop differentiates into classical $Ly6C^{hi}CCR2^{hi}$ monocytes that can convert to $Ly6C^{lo}CCR2^{lo}$ monocytes [87, 93-95]. While it is still under debate that short-lived $Ly6C^{hi}$ monocytes [72, 93] can convert into $Ly6C^{lo}$ monocytes [65], it is well established that they give rise to short-lived $Ly6C^{hi}CD11b^+$ moDCs [96-98]. Equally, $Ly6C^{lo}$ monocytes can differentiate into long-lived $Ly6C^{lo}CD11b^+$ moDCs. Since, not all $Ly6C^{hi}$ monocytes that enter the lung differentiate into DCs, but nevertheless migrate towards the lymph nodes [97], it was suggested that further stimuli are necessary to drive monocyte differentiation inside the lung.

MoDCs were defined as $CD11c^+CD11b^+CD64^+Ly6C^+Fc\varepsilon R1^+$ cells [51]. However, it was shown that they lose the expression of Ly6C during their maturation from monocytes into moDCs [51, 88]. The development of moDCs is dependent on CCL2 signaling that drives the migration of $Ly6C^{hi}CCR2^{hi}$ monocytes to the lung [88, 99-102]. Differentiation of moDCs is then mediated by CCL2 [51] and colony stimulating factor (CSF)1 [84].

Alveolar Macrophages

Differentiation of AMs starts during embryonic development as they derive from yolk sac macrophages or fetal liver monocytes [103]. These cells leave their sites of origin and migrate to the lung to colonize the alveolar space during the first days after birth. It was also shown that the recruitment of precursors to the lung is dependent on CSF2, since it was abolished in the absence of CSF2 [103]. After colonization of the lung the AM population is maintained by self-renewal throughout the host's lifetime.

Monocytes that enter the lung during inflammatory conditions differentiate into $CD11c^{lo}CD11b^{hi}$ macrophages which rather resemble IMs than AMs, but data suggested that those IMs might be an intermediate stage during the differentiation to AMs [104].

Interstitial Macrophages

IMs are a rather poorly defined cell population characterized by the expression of F4/80 and CD11b but lack expression of CD11c [2, 105]. A similar cell called non-migratory myeloid cell ($CD11b^{+}Gr\text{-}1^{int}F4/80^{+}$) was described that might match the IM phenotype [106, 107]. However, due to inconsistent data about IMs no study has focused on their origin so far, but it is likely that they might originate from the macrophage or monocyte lineage. This suggestion is supported by the commonality of IMs and the macrophage/-monocyte lineage to suppress Th2 responses [2, 106].

Taken together, the origin of most pulmonary phagocytes is mainly understood, although there are remaining questions for some populations as $CD11b^{+}$ DCs and IMs. Understanding the development of the single populations will help to understand their specific functions in allergic airway inflammation. Understanding of specific functions is again the basement for the development of new therapeutics that will directly target a specific population.

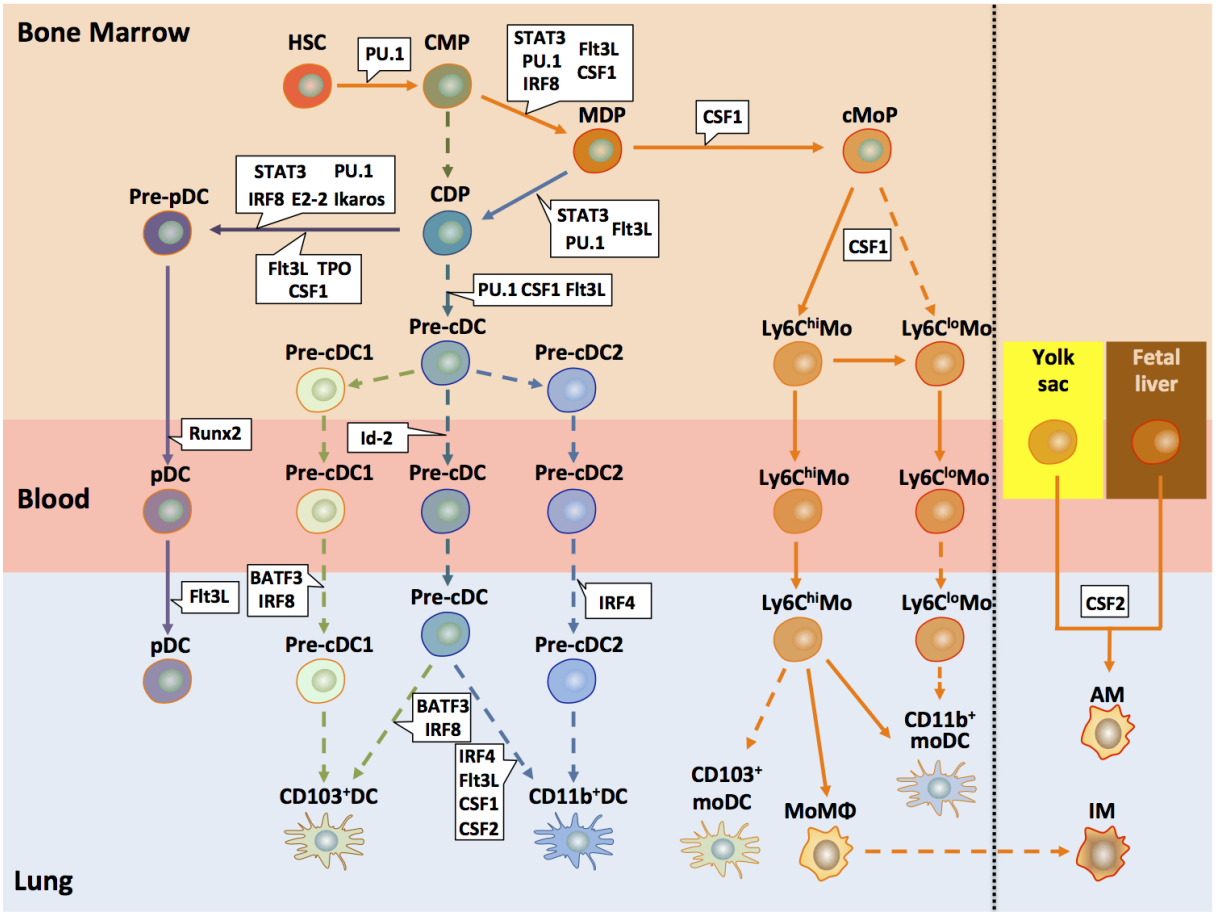

Figure 1: Origin of dendritic cells, monocytes, and macrophages. This figure summarizes the differentiation of pulmonary DC and macrophage subsets starting in the bone marrow (BM). DC development starts with a hematopoietic progenitor (HSC) that differentiates into a common myeloid

progenitor (CMP). This CMP gives rise to either a common DC progenitor (CDP) or macrophage DC progenitor (MDP) [3, 75, 108]. The CDP gives rise to a pre-DC which is a common progenitor for pDCs and cDCs. While pDCs mature in the BM in a Runx2-dependent manner, pre-DCs, giving rise to cDCs, leave the BM and mature in the tissue. Development of $CD103^+$ cDCs is dependent on BATF3 and IRF8, $CD11b^+$ cDCs are dependent on IRF4, Flt3L, CSF1 (M-CSF), and CSF2 (GM-CSF). It was also suggested that the pre-DC fate is already decided before leaving the BM with pre-DC1 and pre-DC2 intermediate stages [109]. The MDP differentiates with an intermediate cMop step into $Ly6C^{hi}$ or $Ly6C^{lo}$ monocytes in a CSF1 dependent manner. In the tissue $Ly6C^{hi}$ monocytes give rise to monocyte-derived macrophages (MoMΦ) and $CD11b^+$ moDCs [3, 65]. AMs derive from yolk sac and fetal liver progenitors that colonize the embryonic lung and are maintained by self-renewal at steady-state [3]. The origin of IMs still needs to be unraveled. However, some data suggest that they represent monocyte-derived macrophages [106, 107]. HSC- hematopoietic stem cells, CMP- common myeloid progenitor; MDP- monocyte–macrophage DC progenitor, CDP- common DC progenitor, cMoP- common monocyte progenitor, Mo- monocyte, MoMΦ- monocyte-derived macrophage, cDC- conventional DC, moDC- monocyte-derived DC, AM- alveolar macrophage, IM- interstitial macrophage.

This figure was published before in Hoffmann *et al*. [66] and is reproduced according to the guidelines for redistribution of material published in Frontiers in Immunology under the terms of the Creative Commons Attribution 4.0 International Public License (https://creativecommons.org/licenses/by/4.0/legalcode#languages).

3.2.4 Localization of Pulmonary Phagocytes

It is known, that pulmonary phagocytes and especially DCs are critical for antigen uptake and the development of an immune response. After distinction of phagocyte subsets, knowledge of cell localization is an important basis for understanding of antigen uptake and the onset of the immune response. However, there is no study that gives a detailed overview about the localization of pulmonary phagocytes. The lung is a complex organ consisting of different compartments including airways, alveolar compartment, arteries, veins, and the pleura. In addition, the lung comprises a dense network of lymph vessels (LV) that run with veins, airways, and in the connective tissue between airway and pulmonary artery [110]. Since DCs use LVs for their trafficking to the draining lymph node these compartments are likely areas for DC localization.

Early studies defining DCs only by the expression of MHCII described them to be located in many lung compartments including large conducting airways, alveolar compartment, lung

parenchyma, pleura, perivascular space, and inside of pulmonary vessels [61, 111]. However, it became clear that the expression of MHCII is not only restricted to DCs but also IMs and type II pneumocytes and therefore, further studies are needed to verify the localization of pulmonary phagocytes based on a detailed surface marker panel.

CD103$^+$ Conventional DCs

Originally, pulmonary CD103$^+$ cDCs were described as MHCII$^+$ intraepithelial DCs [112, 113] in the trachea of rats [101]. However, immunohistochemistry (IHC) for CD103$^+$ cDCs originally showed their localization close to the airway epithelium and cell bodies were rarely observed in the epithelium itself [70]. Therefore, it was suggested that the intraepithelial network, described to sample antigen through the epithelial barrier [112, 113], mainly consists of extensions [70]. Two-photon analyses on precision-cut-lung-slices (PCLS) from CD11c-eYFP mice showed a fourfold higher number for subepithelial DCs compared to intraepithelial DCs [114]. Accordingly, a study using OVA-sensitized mice showed no extension of dendrites into the airway lumen. Interestingly, there was a high activity in the alveolar region [115]. These findings support the hypothesis that DC localization in the trachea is different to the lung. Sung *et al.* [70] further showed that CD103$^+$ cDCs account for approximately 70-75% of the CD11c$^+$MHCII$^+$ DCs in the proximal subepithelial and periarterial regions. Furthermore, CD103$^+$ DCs were described on the parenchymal side of arteriole walls underneath the vascular endothelial cells and perhaps attached to the basal lamina but absent in the alveolar region. Regarding the ability of CD103$^+$ cDCs to extend dendrites into the airway lumen it was shown that CD103 (alpha integrin) and beta7 integrin interact with E-cadherin that is expressed at the basal side of epithelial cells [70]. Additionally, CD103$^+$ cDCs have a higher expression of some tight-junction proteins including Claudin-1, Claudin-7, and Z0-2 compared to other DC subsets. This might facilitate the extension of dendrites through the epithelial barrier into the airway lumen [70].

CD11b$^+$ Conventional DCs

The first study describing the localization of CD11b$^+$ cDCs used a flow cytometry-based method. They separated the lung into main conducting airways (trachea, main bronchi) and lung parenchyma (peripheral third of the lung) to determine the localization of different antigen presenting cell (APC) subsets. According to them, CD11b$^+$ cDCs are present in the lung

parenchyma and also at the airways [62]. A second study based on immunohistochemistry showed $CD11b^+$ cDCs in perivascular regions but only few cells in the epithelial region [70]. Two-photon analyses on living lung slices showed that $CD11b^+$ cDCs can be found at the airways up to distance of about 200 µm. Furthermore, an accumulation of $CD11b^+$ cDCs around the airways was shown after OVA challenge. However, it is not clear if the accumulating cells are $CD11b^+$ cDCs, $CD11b^+$ moDCs or both [115].

Monocyte-Derived DCs

Since most of the studies dealing with lung DCs concentrate on functional analyses and not localization, very few data exist for the moDC subset. Localization of moDCs might be even more difficult because of their similar marker expression compared to $CD11b^+$ cDCs. Nevertheless, a population similar to $CD11b^+$ cDCs was described to be recruited to the alveolar region after infection with *B. anthracis* [116]. MoDCs and $CD11b^+$ cDCs can easily be confused and multiparameter analyses are needed to allow a clear distinction. A reliable strategy for the distinction based on CD64 and FcεR1 was first published in 2013 [51]. This study also reported that moDCs are recruited to the lung in high numbers after allergen challenge. Therefore, it is not unlikely that the population recruited to the alveolar region might be moDCs. However, currently there is a disagreement about the frequency of resident moDCs in the lung. Resident moDCs were initially reported to be a minor population at steady-state [51]. Another study proposed that 50% of $CD11b^+$ DCs derive from a monocytic origin [52]. Nevertheless, both studies agree, that there is a high influx of inflammatory moDCs under inflammatory conditions.

Plasmacytoid DCs

Similar to the moDC subset very limited data are available for the localization of pDCs. They comprise a very small fraction in the naïve lung which makes them difficult to detect but they were reported to be present in large conducting airways as well as in the lung interstitium [70, 117]. However, immunohistochemical data, defining them as B220 and Gr-1 expressing cells, described pDCs to be mainly located in the alveolar interstitium [70, 118].

Alveolar Macrophages

In contrast to all other population described here, AMs are not located in the lung tissue itself but the alveolar lumen [62, 119, 120]. Soroosh *et al.* [119] also reported about tissue-resident AMs, but since they did not perform any histological studies it remains unclear whether these cells were inside the lung parenchyma or attached to the alveolar wall and, therefore, not washed out during bronchoalveolar lavage (BAL). Recently, the division of AMs into a alveolus-adherent and a alveolus-non-adherent fraction was shown supporting the second hypothesis [55].

Interstitial Macrophages

Different groups have defined the marker set of IMs differently and several descriptions exist in the literature [2, 105]. Only one paper examined the localization of IMs based on their $CD11c^{-}F4/80^{+}$ phenotype. They found these cells exclusively in the alveolar interstitium, where they can be detected close to DCs [2]. Since the marker expression of IMs is poorly characterized, it is likely that not all macrophage populations in the lung were stained in this paper and further studies are needed to identify the localization of IMs in the lung.

Taken together, valid data for the localization of some phagocyte populations is still missing. The localization of $CD103^{+}$ cDCs, pDCs and AMs seems to be well defined, although there might be misunderstandings regarding intraepithelial $CD103^{+}$ cDCs. In contrast, there is a lack of data concerning localization of the other populations ($CD11b^{+}$ cDCs, moDCs, monocytes, IMs) and a comprehensive study is missing that is examining the location of all pulmonary phagocytes. Such a study, that allows the analysis of different phagocytes in their natural environment, would also enable the examination of cell contacts or interactions. This might be interesting since it has already been shown that sessile AMs communicate with the alveolar epithelium [55] and further interactions between different cell subsets are conceivable.

3.2.5 The Role of Lung Phagocytes in Allergic Asthma

As outlined above there are different subsets of DCs each with specific origin and localization. In the same line, also different functions during the allergic sensitization were reported for the different subsets.

CD103$^+$ Conventional DCs

It was shown that CD103$^+$ cDCs are efficient uptakers of viral particles [121]. In addition, they have also been shown to induce an antiviral response of CD8$^+$ T cells by cross-presentation via MHCI [122]. In allergic airway responses they appeared as less prominent antigen uptakers compared to CD11b$^+$ cDCs [51]. Further, for a long time CD103$^+$ cDCs were thought to sample antigen through the epithelial barrier based on their ability to form tight-junctions with epithelial cells by their expression of tight-junctional proteins (Claudin-1, Claudin-7, ZO-2) [70], but as described above there is no data proving this suggestion. The lung is a mucosal surface and due to this it is often compared to the gut. In the gut CD103$^+$ DCs were shown to interact with macrophages leading to the induction of tolerance. In this model macrophages took up antigen and transferred membrane particles with MHCII-bound peptides via connexin43 (Cx43) channels to the DC [1]. Although, alveolus-adherent AMs were shown to communicate with epithelial cells in a Cx43 dependent manner [55], so far no hints were found for a similar mechanism of CD103$^+$ cDC-macrophage crosstalk as reported in the gut.

In the context of allergic asthma their role is still controversial since different functions were reported. As mentioned above Plantinga *et al.* [51] described them as minor antigen uptaking population after HDM sensitization, while in another model based on lipopolysaccharide (LPS) Nakano *et al.* [52] described them as potent inducers of a Th2 response. In contrast, to these findings, CD103$^+$ cDCs were also associated with the induction of tolerance [49, 50]. Moreover, they might play an important role in T cell homing to the pulmonary compartment since they are a major source of CCL17 and CCL22 [51, 123].

CD11b$^+$ Conventional DCs

Compared to CD103$^+$ cDCs the proposed function of CD11b$^+$ cDCs seems less versatile. As mentioned, CD11b$^+$ cDCs are very efficient allergen uptakers compared to CD103$^+$ cDCs [51, 53] and were also reported to be the main migratory subset in a HDM-based allergic asthma model. Thus, they were also identified to be essential for the allergen-induced Th2 response [51, 53, 124]. In addition, they were also shown to be efficient in inducing a Th17 response in a fungal infection model [85] and a HDM-mediated model [54]. Induction of Th2 and Th17 were promoted via a dectin-2-dependent mechanism by CD11b$^+$ cDCs [54].

Monocyte-Derived DCs

As described above moDCs and CD11b$^+$ cDCs are difficult to distinguish due to a similar marker profile. Today, there is only a single study focusing on the different roles of CD11b$^+$ cDCs and moDCs in a HDM-mediated allergic inflammation. In this study, moDCs showed a maximum 48 h and 72 h after challenge in lung and lymph node, respectively [51], while there were only few moDCs present at steady-state. In contrast, another study reported that about 50% of steady-state CD11b$^+$ DCs derive from a monocytic lineage using C5aR1/CD88 as discriminative marker [52]. In addition to this resident moDCs they identified a third CD11b$^+$ DC population, that was recruited to the lung under inflammatory conditions probably matching the moDCs reported by Plantinga *et al.* [51]. Massive recruitment of moDCs to the lung was shown to be dependent on the CCL2/CCR2 axis as well as formyl peptide receptor [51, 125]. Although they are efficient uptakers, their potential to drive a Th2 response is lower compared to CD11b$^+$ cDCs, in particular at low allergen doses. Therefore, the production of cytokines and chemokines (CCL24, CCL2, CCL4, CCL7, CCL9, and CCL12) that are critical for the activation and recruitment of eosinophils and macrophages in response to allergen challenge has been suggested as their main function [51].

Plasmacytoid DCs

Compared to cDCs pDCs represent a smaller population of lung DCs. At steady-state pDCs maintain pulmonary tolerance to harmless antigens [126, 127]. After allergen encounter the number of pDCs increases [128], at least partly due to the release of IL-15 by epithelial cells [129]. However, different studies pointed out that pDCs are poor allergen presenters compared to cDCs in the context of allergic asthma [51, 118, 128]. Plasmacytoid DCs were deemed as tolerogenic since they are able to drive the differentiation of regulatory T cells ($T_{regs)}$ in response to allergen uptake [118, 130, 131]. In addition, selected depletion of pDCs resulted in impaired tolerance [132]. An important factor during the induction of tolerance is the expression of retinal dehydroxygenases (RALDHs) resulting in the generation of retinoic acid, which is a critical metabolite for the development of T_{reg} cells [133]. However, the role of pDCs in allergic asthma is questioned since CD103$^+$ cDCs instead of pDCs were shown to express increased amounts of RALDHs after allergen administration [50].

Alveolar Macrophages

The role of AMs in allergic asthma remained disregarded for a long time since DCs were considered to be the main important cells depending on their ability to prime naïve T cells. In contrast, AMs were thought to act as garbage collectors for apoptotic cells or airborne particles, that had entered the lung. However, more recently several studies were focusing on the role of AMs highlighting that this population seems to be much more important than originally thought. AMs outline the alveolar space and take up huge amounts of harmless und harmful antigens. To enable this, they are equipped with a wide range of PRRs [134]. Alveolus-adherent AMs were described to suppress the secretion of proinflammatory chemokines by a crosstalk with epithelial cells [55]. Congruent with these observations another study showed that depletion of AMs resulted in decreased TGF-β production [56]. On the other hand, AMs were described as the main source of IL-17 in an OVA-mediated experimental asthma model [57]. In order to combine the anti- and proinflammatory capacities inside the population different models were suggested. The first model suggested that there is a difference between direct or indirect uptake of pathogenic particles leading to tolerance or inflammation respectively [58]. Hussel and Bell [135] suggested that the location of AMs inside the alveoli or the mucus layer of bigger airways might influence their function.

Interstitial Macrophages

Since IMs are a poorly defined population in the lung, little is known about their function. Further, studies defining IMs used different approaches to define these cells. However, there is a slight agreement, that those cells have a $CD11c^{-}CD11b^{+}F4/80^{+}MHCII^{+}$ phenotype. According to one report the majority of circulating monocytes differentiates into IMs and starts expressing MHCII and COX-2 after migration to the lung [97]. Depletion of those circulating monocytes resulted in increased inflammation suggesting an anti-inflammatory function for IMs [56]. IMs were also reported to be a source of IL-10 after low dose LPS treatment [2]. Further, a similar cell called non-migratory myeloid cell ($CD11b^{+}Gr\text{-}1^{int}F4/80^{+}$) potentially matching the IM phenotype was described [106, 107]. These cells were shown to suppress the ability of DCs to reactivate primed Th2 cells in LPS-mediated model. In contrast, IMs were also shown to express IL-17 [57]. The depletion of AMs in IL-13-driven airway inflammation also resulted in higher numbers of IMs in the tissue [136].

Monocytes

The role of monocytes in allergic asthma is ill defined, since for a long time monocytes were thought to act as blood precursors for moDCs and macrophages only. However, it was shown that tissue macrophages develop during embryogenesis and maintain the population by self-renewal [103]. In addition, blood monocytes that enter the lung can preserve their monocytic status and do not mature to moDCs or macrophages, although they start to express MHCII. Further, these tissue-resident monocytes have been shown to take up antigen and transport it towards the lymph nodes in a CD62L dependent manner at steady-state [97].

3.2.6 Migratory Potential of Pulmonary Dendritic Cells

Migration of activated DCs towards the lung draining lymph nodes is essential for the induction of an appropriate immune response, since naïve T cells get primed in the lymph nodes [45, 137, 138]. It is general accepted that activated DCs upregulate CCR7 and migrate in a CCL19/CCL21 dependent manner via LVs towards the draining lymph nodes. Although this mechanism is well described for the skin [139-141] there is a lack of data for the migration of pulmonary DCs. Studies on their migratory potential in the lung are mainly based on the comparison of wildtype (wt) mice and $CCR7^{-/-}$ mice. It was shown that $CD103^{+}$ cDCs lose their ability to home the lung draining lymph node in an allergic mouse model. At the same time, it was described that $CCR7^{-/-}$ mice show an exacerbated inflammation [142, 143]. In accordance with the inability of $CD103^{+}$ cDCs to migrate to the lymph nodes in a $CCR7^{-/-}$ mouse model, it was shown that homing of T_{reg} cells to the lymph nodes was strongly impaired [144]. However, there was a slight increase in tissue-resident T_{reg} cells.

These findings indicate a necessary role for the bronchial lymph nodes during the induction of tolerance, while there is a lymph node independent mechanism for the induction of an inflammatory response. A recent study [115] showed interactions between $CD11b^{+}$ DCs and T cells close to the airways in OVA-sensitized mice 48 h after allergen challenge. By an indirect tracking approach, they have shown that those $CD11b^{+}$ DCs ingested antigen in the alveolar space and where found at the airways interacting with T cells 48 h later. In contrast, another study [51] defined $CD11b^{+}$ cDCs as the main migratory subset in a HDM-based allergic asthma model based on the number of $CCR7^{+}$ $CD11b^{+}$ cDCs in the lymph nodes indicating an important role for the lymph node during inflammation. In a dose-dependent analysis they also showed that $CD103^{+}$ cDCs or moDCs were only found at higher numbers in the lymph nodes with high

or moderate doses of HDM, while no migratory pDCs were observed. An OVA-based study identified $CD103^+$ cDCs as the main migratory subset in the first 24 h hours after instillation of allergen [74], while only a smaller subpopulation of $CD11b^+$ DCs showed migratory potential. In accordance with this finding they also reported higher mRNA expression for CCR7 in $CD103^+$ cDCs than in $CD11b^+$ DCs. Nevertheless, an *in vitro* experiment showed that about 50% of both cDC populations expressed CCR7 24 h after stimulation with LPS in an *in vitro* model using CCR7 green fluorecent protein (GFP)-mice. Different studies, notwithstanding of different cell definition, identified moDCs as a minor migratory subset compared to cDCs. Consistently, moDCs also expressed lower amounts of CCR7 compared to cDCs [51, 73, 74].

There is still an ongoing debate about the presence of steady-state DC migration in the lung. [51] showed CCR7 expression in smaller fractions of both cDC subsets in their control mice indicating the presence of steady-state migration. But since those mice were treated with PBS it remains unclear whether they really represent steady-state conditions. Other studies mentioning steady-state migration and rapid turnover of lung DCs are referring to a single study that showed a high turnover of pulmonary $MHCII^+$ cells in rats [112] or on studies focusing on skin [140]. Based on the data so far, the presence of steady-state migration remains unclear, despite a study showing no migratory potential for DCs at steady-state using an indirect tracking approach [145]. CCL21 was shown to be expressed by endothelial cells of LVs in the skin [140, 146], but there is lacking data dealing with the origin of CCL21 in the lung. Nevertheless, it was shown that cells expressing CCL21 cluster within bronchus associated lymphoid tissue preferentially close to perivascular areas in $CCR7^{-/-}$ mice [144].

Taken together it is well established that $CD103^+$ cDCs and a subpopulation of $CD11b^+$ DCs are able to express CCR7 and migrate to the draining lymph node after stimulation. However, there are contradictory results concerning DC migration which may at least partly be due to different models that were used. The site of DC activation and where $CRR7^+$ DCs are located in the murine lung is still unclear. Further there is no reliable data concerning the presence of steady-state turnover.

3.3 Comparison of Flow Cytometry and Confocal Laser Scanning Microscopy

Most studies dealing with DCs and macrophages are mainly based on flow cytometry. Flow cytometry is an easy way to define different subsets based on various surface markers in order to perform quantitative analyses. Once a gating strategy is set up successfully cells can also be sorted in order to perform different functional analyses either *in vitro* or *in vivo* via adoptive transfer to recipient mice.

Besides all advantages of flow cytometry, the need for compensation might be kind of a disadvantage because it needs to be done very carefully and can get very complicated with increasing number of colors. Compensation is necessary since each fluorophore has a specific excitation maximum but the spectra of some fluorophores show some overlap at the edges. This overlap causes false positive signals which can be eliminated by compensation. In addition, there is often no clear separation for gating positive and negative populations especially regarding lung DCs and macrophages [147]. To solve this problem, the right controls are needed. Possible controls are isotype controls for the antibodies itself and fluorescence minus one (FMO) controls to facilitate the gate set up at the right places. For best results antibody colors need to be chosen carefully depending on the brightness of the fluorochrome and the amount of antigen at the cell surface. In addition, it might be useful to take the gating strategy into account to avoid similar colors or fluorochromes, which are excited by the same laser in the same gating step. Gating itself also includes a risk as subjectivity and manual gating leads to minor differences between single experiments. To patch this issue there is an increase in the development of automatic gating tools [148].

Modern microscopic techniques like confocal laser scanning microscopy (CLSM) or two-photon microscopy allow the observation of immune cells in their natural environment on fixed sections, *ex vivo* on tissue sections [110, 114], and even *in vivo* [115, 149]. Depending on the technique there are several limitations compared to flow cytometry. Simple fluorescence microscopes are only equipped with a small set of filters that allow a maximum of four colors. In addition, it is only possible to analyze thin sections because there is no vertical resolution. Using CLSM it is possible to make three-dimensional images by scanning different layers of a defined region. This allows the analysis of cell morphology and contacts with other cells, since every layer can be observed individually and the whole stack can be turned around for different views. Depending on the setup a CLSM offers many other possibilities for the observation of

living cell or tissues over a certain time. Further, it is possible to use additional fluorophores compared to classical fluorescence microscopy by combining laser and filter settings in the same way as for flow cytometry, but until now, there are only few studies performing microscopy with more than four colors [150, 151].

As for flow cytometry, there are several advantages and disadvantages of microscopic analyses. A striking advantage is that cells can be observed in their natural environment, this allows statements about morphology, localization, and even cell contacts. None of these findings can be defined by flow cytometry. In contrast, the problems of background fluorescence of the tissue are much higher and depending on fixation antigen might be masked. Quantitative analyses are also more difficult compared to flow cytometry. On the one hand because microscopic analyses are more time consuming than flow cytometry and on the other hand a technique is needed that allows a random selection of regions of interest. These regions must represent the whole section because imaging a complete tissue section is not possible. Further, software for counting is needed, otherwise counting must be performed by hand. In a final step the counted results need to be extrapolated to the whole tissue or organ. Thus, microscopy based quantification seems to be a great expenditure compared to easy quantification by flow cytometry, but a recent study highlighted that there might be some problems with the latter depending on the tissue. Steinert *et al.* [152] compared the numbers of resident $CD8^+$ memory T cells in various organs including the lung. It turned out that cell numbers obtained by flow cytometry have underestimated cell numbers up to 70-fold compared to the microscopic analysis in such non-lymphatic organs (lung 69.1-fold) while it was roughly the same for both techniques in spleen (1.92-fold) and lymph nodes (1.19-fold). These differences can be explained by structures of the different organs. Lymphoid organs only contain small amounts of connective tissue while non-lymphoid organs mainly consist of connective tissue. Phagocytes in those organs are sometimes tightly attached to the tissue which complicates cell isolation and an enzymatic digestion of the tissue is necessary. However, depending on cell type and organ it seems that the digestion does not enable the isolation of the complete population.

3.4 Aims

As described the activation of DCs after allergen inhalation is crucial for the induction of an allergic airway response. It is therefore likely that asthma prevalence is linked to differential antigen uptake by DC and macrophage subsets in different areas of the lung in mouse strains with low (C57BL/6) and high susceptibility (BALB/c) for allergic asthma. To shed light on the steady-state conditions and the comparison with the circumstances under early inflammation this study set the following aims:

1) Identification of DC and macrophage subsets in the lung by a four-color panel for immunohistochemistry.
2) Quantification of DC and macrophage subsets in the murine lung based on microscopy.
3) Localization of the different DC and macrophage subsets to determine preferred sites of localization or possible areas with high cell density. Further, possible cell interactions will be analyzed.
4) Determination of changes regarding cell numbers and cell localization after allergen challenge.
5) Examination of migratory properties of pulmonary phagocytes based on their CCR7 expression in the naïve and the allergen treated lung.

4 Material and Methods

4.1 Material

The following chapter summarizes the material and equipment used in this study.

4.1.1 Animals

Mice used for immunohistochemical essays at steady-state conditions were purchased from Charles River Laboratories Research Models and Services Germany GmbH (see tab. 1) and sacrificed 8 to 16 weeks after birth. HDM-treated mice were provided by the Institute of Systemic Inflammation Research, Lübeck.

Table 1: Used mouse strains

Mouse Strain	Supplier	Application	Treatment
BALB/cAnNCrl	Charles River Laboratories Research Models and Services Germany GmbH, Sulzfeld, Deutschalnd	IHC	naïve/ HDM-treated
C57BL/6NCrl	Charles River Laboratories Research Models and Services Germany GmbH, Sulzfeld, Deutschland	IHC/ Flow Cytometry	naïve/ HDM-treated
C57BL/6NCrl	JAX® Mice, The Jackson Laboratory, Bar Harbor, USA	Flow Cytometry	naïve

4.1.2 Chemicals

Table 2: Chemicals and other reagents used in this study

Chemicals and other Reagents	
ACK Lysing Buffer	Life technologies Corporation, Carlsbad, USA
Ampuwa Spüllösung	Fresenius Kabi, Bad HomburgGermany
Bovine serum albumin (BSA)	Sigma-Aldrich Chemie GmbH, Steinheim, Germany
Calcium chloride ($CaCl_{2)}$	Merck KGaA, Darmstadt, Germany
CD11c MicroBeads Ultrapure	Miltenyi Biotec Inc., San Diego, USA
Certified PCR Low Melt Agarose	Bio-Rad Laboratories, München, Germany
Collagenase IV	Sigma-Aldrich Chemie GmbH, Steinheim, Germany
Disodium hydrogen phosphate (Na_2HPO_4) >99% p.a.	Merck KGaA, Darmstadt, Germany
DNAse I	Sigma-Aldrich Chemie GmbH, Steinheim, Germany
Ethylendiamintetraessigsäure (EDTA)	Sigma-Aldrich Chemie GmbH, Steinheim, Germany

Ethanol 70 %	Carl Roth GmbH & Co. KG, Karlsruhe, Germany
Fetal bovine serum (FBS)	PAA Laboratories GmbH, Pasching, Austria
Formaldehyde	Merck KGaA, Darmstadt, Germany
D-(+)-Glucose	Sigma-Aldrich Chemie GmbH, Taufkirchen, Germany
GM-CSF, recombinant murine	Peprotech Corporation, Rocky Hill, USA
Glycerine 90% GC	Merck KGaA, Darmstadt, Germany
HCl	
2-(4-(2-Hydroxyethyl)-1-piperazinyl)-ethansulfonsäure (HEPES)	C. Roth GmbH & Co. KG, Karlsruhe, Germany
House Dust Mite Extract	Greerlabs Laboratories Inc., Lenoir, USA
Immersion Oil Type F	Olympus Corporation, Tokio, Japan
Immersion Oil 518 F	Carl Zeiss MicroImaging Göttingen GmbH, Göttingen, Germany
Isofluran	Baxter, Unterschleißheim, Germany
KCl p.a.	Merck KGaA, Darmstadt, Germany
L-Glutamin	PAA Laboratories GmbH, Pasching, Austria
Magnesium Chloride ($MgCl_2$)	Merck KGaA, Darmstadt, Germany
Mowiol 4-88	Höchst GmbH, Frankfurt, Germany
Natriumchloride (NaCl) ≥99.5% p.a.	C. Roth GmbH & Co. KG, Karlsruhe, Germany
Normal donkey serum	Linaris, Biologische Produkte GmbH, Wertheim-Bettingen, Germany
Penicillin/Streptomycin	PAA Laboratories GmbH, Pasching, Austria
RPMI 1640	PAA Laboratories GmbH, Pasching, Austria
Sodium hydroxide (NaOH) >98% (Fluka)	Sigma Aldrich Chemie GmbH, Taufkirchen, Germany
Sodium Penthotal	Abott Laboratories, Lake Bluff, USA
D(+)-Sucrose	Merck KGaA, Darmstadt, Germany
Tris-HCl	C. Roth GmbH & Co. KG, Karlsruhe, Germany
Trizol Reagent	Life technologies Corporation, Carlsbad, USA
Trypan Blue	Life technologies Corporation, Carlsbad, USA
UHU Superglue	UHU GmbH & Co. KG, Bühl/Baden, Germany

4.1.3 Buffers and Fluids

Table 3: Buffers and fluids used in this study

Buffer/ Fluid	Substance
Digestion medium	RPMI
	1% Penicillin/Streptavidin
	1% L-Glutamin
	0.5 mg/ml DNase I
	0.25 mg/ml Liberase
HEPES-buffered Ringer solution	1000 ml Aqua bidest.
	0.418 g KCl

	7.97 g NaCl 1 ml $MgCl_2$ x 6 H_2O 2.2 ml $CaCl_2$ x 6 H_2O 1.89 g Glucose 2.38 g HEPES pH 7.4
Lysis Buffer	Aqua bidest. 155 mM NH_4Cl 10 mM $NaHCO_3$ 0.1 mM EDTA
MACS Buffer, pH 7.2	PBS 0.5% BSA 2 mM EDTA
Mowiol, buffered	12 g Mowiol 4-88 30 ml Aqua bidest. 60 ml 0.2 m Tris-Buffer 30 g Glycerine pH 8.5
Paraformaldehyde 1%, buffered	1000 ml Aqua bidest. 1000 ml 2x PBS 20 g Paraformaldehyde 1 N NaOH pH 7.4
PBS (20x)	2000 ml Aqua bidest. 90 g NaCl 2.704 g Na_2HPO_4 x H_2O 28.794 g Na_2HPO_4 12 x H_2O pH 7.4
TBS (10x)	1000 ml Aqua bidest. 9 g Tris 68.5 g Tris-HCl 88 g NaCl pH 7.4
Wash Medium	RPMI 1% Penicillin/Streptavidin 1% L-Glutamin 0.5 mg/ml DNase I

4.1.4 Antibodies

4.1.4.1 Antibodies for Immunohistochemistry

Table 4: Primary antibodies used for immunohistochemistry

Antibody	Clone	Species	Label	Manufacturer	Concentration
Anti-mouse CD11b	M1/70	Rat	Brilliant Violet 421	Biolegend Inc., San Diego, USA	0.5 µg/ml
Anti-mouse CD11b	M1/70	Rat	PE	Biolegend Inc., San Diego, USA	0.25 µg/ml
Anti-mouse CD11b	M1/70	Rat	Alexa Fluor 647	Biolegend Inc., San Diego, USA	0.313 µg/ml
Anti-mouse CD11c	N418	Armenian Hamster	Alexa Fluor 488	eBioscience Inc, San Diego, USA	1.25 µg/ml
Anti-mouse CD11c	N418	Armenian Hamster	Alexa Fluor 647	Biolegend Inc., San Diego, USA	1.25 µg/ml
Anti-mouse CD11c	N418	Armenian Hamster	Brilliant Violet 421	Biolegend Inc., San Diego, USA	1 µg/ml
Anti-mouse CD11c	N418	Armenian Hamster	PE	Biolegend Inc., San Diego, USA	0.5 µg/ml
Anti-mouse CD64	X54-5/7.1	Mouse	Alexa Fluor 647	Biolegend Inc., San Diego, USA	1 µg/ml
Anti-mouse CD64	X54-5/7.1	Mouse	PE	Biolegend Inc., San Diego, USA	0.25 µg/ml
Anti-mouse CD88/ C5aR1	20/70	Rat	APC	Biolegend Inc., San Diego, USA	0.25 µg/ml
Anti-mouse CD90.2	30-H12	Rat	Alexa Fluor 488	Biolegend Inc., San Diego, USA	0.5 µg/ml
Anti-mouse CD90.2	30-H12	Rat	Alexa Fluor 647	Biolegend Inc., San Diego, USA	0.313 µg/ml
Anti-mouse CD197/ CCR7	4B12	Rat	Alexa Fluor 488	Biolegend Inc., San Diego, USA	2.5 µg/ml
Anti-mouse CD197/ CCR7	4B12	Rat	Alexa Fluor 647	Biolegend Inc., San Diego, USA	2.5 µg/ml
Anti-mouse CD207/ Langerin	polyclonal (E-17)	Goat	pure	Santa Cruz, Dallas, USA	0.03 µg/ml
Anti-mouse CD317/ PDCA-1	927	Rat	PE	Biolegend Inc., San Diego, USA	0.125 µg/ml

Anti-mouse CCL21	polyclonal	Goat	pure	R&D Systems, Wiesbaden, Germany	0.125 µg/ml
Anti-mouse Connexin43	polyclonal	Rabbit	pure	Cell Signaling Technologies, Cambridge, UK	Dilution 1:400
Anti-mouse F4/80	CI:A3-1	Rat	Alexa Fluor 647	AbD Serotec, Hercules, USA	0.25 µg/ml
Anti-mouse MHC II	M5/114.15.2	Rat	Alexa Fluor 647	Biolegend Inc., San Diego, USA	0.313 µg/ml
Anti-mouse MHC II	M5/114.15.2	Rat	PE	Biolegend Inc., San Diego, USA	0.125 µg/ml
Anti-mouse Siglec-F	E50-2440	Rat	Alexa Fluor 647	BD Biosciences Pharmingen, Heidelberg, Germany	0.5 µg/ml
Anti-mouse α-SMA	1A4	Mouse	FITC	Sigma-Aldrich Chemie GmbH, Steinheim, Germany	Dilution 1:800
Anti-mouse α-SMA	1A4	Mouse	Cy3	Sigma-Aldrich Chemie GmbH, Steinheim, Germany	0.433 µg/ml

Table 5: Secondary antibodies used for immunohistochemistry

Host	Reactivity	Label	Company	Concentration
Donkey	Goat IgG	Alexa Fluor 488	Invitrogen, GmbH, Karlsruhe, Germany	10 µg/ml
Donkey	Goat IgG	Alexa Fluor 647	Invitrogen, GmbH, Karlsruhe, Germany	10 µg/ml
Donkey	Goat IgG	Cy3	Invitrogen, GmbH, Karlsruhe, Germany	5 µg/ml
Donkey	Rat IgG	Cy3	Invitrogen, GmbH, Karlsruhe, Germany	5 µg/ml

4.1.4.2 Antibodies used for Flow Cytometry

Table 6: Antibodies used for flow cytometry and fluorescence-activated cell sorting (FACS)

Antibody	Clone	Species	Label	Manufacturer	Concentration
Anti-mouse CD3e	145-2C11	Armenian Hamster	eF450	eBioscience Inc, San Diego, USA	0.67 µg/ml
Anti-mouse CD11b	M1/70	Rat	Brilliant Violet 510	Biolegend Inc., San Diego, USA	0.25 µg/ml
Anti-mouse CD11b	M1/70	Rat	PE-Cy7	Biolegend Inc., San Diego, USA	0.25 µg/ml
Anti-mouse CD11c	N418	Armenian Hamster	APC	eBioscience Inc, San Diego, USA	0.25 µg/ml
Anti-mouse CD11c	N418	Armenian Hamster	PE	eBioscience Inc, San Diego, USA	0.25 µg/ml
Anti-mouse CD19	eBio1D3	Rat	eF450	eBioscience Inc, San Diego, USA	0.67 µg/ml
Anti-mouse CD49b	DX5	Rat	eF450	eBioscience Inc, San Diego, USA	0.67 µg/ml
Anti-mouse CD64	X54-5/7.1	Mouse	PE	Biolegend Inc., San Diego, USA	0.25 µg/ml
Anti-mouse CD88/ C5aR1	20/70	Rat	APC	Biolegend Inc., San Diego, USA	0.125 µg/ml
Anti-mouse CD103	2E7	Armenian Hamster	PerCp-Cy5	Biolegend Inc., San Diego, USA	0.25 µg/ml
Anti-mouse Ly6G	1A8	Rat	V450	BD Biosciences Pharmingen Heidelberg, Germany	0.67 µg/ml
Anti-mouse MHC II	M5/114.15.2	Rat	APC-eF780	eBioscience Inc, San Diego, USA	0.13 µg/ml
Anti-mouse Siglec-F	E50-2440	Rat	Brilliant Violet 421	BD Biosciences Pharmingen Heidelberg, Germany	0.67 µg/ml
Functional Grade Purified anti-mouse CD16/32	93	Rat	-	eBioscience Inc, San Diego, USA	10 µl/ $1*10^6$ cells
Compensation Beads anti-rat & anti-hamster				BD Biosciences Pharmingen, Heidelberg, Germany	1 drop/50 µl

Compensation Beads negative control	BD Biosciences Pharmingen, Heidelberg, Germany	1 drop/50 µl

4.1.5 Laboratory Consumables

Table 7: Laboratory consumables used in this study

Laboratory Consumables		Company
Braunüle Vasofix	20 G	B. Braun Melsungen AG, Melsungen, Germany
Cannules Sterican	27 G	B. Braun Melsungen AG, Melsungen, Germany
Cell Strainer	70 µm	Fisher Scientific, Massachusetts, USA
Coverglasses	20 x 20 mm 24 x 32 mm 24 x 40 mm	Menzel Glasbearbeitungswerk GmbH & Co. KG, Braunschweig, Germany
Culture Plates	6-well 24-well	Orange Scientific, Braine-l'Alleud, Belgium
Diff-Quik® System		Siemens Healthcare Diagnostics GmbH, Eschborn, Germany
Disposable Syringes	1 ml 2 ml 5 ml	B. Braun Melsungen AG, Melsungen, Germany
FACS Tubes		BD Biosciences Pharmingen Heidelberg, Germany
Falcon Tubes	15 ml 50 ml	BD Biosciences Pharmingen Heidelberg, Germany
Peha-soft-powderfree GlovesGr.S		Paul Hartmann AG, Hartheim, Germany
Pipette Tips	0.1-10 µl 20-200 µl 100-1000 µl	Eppendorf AG, Hamburg, Germany
Pipette Filter Tips	0,1-10 µl 20-200 µl 100-1000 µl	Eppendorf AG, Hamburg, Germany
Parafilm M		American National Can, Greenwich, USA
Razor Blades		Wilkinson Sword, High Wycombe, UK
Scalpel Blades		B. Braun Melsungen AG, Melsungen, Germany
Slides	Superfrost Plus	Thermo Scientific, Massachusetts, USA

Thread	Gütermann A	Gütermann GmbH, Gutach-Breisgau, Germany
Tubes	1500 µl 2000 µl	Eppendorf AG, Hamburg, Germany

4.1.6 Hardware

Table 8: Surgical material used for lung preparation

Surgical Material		Company
Microscissors		Fine Science Tools, Heidelberg, Germany
Dissecting Scissors	small	Fine Science Tools, Heidelberg, Germany
	big	Fine Science Tools, Heidelberg, Germany
Tweezers	bent	Fine Science Tools, Heidelberg, Germany
	fine	Fine Science Tools, Heidelberg, Germany
	round	Fine Science Tools, Heidelberg, Germany

Table 9: Hardware used in this study

Hardware		Company
BD FACSAria III		BD Biosciences Pharmingen, Heidelberg, Germany
Centrifuge 5810R		Eppendorf AG, Hamburg, Germany
Centrifuge 5424R		Eppendorf AG, Hamburg, Germany
Chemical Balance		Sartorius AG, Göttingen, Germany
Cold Light source	CL100	Classen & Co., Hamburg, Germany
Heating Plate	MR Hei-Tec	Heidolph Instruments GmbH & Co. KG, Schwabach, Germany
Hera Safe		Heraeus, Hanau, Germany
Incubator	Heraeus B5050E	Heraeus, Hanau, Germany
MACS Columns	LS	Miltenyi Biotec Inc., San Diego, USA
MACS Separator	QuadroMACS	Miltenyi Biotec Inc., San Diego, USA
Microcentrifuge		Carl Roth GmbH, Karlsruhe, Germany
MoFlo XDP		Beckman Coulter, California, USA
Neubauer Chamber		Brand GmbH & Co. KG, Mannheim, Germany
pH meter		Knick Elektronische Messgeräte GmbH & Co. KG, Berlin, Germany
Pipetboy		Integra Biosciences AG, Zizers, Switzerland
Pipettes	0.5 - 2 µl	Eppendorf AG, Hamburg, Germany
	1 - 10 µl	
	2 - 200 µl	
	100 - 1000 µl	
	500 µl	
	1000 µl	

Shaker	Titramax 100	Heidolph Instruments GmbH & Co. KG, Schwabach, Germany
Vacusafe 158210		Integra Biosciences GmbH, Freiwald, Germany
Vibratome	1000/2	TBI Vibratome, GaLa Gabler Labor Instrumente Handels GmBH, Germany
Vibratome	VT1200S	Leica Camera AG, Wetzlar, Germany
Vortex Genie 2		Heidolph Instruments GmbH & Co. KG, Schwabach, Germany

Table 10: Microscopes used in this study

Microscopes and objectives		**Company**
Bionocular	Wild M3C	Wild, Heerbrugg, Switzerland
Microscope	Axioskop 2 Plus	Carl Zeiss Göttingen GmbH, Göttingen, Germany
Objectives	Plan Apochromat 20x/0.75	Carl Zeiss Göttingen GmbH, Göttingen, Germany
	Plan Apochromat 40x/0.95	Carl Zeiss Göttingen GmbH, Göttingen, Germany
Camera	DP72	Olympus Corporation, Tokio, Japan
Lamp	MBQ 52 AC	Carl Zeiss Göttingen GmbH, Göttingen, Germany
Microscope	LSM 510 Meta	Carl Zeiss MicroImaging Göttingen GmbH, Göttingen, Germany
Objectives	Plan Apochromat 20x/0.75	Carl Zeiss MicroImaging Göttingen GmbH, Göttingen, Germany
	C-Apochromat 40x/1.2W oil	Carl Zeiss MicroImaging Göttingen GmbH, Göttingen, Germany
Lamp	MBQ 52 AC	Carl Zeiss Göttingen GmbH, Göttingen, Germany
Microscope	LSM 710	Carl Zeiss MicroImaging Göttingen GmbH, Göttingen, Germany
Objective	EC-Plan-Neofluar 40x/1.30 oil	Carl Zeiss MicroImaging Göttingen GmbH, Göttingen, Germany
Lamp	HBO 100	Carl Zeiss MicroImaging Göttingen GmbH, Göttingen, Germany
Microscope	FV1000	Olympus Corporation, Tokio, Japan
Objectives	UPlanSApo Super Apochromat 20x/0.85 oil	Olympus Corporation, Tokio, Japan
	UPlanSApo Super Apochromat 60x/1.35 oil	Olympus Corporation, Tokio, Japan
Lamp	Olympus U-RFL-T	Olympus Corporation, Tokio, Japan

4.1.7 Software

Table 11: Software used in this study

Software	Company
Adobe Acrobat Reader DC 2015	Adobe Systems Inc., San Jose, CA, USA
BD FACSDiva 7.0	BD Biosciences Pharmingen, Heidelberg, Germany
Endnote X7	Endnote™, Pennsylvania, USA
GraphPad Prism 5	GraphPad Software Inc., La Jolla, CA USA
FlowJo 10.2	FlowJo, LLC, Oregon, USA
Imaris x64 7.6.4	Bitplane AG, Zürich, Switzerland
LSM 510 Meta 3.2	Carl Zeiss MicroImaging Göttingen GmbH, Göttingen, Germany
Microsoft Excel, Version 2013	Microsoft Cooperation, Mountain View, CA, USA
Microsoft Power Point, Version 2013	Microsoft Cooperation, Mountain View, CA, USA
Microsoft Word, Version 2013	Microsoft Cooperation, Mountain View, CA, USA
Olympus FluoView FV10-ASW Ver.04.02	Olympus Corporation, Tokio, Japan
Summit 5.4	Beckman Coulter, CA, USA
Zen 2011	Carl Zeiss MicroImaging Göttingen GmbH, Göttingen, Germany

4.2 Methods

4.2.1 Animal Housing

Mice were kept under specific pathogen free (SPF) conditions at the animal facility of the University of Lübeck according with the guidelines of the German law for animal protection. Mice used for cell sorting were delivered from JAX® Mice and housed for a single night in the animal facility of the Cincinnati Children's Hospital Medical Center. Animal experiments and animal sacrificing for lung removal were approved by the Ministerium für Energiewende, Landwirtschaft, Umwelt und ländliche Räume des Landes Schleswig-Holstein (V312-72241.122-1, V242-389/2016 (75-6/16)).

4.2.2 Animals and Treatment

In this study, naïve and HDM-treated wt BALB/c and C57BL/6 were used. HDM was administered intra-tracheally (i.t.) with a dose of 100 µg HDM in 50 µl PBS by members of the Institute for Systemic Inflammation Research from the group of Professor Köhl. Naïve and HDM-treated (24 h) mice were sacrificed with an overdose of isoflurane. Mice used for DC analyses based on C5aR1/CD88 by flow cytometry were euthanized with 300 µl Sodium Pentothal intra-peritoneally (i.p.).

4.2.3 Lung Explantation for Precision Cut Lung Slices

For the preparation of precision cut lung slices (PCLS) 0.3 g agarose was dissolved in 10 ml HEPES-buffererd Ringer solution for each mouse using a magnetic stirrer at 80 °C. Then, the agarose was filled into 2 ml syringes and kept inside of an incubator at 37 °C until usage. Further, a 5 ml syringe with 4.7 ml HEPES-buffered Ringer solution and 0.3 ml heparin sodium with a 27 G canula, a 2 ml syringe filled with 1% PFA and two 2 ml syringes filled with PBS were prepared before preparation of the lung. Following the death of the animal, the thorax was opened at the sternum to expose lung, heart, and trachea by removing ribs, muscles, thymus, and salivary glands. The left auricle was cut and the lung circulation was rinsed with the PBS heparin solution through the right ventricle. Next, the heart was removed. A small cut was set at the trachea, a catheter (BraunüleVasofix 20 G) was inserted into the trachea and the lung was filled with 1.5 ml 1% PFA. To avoid leakage a thread was placed around the trachea and the catheter was held in place by a knot and the mouse was not moved. After 20 min of fixation the

formaldehyde solution was removed from the lung and the lung was flushed two times with 1.5 ml PBS for 5 min. The PBS was removed and the lung was filled with 1.5 ml agarose and to avoid leakage of agarose the trachea was closed again using a string. Subsequently, the lung was removed carefully from the thorax and put into HEPES-buffered Ringer solution at 4 °C to harden the agarose. Next, the complete lung was weighed. In addition, the left lung and the right lung were weighed separately. Single lobes were glued on precooled metal plates with superglue and a metal ring was placed around the lung. The ring was filled with agarose to enclose the lobe and after cooling the ring was removed. For the preparation of PCLS the agarose block was set into the cutting chamber of a vibratome which contained HEPES-buffered Ringer solution at 4°C and cut into 300 µm thick slices. The slices were collected in HEPES-buffered Ringer solution, transferred to 20% sucrose and stored over night at room temperature (RT). On the next day the slices were frozen at -20 °C until further usage.

Alternatively, the lung was filled with agarose before fixation. For this protocol the slices had to be collected at 4 °C to avoid any cell activation. Slices were then fixed with 1% PFA for 10 min at 4 °C and washed three times for 10 min with PBS at room temperature (RT). Afterwards the slices were transferred to 20% sucrose and stored over night at RT. On the next day the slices were frozen at -20 °C until further usage.

4.2.4 Direct and Indirect Immunohistochemistry

Immunohistochemical stainings were performed in 24-well plates in the dark to protect the fluorophores from light. PCLS were defrosted at RT on a shaker and washed three times in 1 ml TBS for 10 min. If indirect antibodies were used, slices were incubated with 5% normal serum (same species as secondary antibody) in 500 µl TBS for 30 min afterwards to block unspecific binding sites of the secondary antibody. Blocking was not necessary for stainings with direct labeled antibodies. Antibodies used for IHC are listed in tab. 4 and 5. Coincubation with different unlabeled antibodies was possible when host species were different. Primary antibodies were diluted in 500 µl TBS and incubated on a shaker overnight at RT in the dark. The next day the slices were rinsed three times in TBS for 10 min. If no secondary antibody was needed, slices were transferred to an object slide, dried carefully, and coverslipped with Mowiol. Secondary antibodies were diluted in 500 µl TBS and slices were incubated for 60 min in the dark. Afterwards slices were rinsed three times with TBS for 10 min and coverslipped as described above.

4.2.5 Evaluation with Confocal Microscopy

Stained slices were evaluated with confocal microscopy and z-stacks were recorded to allow a three-dimensional presentation of lung structures including possible cell interactions. Analysis was done at the FV1000 (Olympus), LSM 510Meta (Zeiss), and LSM 710 (Zeiss).

4.2.6 Quantification

4.2.6.1 Quantification of DCs and Macrophages

To allow the quantification of DCs and macrophages in the lung it was necessary to weigh the total lung as well as the single lobes before cutting. PCLS were prepared and stained as described above but the slices were weighed before mounting. Areas of image acquisition were distributed randomly by blind relocation of the slice. Images were acquired using a confocal microscope with specified parameters (see below) using a 20x immersion objective. In addition, the thickness of the slice was measured at the microscope. This step was necessary because the 300 µm thick PCLS shrank during the mounting procedure. Due to this shrinkage, the measured instead of the original thickness was used for extrapolation. Further, the area of the slice was determined by hand. During image analysis, cells were counted manually and assigned by their surface marker expression using the Imaris software. To calculate the number of cells per lung, several steps were performed. First, the cell number per slice was determined by the ratio of counted cells to the area. Second, the cell number of the lobe was calculated by the weight ratio from slice to lobe. Third, the total cell number was determined by the weight ratio from the left lung to the total lung.

The calculation of the total cell number (x) was done using the following formula:

$$x = a \times \left(\frac{e}{c \times b}\right) \times \left(\frac{f}{d}\right) \times \left(\frac{h}{g}\right) \times (i)$$

a= counted cell numbers
b= number of images
c= area (image) = 636 x 636 µm
d= thickness of the stack = 40 µm
e= area (slice)
f= measured thickness of the slice
g=weight of the slice
h= weight of the lobe
i= weight ratio left lung to total lung
= 2.79 (see fig. 1 C, appendix tab. 1+ 2)
x= cell number

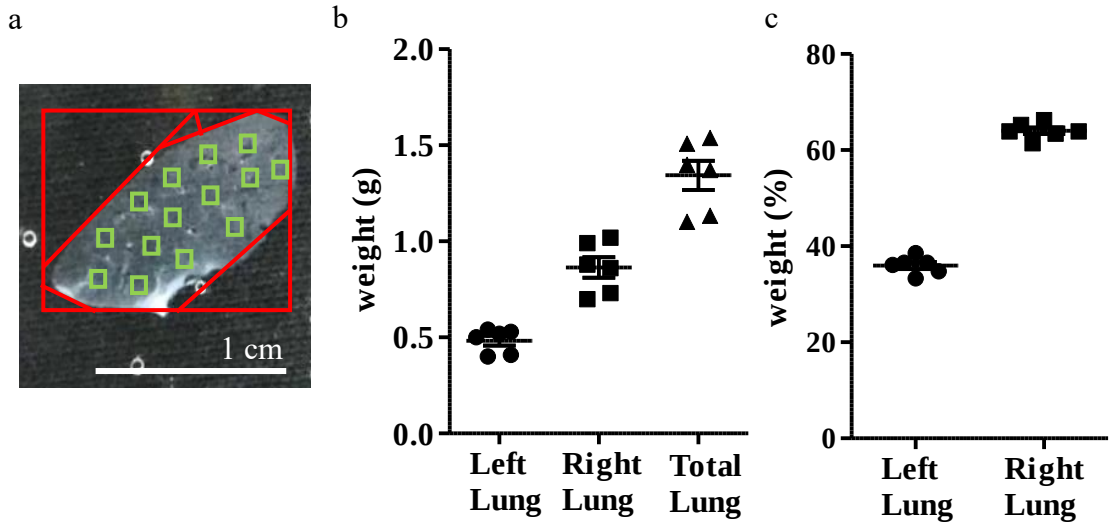

Figure 2: Cell counting and extrapolation. (a) Stained PCLS were coverslipped and random areas of defined size (green squares) were imaged. Slice area was measured manually (red lines). Agarose-filled lungs were measured and total (b) and relative (c) weights were measured (n= 6).

4.2.6.2 Quantification of CD64-Expressing Cells in the CD11b$^+$ DC Population

To determine the proportion of CD11b$^+$ DCs with monocytic origin in the lung CD64$^+$ CD11b$^+$ DCs were counted in naïve and HDM-treated mice. To allow this, images were taken randomly at regions with high DC density which includes airways and blood vessels. CD64$^+$CD11b$^+$ DCs and CD64$^-$CD11b$^+$ DCs were counted manually using Imaris software and the ratio was determined.

4.2.6.3 Quantification of CCR7$^+$ DCs in the Lung

Quantification of activated CCR7$^+$ DCs was performed as described above for CD64-expressing CD11b$^+$ DCs.

4.2.6.4 Quantification of Cell Accumulations in LVs

In addition to the ratio of CCR7$^+$ DCs in the lung the ratio of cell accumulations within the LVs were determined. For this purpose, LVs that run with airways were imaged randomly. A lymph vessel was counted as positive, if a CCR7$^+$ cell accumulation ≥ 5 cells was present in the vessel. Multiple accumulations were not counted because evaluation was done based on a positive-negative-principle. The ratio of LVs which were positive for these accumulations was determined in naïve and HDM-treated mice.

4.2.7 Flow Cytometry and Fluorescence-Activated Cell Sorting (FACS)

4.2.7.1 Lung extraction for Flow Cytometry

To explant the lung for flow cytometry the thorax was opened and ribs were removed to expose lung and trachea. The trachea was opened by a small cut and the lung was flushed through a catheter with 1 ml PBS to perform a BAL in order to remove cells from the lumen. The lobes were cut out and transferred into a 6-well plate containing a cell strainer and 5 ml sterile pure medium at 4 °C. The fluid from the BAL was discarded.

4.2.7.2 Cell Isolation

Cells had to be isolated from the lung tissue. To remove cells from the tissue the lung needs to be digested. For digestion, the lobes were cut into small pieces using a scissor and 0.5 mg/ml DNAse I and 0.25 mg/ml Liberase were added to the medium under sterile conditions. Next, the lung was incubated for 45 min at 37 °C and shaken gently. After incubation the strainer was put in a 50 ml Falcon tube and the cells were pushed through the strainer with the plunger of a 2 ml syringe. The medium from the well was pipetted through the strainer to transfer cells that were already eluted during the digestion. Then, the remaining tissue was pushed through the strainer again and the strainer was rinsed with 5 ml wash medium. This step was repeated one more time. The suspension was centrifuged at 350 g for 10 min at RT. Afterwards, the supernatant was aspirated, the pellet was resuspended in 3 ml RBC lysis buffer, and incubated for 3 min. The solution was diluted 10 times with PBS to inactivate the RBC lysis buffer.

4.2.7.3 Counting of Cells from Cell Suspension

To determine the cell number in the cell suspension an aliquot of 10 µl was stained with trypan blue (ratio 1:2) and cells were counted with the help of a Neubauer counting chamber under a microscope. Calculation was done according to the following formula:

$$cell\ number\ x\ 10^4 = \frac{counted\ cell\ number\ x\ dilution\ with\ trypan\ blue\ x\ volume\ (ml)}{counted\ quadrants}$$

After counting, the suspension was centrifuged at 350 g for 5 min at RT and the pellet was resuspended in MACS buffer ($1x10^6$ cells/100 µl).

4.2.7.4 Cell Staining for Flow Cytometry

To block unspecific binding sites cells were incubated with anti-CD16/32 (1 µl per $1x10^6$ cells/100 µl) for at least 15 min at 4°C. The cell suspension was centrifuged for 30 s (maximal speed), the supernatant was removed and the pellet was washed with 500 µl MACS buffer to remove unbound antibodies. MACS buffer was removed by centrifugation (30 s, maximal speed) and removing of supernatant. Next, the cells were stained with specific antibodies for 20 min at 4 °C. Antibodies were diluted in MACS buffer according to the concentrations listed in tab. 6 and 100 µl mastermix containing the suitable antibodies were applied to $1x10^6$ cells. After this step, cells needed to be washed again (s.a.). The pellet was resuspended in 300 µl MACS buffer and transferred into tubes for flow cytometry. Samples were analyzed using a flow cytometer. During analysis a maximum of 1,000 cells/s was measured and 200,000 events were counted.

.

4.2.7.5 Cell Enrichment Using CD11c MicroBeads

To perform a positive selection of $CD11c^+$ cells, cells were isolated and a cell suspension was prepared as described above. After blocking of unspecific binding sites the cell suspension was centrifuged at 300 g for 10 min and the supernatant was removed completely. The pellet was resuspended in 400 µl pre-cooled MACS buffer per 10^8 total cells and 100 µl of CD11c MicroBeads UltraPure per 10^8 cells were added. Cell suspension was mixed and incubated for 10 min in the dark at 4 °C. Afterwards, cells were washed by adding 10 ml of cooled MACS buffer and centrifuged at 300 g for 10 min. The supernatant was aspirated completely and the pellet was resuspended in 500 µl cooled MACS buffer per 10^8 cells. To perform the magnetic cell separation the LS MACS Column was placed into the QuadroMACS Separator and adequate collecting tubes were placed under the column. Each column was then rinsed with 3 ml cooled MACS buffer. After the fluid reservoir of the column was empty, the cell suspension was applied to the column. The column was washed three times with 3 ml cooled MACS buffer after the fluid reservoir was empty. The column was removed from the MACS separator and placed in a 15 ml tube. Next, 5 ml of cooled MACS buffer was applied to the column and $CD11c^+$ cells were flushed out from the column by pushing the plunger into the column. After enrichment cells were stained as described above.

4.2.7.6 Fluorescence Activated Cell Sorting

Sorting of cell populations allows further characterization and experimental setups. Cells were stained as described above. Populations were defined by gating and all events were counted and the cells sorted into different FACS tubes filled with wash medium containing 20% FBS and 10 µg/ml GM-CSF. For small populations it was necessary to pool animals to get enough cells.

4.2.8 Preparation of Cytospins

To ensure the purity of the sorted cells, 10,000 cells were removed from the cell suspension after sorting and used for cytospins. Cells were transferred to a 1.5 ml tube and centrifuged for 30 s at maximal speed, the supernatant was removed, and the pellet was washed with 500 µl PBS for 30 s at maximum. The supernatant was aspirated and the pellet was dissolved in 200 µl PBS. The cell suspension was centrifuged to slides using a cytospin centrifuge at 400 rpm for 4 min. Cytospins were dried overnight and were stored at room temperature for up to one week.

4.2.8.1 Analysis of Cell Morphology

To analyze cell morphology cells were stained with the Diff-Quik Stain Kit. Slides were dipped seven times in solution I, seven times in solution II, and six times in solution III. Slides were rinsed with water and dried before mounting. Cell morphology was analyzed using a light microscope.

4.2.9 Statistics

Statistical analyses were done with GraphPad Prism 5.0. Data were presented in dotplots with mean and standard error of the mean (SEM). Samples were too small to allow testing for a Gaussian distribution; therefore, data was analyzed with the Mann-Whitney U-test. P-values ≤ 0.05 were termed as significant.

5 Results

5.1 Identification of Pulmonary Phagocytes

5.1.1 Conventional Dendritic Cells and Macrophages

Usually, lung phagocytes are defined by flow cytometry using a panel with at least six colors. The establishment of a panel with that many colors was not possible for immunohistochemistry due to the limitation of separable dyes. Therefore, a four-color panel was established to identify the main phagocytic populations including CD11b$^+$ cDCs, CD103$^+$ cDCs, AMs, as well as the population of poorly characterized IMs. For the comparability of this study with studies based on flow cytometry, if possible, the same antibodies and clones were used as published before [51]. This panel consists of CD11c, MHCII, CD11b, and Langerin. Since it turned out that the specificity of the anti-CD103 antibody was dependent on the fixation, divergent from established panels for flow cytometry, Langerin was used instead of CD103 as specific marker for CD103$^+$ cDCs (fig. 3). The anti-Langerin antibody was totally independent from the type of fixation and was therefore more suitable for IHC. Both proteins are located at different sites in the cell, CD103 is expressed at the cell surface but not in the cytosol, while Langerin is almost exclusively located intracellularly. Although CD103 was not used for IHC in this study, the population was termed as CD103$^+$ cDCs to avoid any confusions regarding nomenclature.

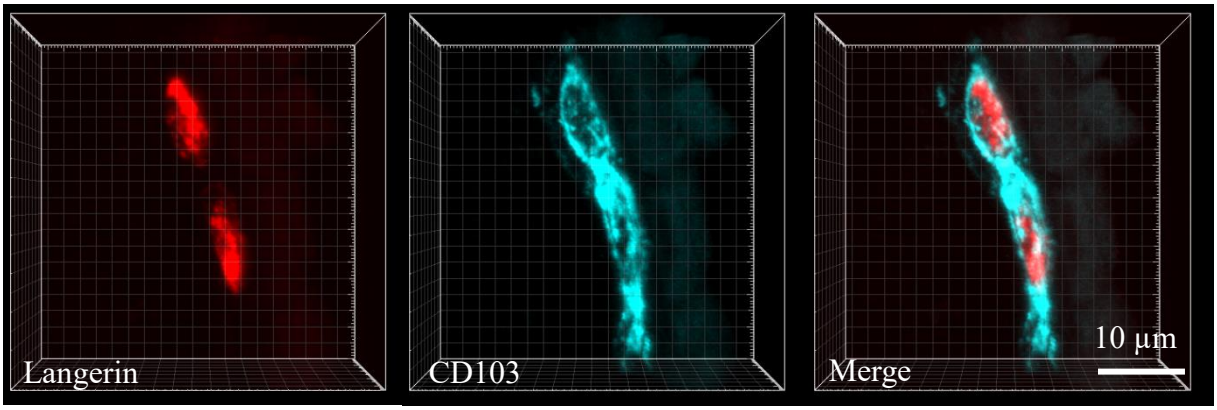

Figure 3: Langerin is a specific marker for CD103$^+$ cDCs. PCLS of a naïve lung stained for Langerin (intracellular, red) and CD103 (cell surface, cyan); n= 4 naïve BALB/c mice.

Both types of DCs express CD11c and MHCII (fig. 4 a and b). In addition, CD11b$^+$ DCs are characterized by the expression of CD11b but lack the expression of Langerin (fig. 4 a) whereas CD103$^+$ cDCs express Langerin but are negative for CD11b (fig. 4 b). AMs express high levels of CD11c but are negative for other markers out of this panel. Further, AMs are autofluorescent. Autofluorescence is best detectable using the ultra violet (UV) or green laser. Usually,

autofluorescence is distinguishable from a real signal because CD11c stains the whole cell surface brightly, while an autofluorescence signal is weaker and does not stain the whole cell (fig. 4 c). As described in the introduction there is no consensus about the definition of lung IMs yet, definition of IMs in this study is based on the findings of Bedoret *et al.* and Hussel and Bell [2, 135]. IMs were therefore characterized by the expression of MHCII and CD11b and a lack of CD11c (fig. 4 d). Stainings for cell identification were performed in naïve BALB/c and C57BL/6 mice; representative data are depicted from BALB/c mice.

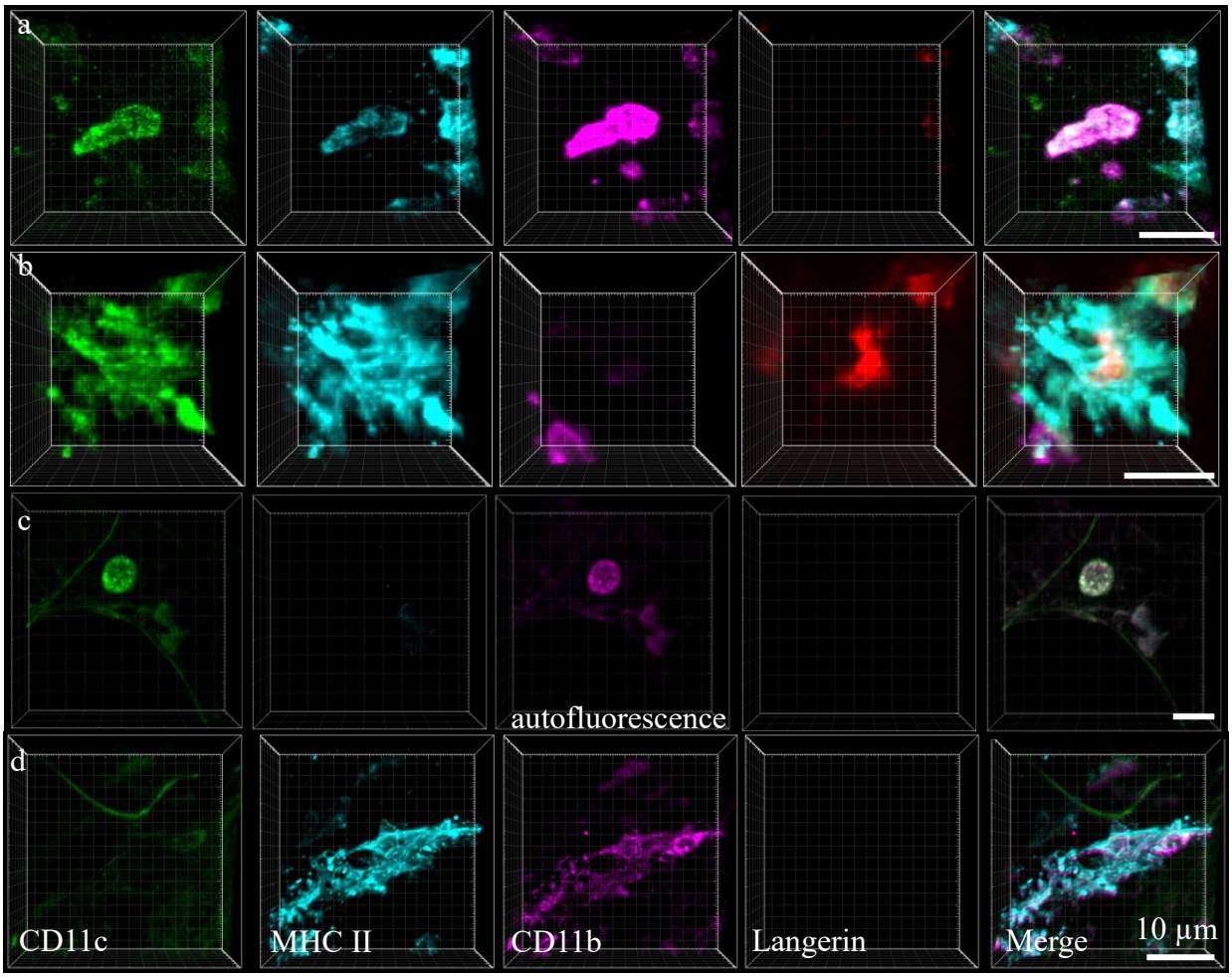

Figure 4: Identification of lung cDCs and macrophages. Cell staining in a PCLS from BALB/c mouse (n= 4) with CD11c (green), MHCII (cyan), CD11b (pink), and Langerin (red). Depicted are $CD11b^+$ DCs (a), $CD103^+$ cDCs (b), AMs (c), and IMs (d).

5.1.2 Cells with Monocytic Origin

Supplementary to the identification of these populations by their classical markers, CD64 was used to identify lung phagocytes with monocytic origin. Because $CD11b^+$ DCs and $CD103^+$ cDCs are characterized by the expression of CD11b or Langerin respectively

(fig. 4 a and b) $CD103^+$ cDCs can also be detected by the lack of CD11b, if staining for Langerin was substituted by CD64-staining. The adapted panel allows the identification of $CD11c^+MHCII^+CD11b^-CD64^-$ $CD103^+$ cDCs (fig. 5 a). The absence of CD64 is in accordance with the monocyte-independent development (Hoffmann, Ender et al. 2016) of this DC population. Using this modified staining panel, it appeared that the population of $CD11b^+$ DCs can be divided into $CD11c^+MHCII^+CD11b^+CD64^-$ $CD11b^+$ cDCs and $CD11c^+MHCII^+CD11b^+CD64^+$ moDCs (fig. 5 b and c). According to their monocytic origin (Guilliams, De Kleer et al. 2013) AMs are $CD11c^+$ and $CD64^+$ (fig. 5 d). Interestingly, $MHCII^+CD11b^+$ IMs also express $CD64^+$ (fig. 5 e). This finding contributed to the better characterization of this population since it provides information about their origin. Lastly, classical monocytes can be defined by the expression of CD11b and CD64 but lack MHCII (fig. 5 f).

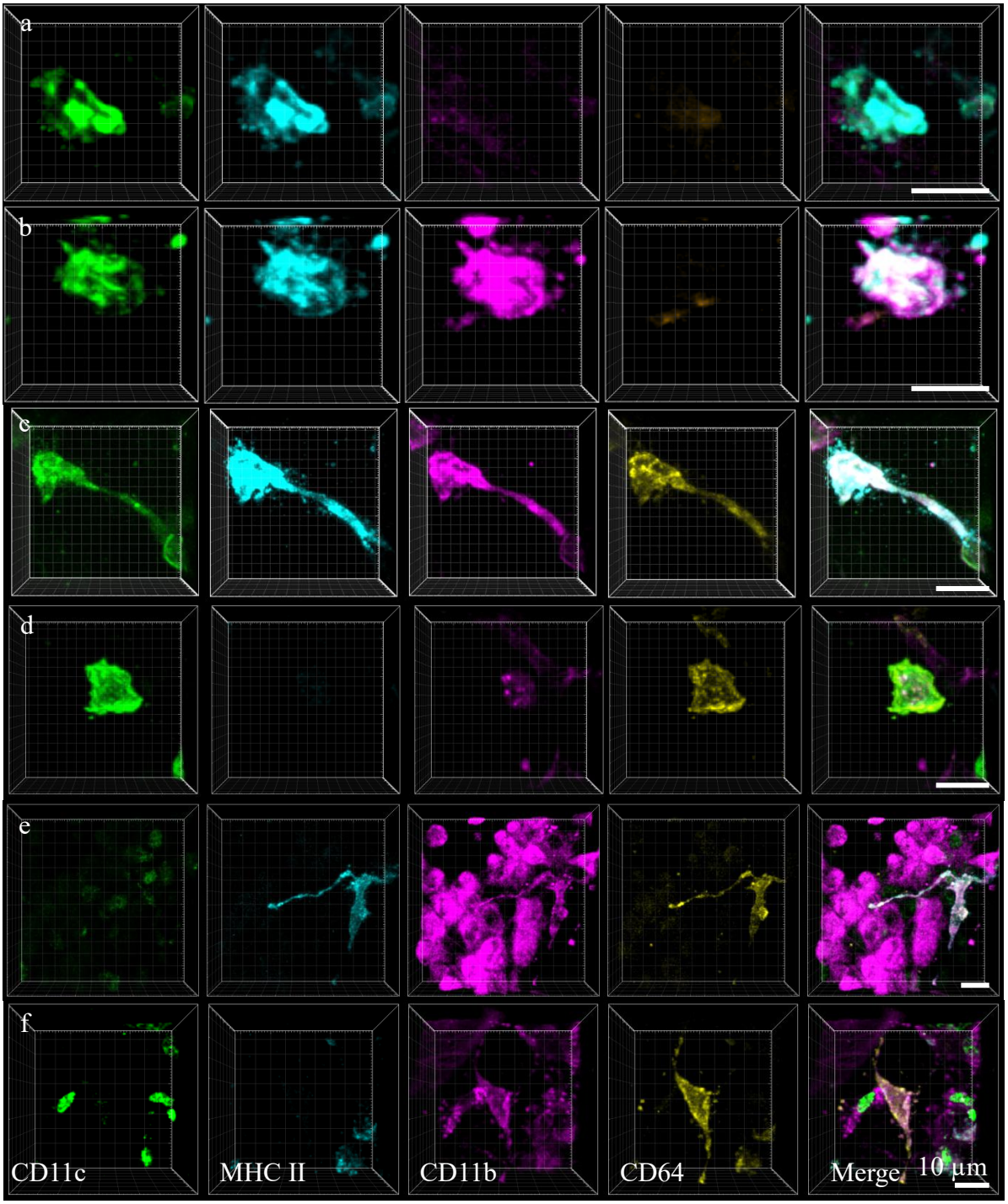

Figure 5: Identification of cells with monocytic origin. PCLS stained for CD11c (green), MHCII (cyan), CD11b (pink), and CD64 (yellow). Analysis was performed in naïve C57BL/6 and BALB/c mice (n= 4 for each strain). Depicted are $CD103^+$ cDCs (a), $CD11b^+$ cDCs (b), $CD11b^+$ moDCs (c), AMs (d), IMs (e), monocytes (f).

5.1.3 Plasmacytoid Dendritic Cells

PDCs are another phagocytic population in the lung. A specific marker for pDCs is PDCA-1. According to literature (reviewed in [66]), pDCs express low amounts of CD11c and CD11b based on flow cytometry, but no labeling for these markers could be detected with IHC in this study (fig. 6).

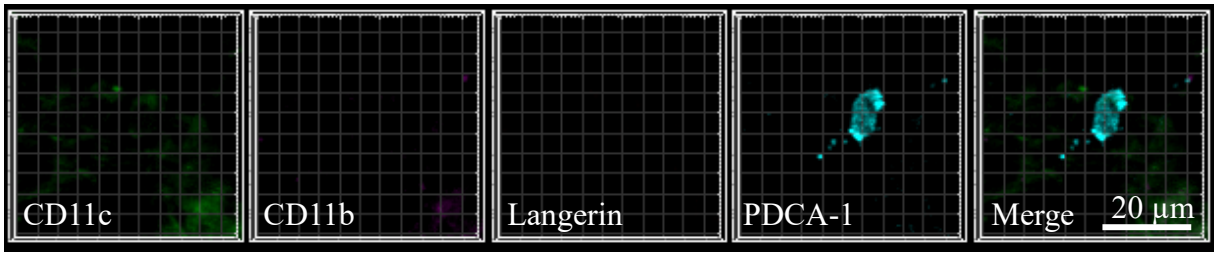

Figure 6: Identification of pDCs. PCLS from naïve C57BL/6 mice (n= 2) stained for CD11c (green), CD11b (pink), Langerin (red), and PDCA-1 (cyan).

5.2 Quantification of Pulmonary Phagocytes in the Naïve Lung

By now there are only a few studies based on flow cytometry dealing with total numbers of lung phagocytes. Often, studies have focused on a single population and comparison between different studies is difficult. Further, there are huge differences in published numbers and proportions. Because no data are available for quantification based on IHC the aim was to quantify pulmonary phagocytes with this technique. The reliable identification of pulmonary phagocytes was the cornerstone for a quantification of these cells by IHC.

Ideally, the quantification of immune cells in the lung should be performed by stereology but since the suitable equipment including a microscope with an automated scanning tool and a software for automated cell counting was not available for this study an alternative quantification method was established. This approach allowed the collection and calculation of reproducible results for absolute numbers and relative cell proportions. Nevertheless, absolute numbers might be overestimated in this study compared to published DC numbers [67, 71]. Problems regarding cell quantification will be discussed later in detail. The single steps are described in part 4.2.6.1. Quantification of DCs and macrophages was done manually and is based on counting an average of 899 cells (min 485, max 1,287) per animal. Quantification of pDCs is based on the counting of only a few cells (min 6, max 9), because pDCs are a rare population. Tables including complete data for any quantification in this study are listed in the appendix.

5.2.1 Conventional Dendritic Cells and Macrophages

Based on the cell identification shown in figure 3, cells were identified and counted in C57BL/6 (n= 4) and BALB/c (n= 4) mice to examine possible differences between the strains. Counted cells were then extrapolated to the whole lung. Under steady-state conditions total numbers for DCs and macrophages were the same with a slight tendency towards lower numbers in C57BL/6 mice (fig. 7) despite no differences in lung size or weight. $CD11b^+$ DCs accounted for 608,534± 200,289 and 531,052± 95,306 cells in BALB/c and C57BL/6 mice respectively. Population sizes for $CD103^+$ cDCs were 602,082± 212,719 and 440,172± 36,433 cells in BALB/c and C57BL/6 mice respectively. During quantification it turns out that cells defined as IMs in this study diverge substantially from their initial description regarding their localization [2], which will be explained in detail in part 3.4.2. To refer on this difference, cells matching the IM phenotype were called IM-like cells (IMLCs) in this study. IMLCs represent a population with a similar population size compared to single DC populations (657,340± 197,679 BALB/c, 492,628± 142453 C57BL/6). AMs represent the largest phagocyte population with a size of 1,676,162± 398,549 cells in BALB/c and 1,509,806± 169,273 cells in C57BL/6 mice. AMs represent the biggest population with an average about $1.5x10^6$ cells. Cell numbers for AMs are in the same range as published data obtained by flow cytometry [67, 70, 71]. Numbers for DCs are higher than reported [71]. There is no published data available for IMs.

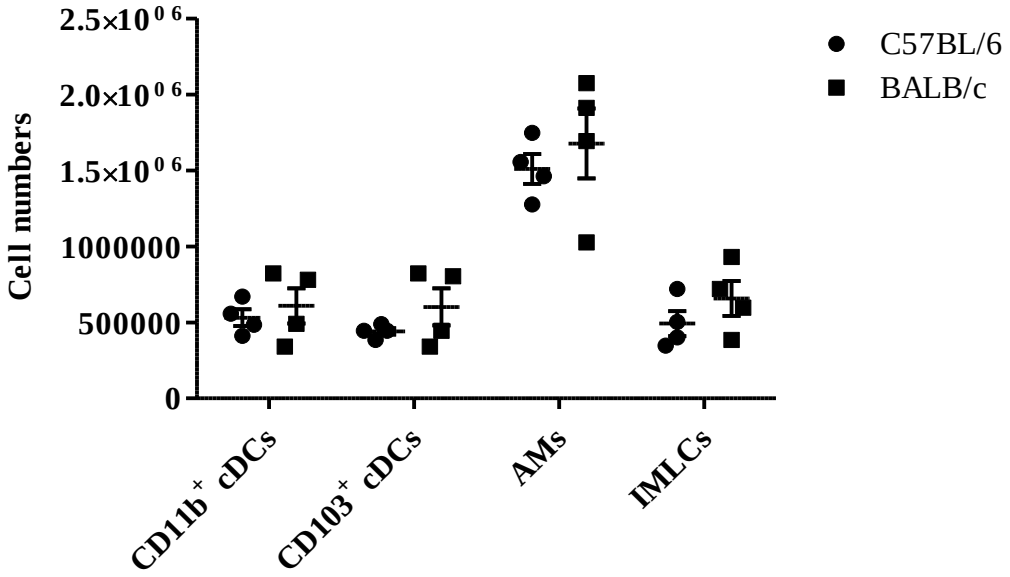

Figure 7: Total cell numbers for DCs and macrophages obtained from naïve BALB/c and C57BL/6 mice. PCLS from naïve BALB/c (n= 4) and C57BL/6 (n= 4) mice were stained for CD11c, MHCII, CD11b, and Langerin. DCs and macrophages were counted and extrapolated to absolute numbers. Depicted are mean and SEM.

In addition, the frequencies of $CD11b^+$ DCs to $CD103^+$ cDCs were determined, because there was a large variation reported in the literature (reviewed in [66]). In this microscopic assay, proportions of $CD103^+$ and $CD11b^+$ DCs were quite similar, although the proportion of $CD11b^+$ DCs (54.22± 3.37%) was significantly higher than the proportion of $CD103^+$ cDCs (45.78± 3.77%) in C57Bl/6 mice (fig. 8 a). This difference was not observed in Balb/c mice. Proportions were 50.5± 1.34% $CD11b^+$ DCs to 49.5± 1.34% $CD103^+$ cDCs (fig. 8 b).

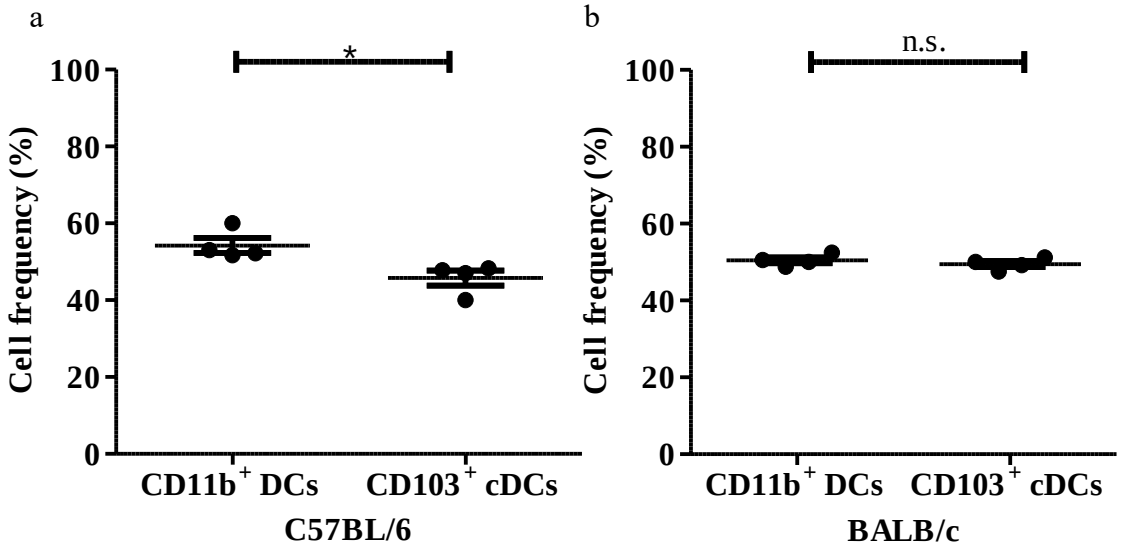

Figure 8: Proportion of CD11b$^+$ DCs and CD103$^+$ cDCs in naïve mice. PCLS from naïve C57BL/6 (a, n= 4) and BALB/c (b, n= 4) mice were stained for CD11c, MHCII, CD11b, and Langerin. CD103$^+$ cDCs and CD11b$^+$ DCs were counted and their proportion was determined. Depicted are mean and SEM; $p \leq 0.05$ (*), statistical test: Mann-Whitney U-test.

5.2.2 CD11b$^+$ Resident Monocyte-Derived Dendritic Cells

The staining panel that was used for quantification did not include CD64. Therefore, another approach was needed to determine the number of CD11b$^+$ moDCs. Analysis was performed in naïve C57BL/6 (n= 4) and BALB/c (n= 4) mice. PCLS were stained for CD11c, MHCII, CD11b and CD64 to allow the distinction between CD11b$^+$ cDCs and CD11b$^+$ moDCs (fig. 9). Images were taken randomly and quantification was based on 218 cells in C57BL/6 and 324 cells in BALB/c. In naïve mice CD11b$^+$ moDCs constituted 51.5± 6.2% in C57BL/6 and 62.15± 4% in BALB/c from the total CD11b$^+$ DC population, indicating that CD11b$^+$ DCs consists of a heterogeneous population at steady-state. Interestingly, the frequency of resident moDCs is significantly higher in BALB/c mice.

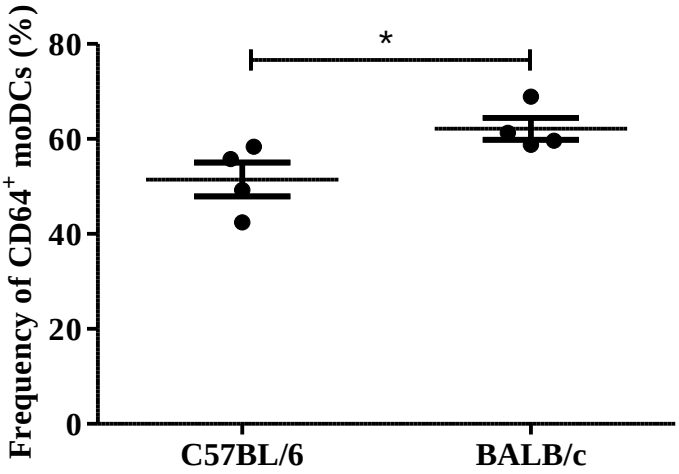

Figure 9: Frequencies of CD64$^+$ moDCs in naïve C57BL/6 and BALB/c mice. PCLS from naïve C57BL/6 and BALB/c mice (n= 4) were stained for CD11c, MHCII, CD11b, and CD64. CD11b$^+$ cDCs and CD11b$^+$ moDCs were counted and the proportion of CD64$^+$ moDCs was determined. Depicted are mean and SEM; p≤ 0.05 (*), statistical test: Mann-Whitney U-test.

5.2.3 Plasmacytoid Dendritic Cells

To complete the quantification of pulmonary phagocytes in the naïve lung, pDCs were quantified in the same way as described above. PDCs represent a small population with a population size of about 36,696± 9,232 cells at steady-state in C57BL/6 mice (n= 3) (fig. 10). Due to their rarity quantification was difficult because maximum one or two cells were present per image.

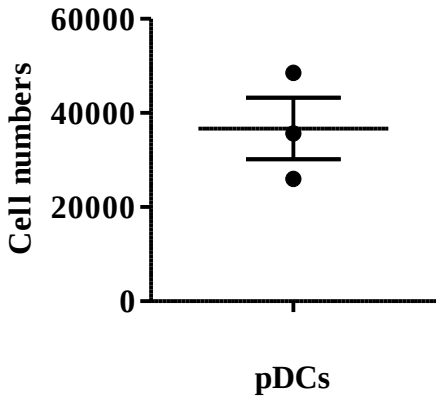

Figure 10: Quantification of pDCs in C57BL/6 mice at steady-state. PCLS from naïve C57BL/6 (n= 3) mice were stained for CD11c, CD11b, Langerin, and PDCA-1. Plasmacytoid DCs were counted and extrapolated to absolute numbers. Depicted are mean and SEM.

5.3 Comparison of IHC and Flow Cytometry for the Identification and Quantification of Pulmonary DCs

As indicated above CD11b$^+$ DCs are not a homogeneous population at steady-state but consists of two different subpopulations (fig. 9). In 2012 the group of Bart Lambrecht has published a new strategy to distinguish between CD11b$^+$ cDCs and moDCs based on the expression of CD64 and FcεR1 [51]. An adapted gating strategy using CD64 as the critical marker was established in a study related to this project [153] enabling the direct comparison of CD64 for IHC and flow cytometry in this study. Reproduction of their DC gating strategy (fig. 11) showed that there are significant differences regarding the percentage of resident moDCs between IHC and flow cytometry. While about 50-60% of CD11b$^+$ DCs are CD64$^+$ by IHC (C57BL/6 51.45± 6.2%; BALB/c 62.15± 4.01%) only a minor population of 4.85± 0.86% was detected by flow cytometry in C57BL/6 mice (fig. 12 b). Similar differences were also observed concerning the ratio of CD11b$^+$ DCs to CD103$^+$ cDCs (fig. 13).

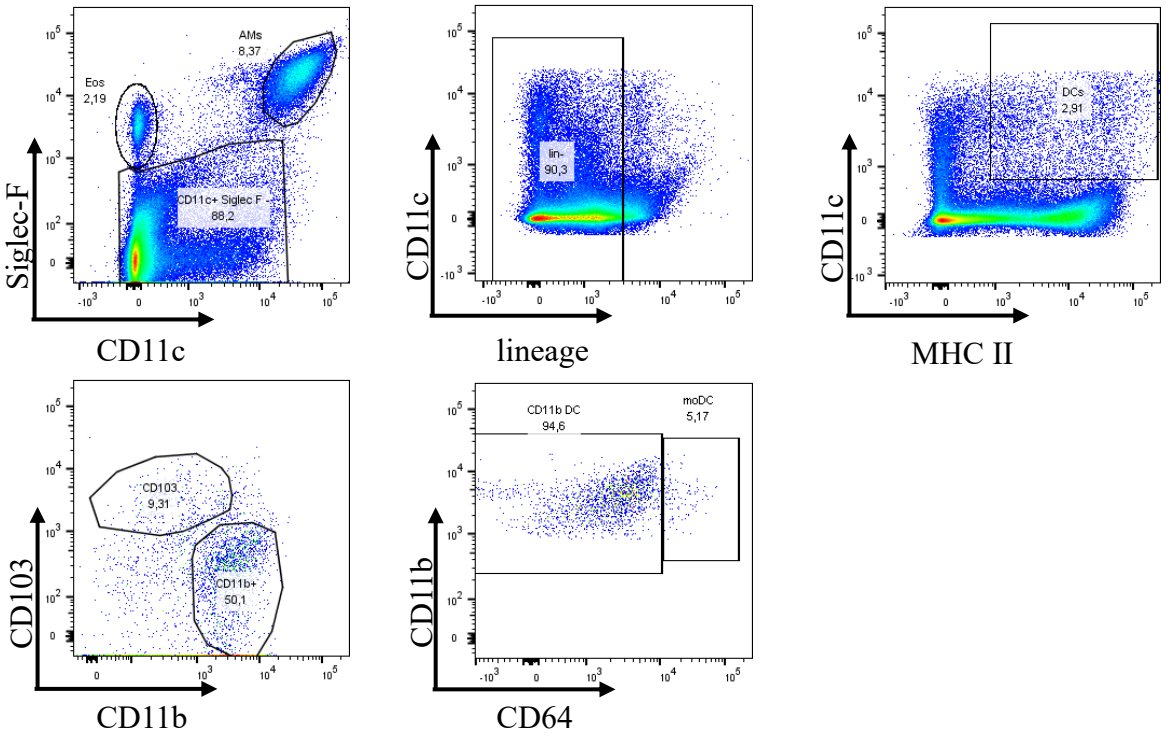

Figure 11: Identification of pulmonary phagocytes using flow cytometry. Living cells were gated for their expression of Siglec-F and CD11c and divided into Siglec-F$^+$CD11c$^-$ eosinophils, Siglec-F$^+$CD11c$^+$ AMs, and Siglec-F$^-$CD11c$^+$ DCs. Cells from the DC gate were then analyzed for their lineage marker expression (CD3e, CD19, CD49b, Ly6G). Lineage-negative cells were gated for CD11c and MHCII. CD11c$^+$MHCII$^+$ cells were separated for their expression of CD11b and CD103 to define CD11b$^+$ DCs and CD103$^+$ cDCs. CD11b$^+$ DCs were then separated into CD11b$^+$ cDCs and CD11b$^+$ resident moDCs using CD64. Experiment was performed using naïve C57BL/6 mice; n= 3.

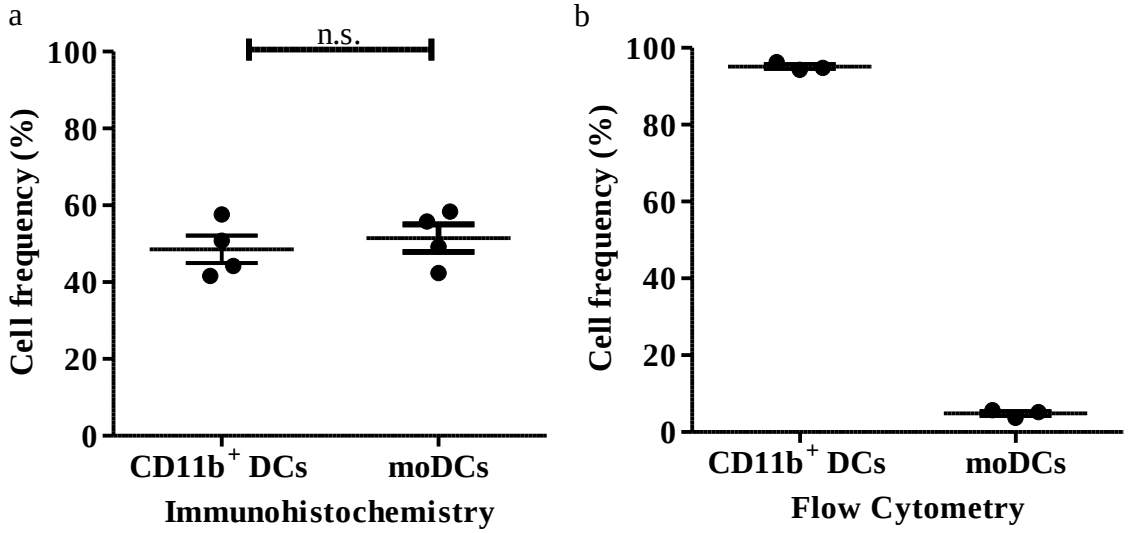

Figure 12: Comparison of resident moDC frequencies based on IHC and flow cytometry. $CD11b^+$ cDCs and $CD11b^+$ resident moDCs were identified and quantified based on their CD64 expression as described. Frequencies in naïve C57BL/6 mice were obtained by IHC (a, n= 4) and flow cytometry (b, n= 3). Depicted are mean and SEM; $p \leq 0.05$ (*), statistical test: Mann-Whitney U-test. Due to low sample number of flow cytometry experiments, no statistical analysis was performed.

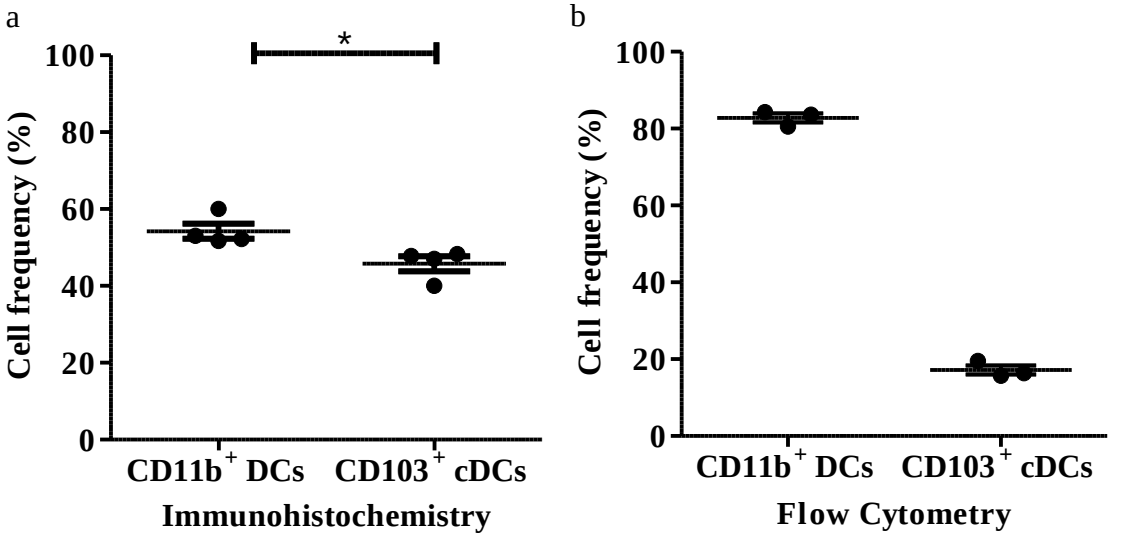

Figure 13: Comparison of $CD11b^+$ DC:$CD103^+$ cDCs ratios based on IHC and flow cytometry. $CD11b^+$ DCs and $CD103^+$ cDCs were identified and quantified based on their reciprocal expression of CD11b and CD103 as described. Frequencies in naïve C57BL/6 mice were obtained by IHC (a, n= 4) and flow cytometry (b, n= 3). Depicted are mean and SEM; $p \leq 0.05$ (*), statistical test: Mann-Whitney U-test. Due to low sample number of flow cytometry experiments, no statistical analysis was performed.

In 2015 Nakano *et al.* [52] identified CD88 (C5aR1) as another marker that is specific for cells from a monocytic lineage in C57BL/6 mice. They reported a ratio of 1:1 for $CD11b^+$ cDCs to $CD11b^+$ resident moDCs matching our results from IHC studies using CD64. Indeed, a costaining of C5aR1 and CD64 using IHC revealed, that both antibody specifically stain the same cells (fig. 14). Therefore, another experiment was done using CD88 as discriminative marker based on IHC and flow cytometry. Using C5aR1/CD88 as discriminative marker it was possible to obtain comparable amounts of $CD11b^+$ resident moDCs by IHC and flow cytometry (fig. 15). This finding indicates, that $CD64^+$ cells were underrepresented in flow cytometry.

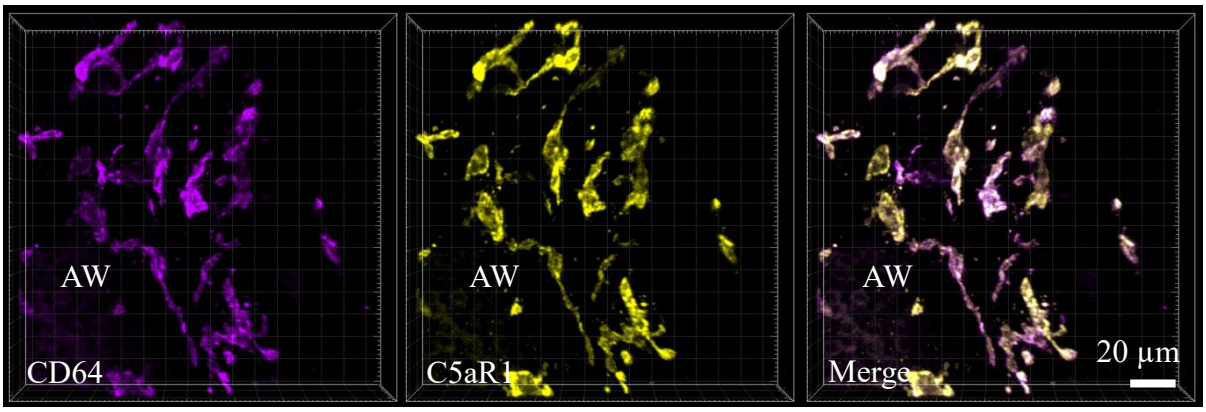

Figure 14: CD64 and C5aR1/CD88 are equivalent markers for cells with monocytic origin. PCLS from naïve C57BL/6 (n= 4) and BALB/c (n= 4) mice were stained with CD64 (purple) and C5aR1/CD88 (yellow). AW- airway. Representative data of BALB/c mice is shown.

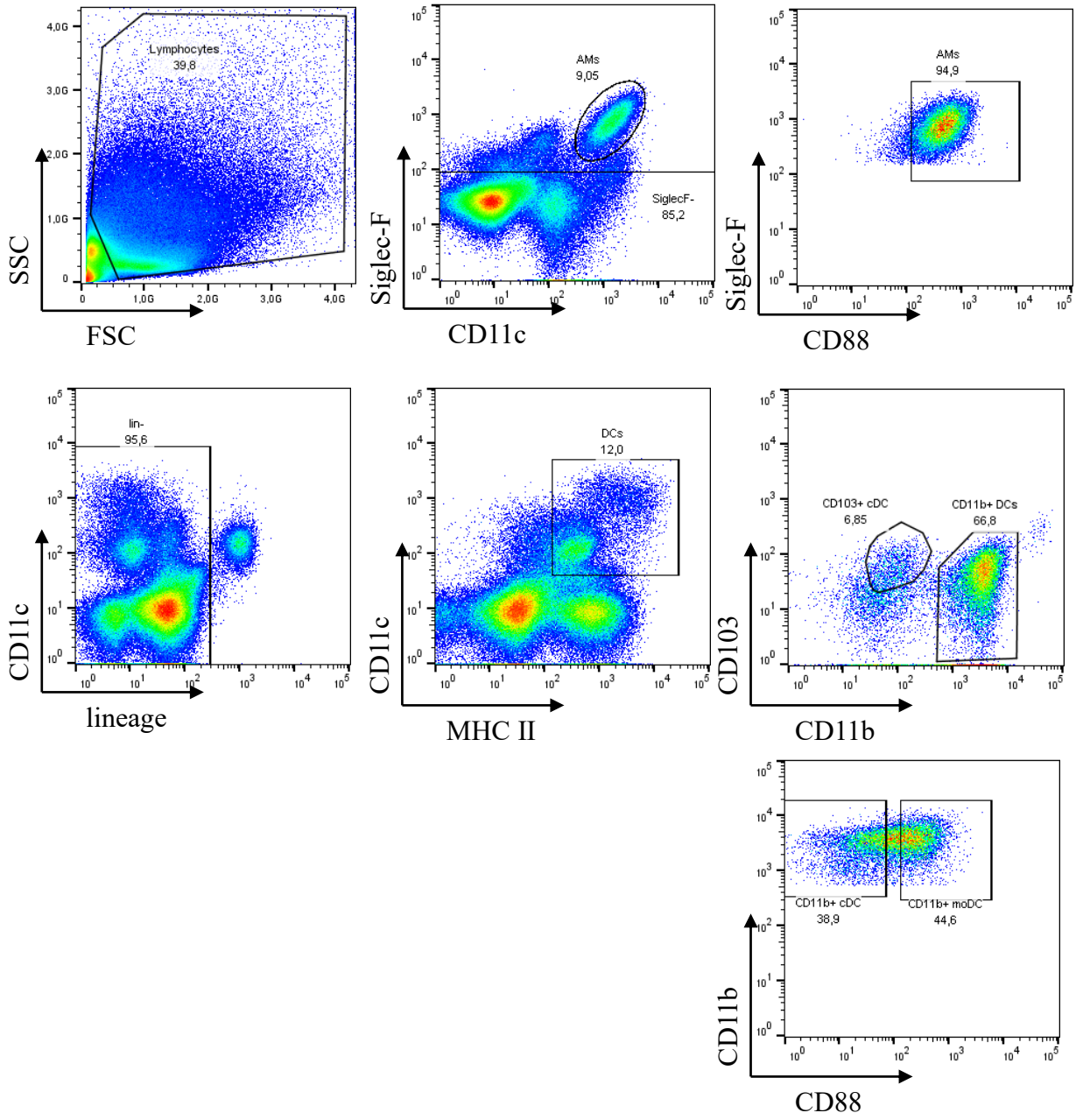

Figure 15: Distinction of CD11b$^+$ cDCs and CD11b$^+$ moDCs based on C5aR1/CD88. Living cells were gated for their expression of Siglec-F and CD11c and divided into Siglec-F$^+$CD11c$^-$ eosinophils, Siglec-F$^+$CD11c$^+$ AMs, and Siglec-F$^-$CD11c$^+$ DCs. Cells from the DC gate were then analyzed for their lineage marker expression (CD3e, CD19, CD49b, Ly6G). Lineage-negative cells were gated for CD11c and MHCII. CD11c$^+$MHCII$^+$ cells were separated for their expression of CD11b and CD103 to define CD11b$^+$ DCs and CD103$^+$ cDCs. CD11b$^+$ DCs were then separated into CD11b$^+$ cDCs and CD11b$^+$ resident moDCs using CD88. Experiment was performed pooling 30 naïve C57BL/6 mice for cell sorting in a single experiment.

5.4 Localization of Pulmonary Phagocytes

This study aimed at characterizing the murine lung at steady-state and after induction of an allergic airway response by IHC. After identification and quantification of DCs and macrophages the next step was the localization of these cell types, because localization, inter alia, is important for the availability of antigen and resulting cell activation.

5.4.1 Structure of the Lung

The lung consists of different compartments and structures. To allow a reliable localization of lung phagocytes the first step was to identify pulmonary compartments like airways, lung interstitium, alveolar lumen, and blood vessels reliably in PCLS. With the staining of α-smooth muscle actin (α-SMA) airways, veins, and arteries could be identified and distinguished based on the structure of their smooth muscle cells. Smooth muscle cells of airways are arranged in horizontal stripes parallel to the airway direction (fig. 16 a), while it is uniformly distributed on pulmonary and intra-acinar arteries (fig. 16 a, b). In contrast, smooth muscle cells of veins are arranged irregularly (fig. 16 c). An alternative way to identify airways and blood vessels is the usage of autofluorescence. This method was used for localization studies of DCs and macrophages, because a four-color panel was needed to identify them reliably (see fig. 4) and a fifth color for α-SMA was not available. Lung tissue is autofluorescent and this autofluorescence can be excited best with the UV or green laser and detected at wavelengths between 420-530 nm. To show how airways and blood vessels can be distinguished by both approaches, they are compared in figure 16. Airways can be identified by airway epithelial cells that are highly autofluorescent (fig. 16 a). The pulmonary artery is located close to the airway and was characterized by a bright homogenous autofluorescence pattern and no single cells were detectable (fig. 16 a). Intra-acinar arteries showed the same autofluorescence as pulmonary arteries, but due to their smaller size/diameter the signal was less intense. In addition, they were surrounded by up to four alveolar ducts depending on the vessel direction, which appeared as deep black holes at both sides of the vessels (fig.16 b). Veins were not accompanied by alveolar ducts and they showed an irregular autofluorescence pattern (fig. 16 c).

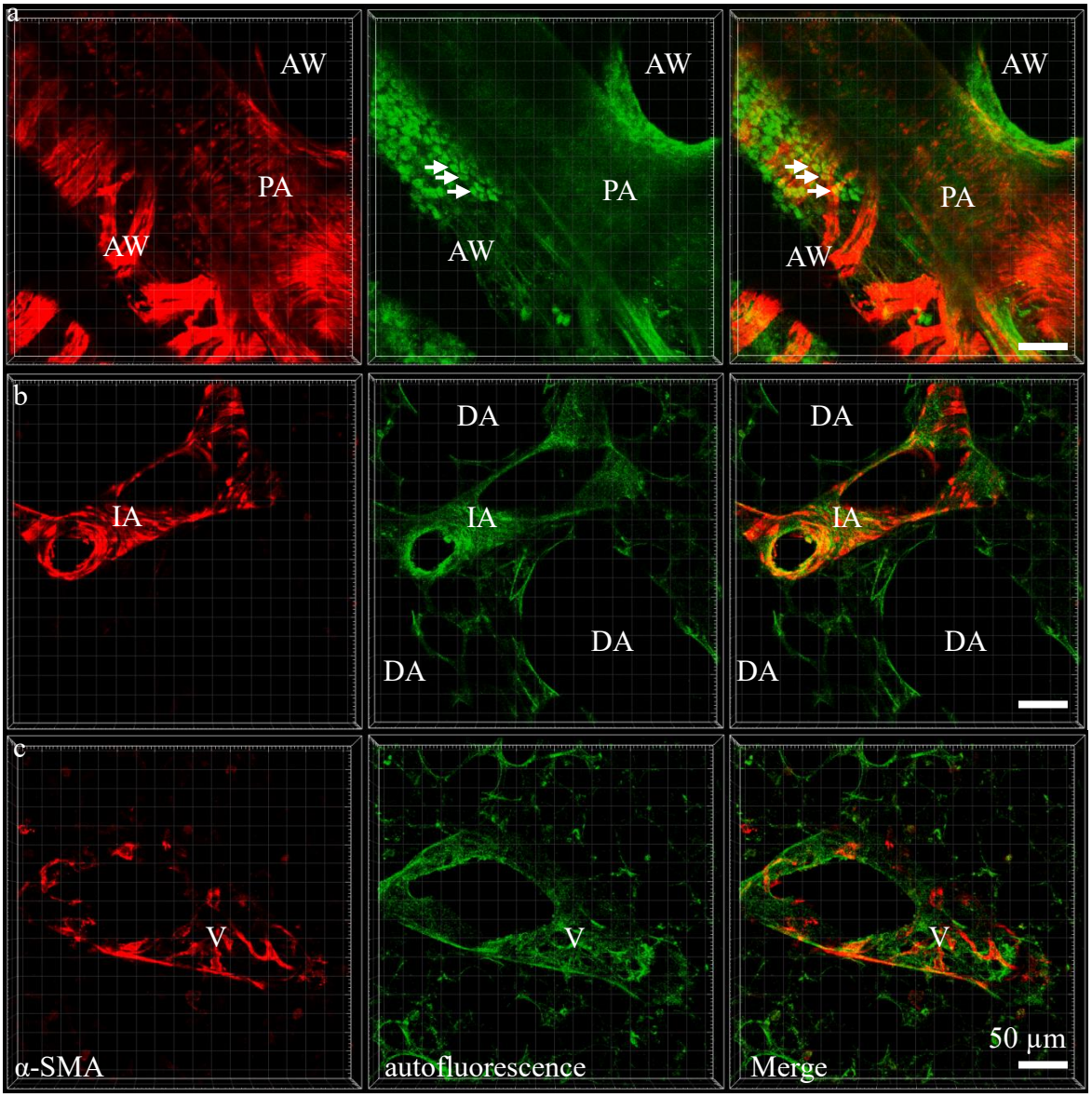

Figure 16: Visualization of airways and blood vessels based on antibody staining or autofluorescence. Airways (a), pulmonary artery (a), intra-acinar arteries (b), and veins (c) were identified with α-SMA (red) or autofluorescence (green) on PCLS from naïve C57BL/6 mice (n= 2). Airway epithelial cells (arrows) show strong autofluorescent signals (a), while blood vessels can be detected by the autofluorescence of their elastic fibers (a-c). Autofluorescence was excited at 488 nm and recorded at wavelengths between 490-530 nm. AW- airway, DA- alveolar ducts, PA- pulmonary artery, IA- intra-acinar artery, V- vein.

5.4.2 Conventional Dendritic Cells and Macrophages

Localization of pulmonary phagocytes was determined based on the anatomical structures described in part 3.1. This study, for the first time, focused on the location of different types of DCs and macrophages. Using the combination of CD11c, MHCII, CD11b and Langerin DCs, AMs, and IMs were identified at the same time. Both types of DCs ($CD11b^+$ DCs and $CD103^+$ cDCs) were distributed in the airway interstitium all along the airways close to the epithelium (fig. 17 a) but no intraepithelial cells were found. Neither, any cell was found that sent dendrites into the lumen through the epithelial barrier. Conventional DCs were also located in the connective tissue between airway and pulmonary artery, around intra-acinar arteries, and around veins (fig. 17 a-c). No DCs were located in the alveolar interstitium apart from airways or blood vessels (fig. 17 d). $CD11b^+$ DCs and $CD103^+$ cDCs were found at the same regions and no spatial separation was observed

IMs were described to be situated in the alveolar interstitium apart from airways [2]. As indicated above cells representing the phenotype of IMs in this study were also located around airways and blood vessels and, therefore, these cells were called interstitial macrophage-like cells (IMLCs) to highlight the differences concerning localization. Further, they were separated into airway adjacent and blood vessel adjacent IMLCs, whereby the latter might represent the population described by Bedoret *et al.* [2]. Different to cDCs and IMLCs, AMs were not situated in the interstitium but in the alveolar lumen. However, AMs were often found very close to the alveolar epithelium indicating, that they were attached to it (fig. 17 b and d), as described before [55]. Cell localization was determined in BALB/c (n= 4) and C57BL/6 (n= 4) mice and no differences were observed between both strains.

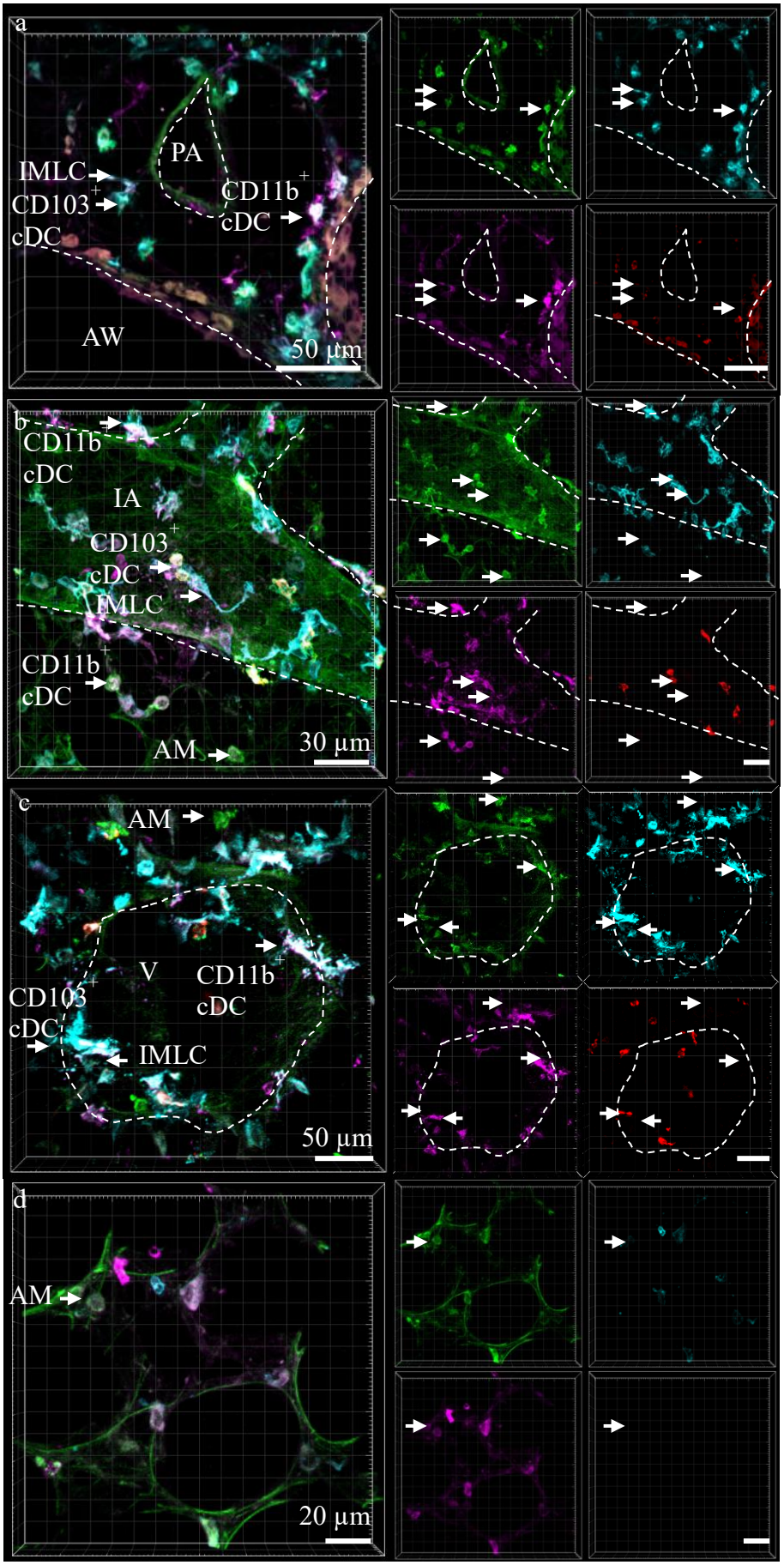
a
PA
IMLC
CD103+
cDC
CD11b+
cDC
AW
50 µm
b
CD11b
cDC
IA
CD103+
cDC
IMLC
CD11b+
cDC
AM
30 µm
c
AM
V
CD11b+
cDC
CD103+
cDC
IMLC
50 µm
d
AM
20 µm

Figure 17: Localization of DCs and macrophages. PCLS from naïve BALB/c (n= 4) and C57BL/6 (n= 4) mice were stained with CD11c (green), MHCII (cyan), CD11b (pink), and Langerin (red). Conventional DCs and IMs were localized in the interstitium around airways and pulmonary arteries (a), around intra-acinar arteries (b), veins (c), while AMs were only located in the alveolar lumen (b-d). Dashed white line indicates borders of airways or vessels. AW-airway, PA, pulmonary artery, V- vein, IA- intra-acinar artery

5.4.3 Cells with Monocytic Origin

With the knowledge that about 50% of $CD11b^+$ DCs have a monocytic background (fig. 9, 12, 15), possible differences regarding localization were examined. Further, location of tissue-resident monocytes was determined. The evaluation of image data showed that there was no difference in localization between resident moDCs and $CD11b^+$ cDCs. Both populations were located around airways and blood vessels. Interestingly, monocytes were mainly located in the airway interstitium close to the epithelium and only a smaller proportion was located around vessels (fig. 18).

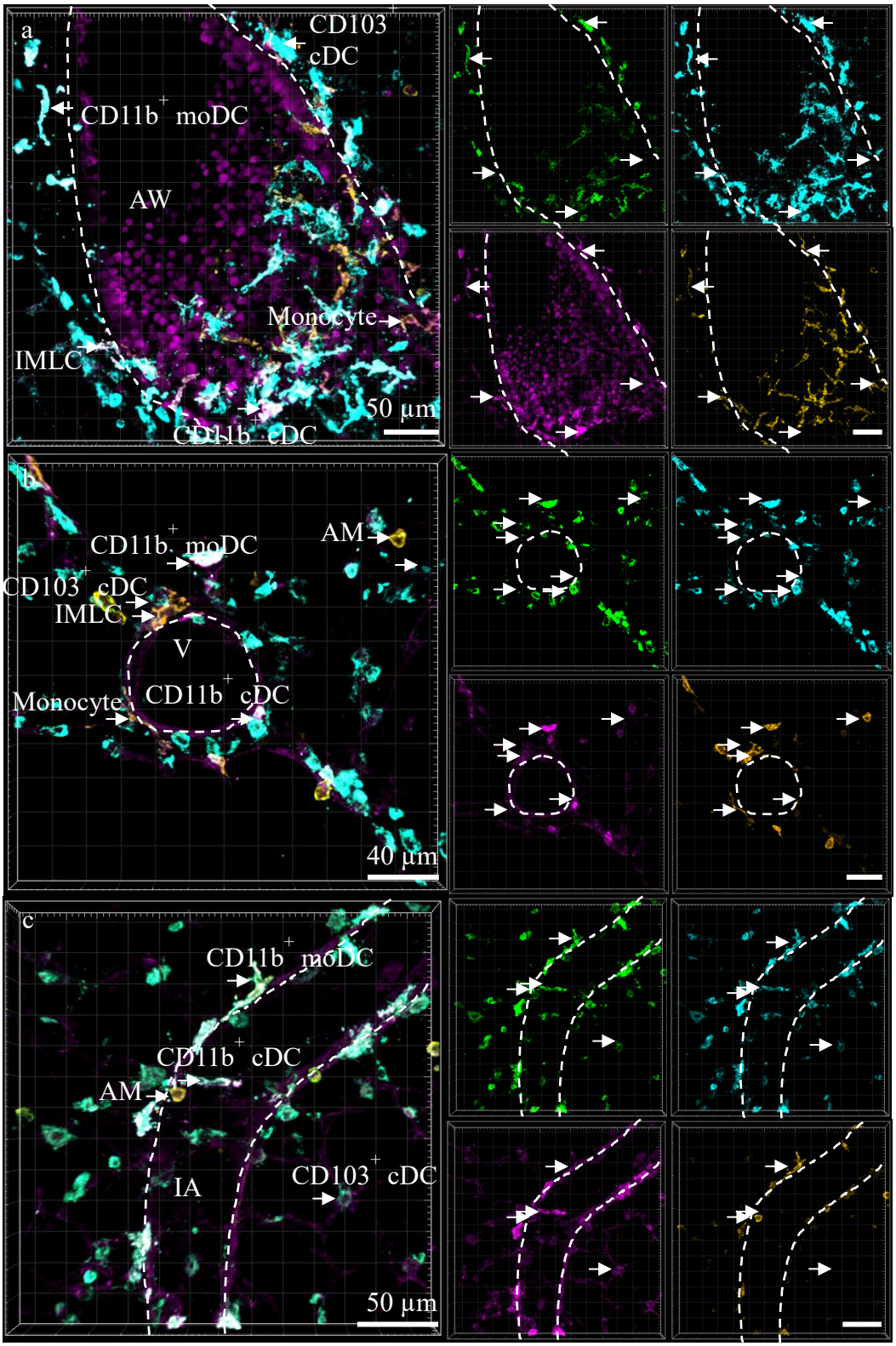

Figure 18: Cells with monocytic origin are located around airways and blood vessels. PCLS from naïve and C57BL/6 mice (n= 4) were stained with CD11c (green), MHCII (cyan), CD11b (pink), and CD64 (yellow). Cells with monocytic origin were localized in the interstitium around airways (a), veins (b), intra-acinar arteries (c), and in the alveolar lumen (a- c). Dashed white line indicates borders of airways and vessels. AW- airway, V- vein, IA- intra-acinar artery.

5.4.4 Plasmacytoid Dendritic Cells

In contrast to the other DC subsets, which were located in the interstitium, localization of pDCs was not restricted to airways and vessels. Actually, they were located widely distributed across the alveolar interstitium (fig. 19 a), only few cells were found close to blood vessels (fig. 19 b), and no pDC was found close to the airway epithelium.

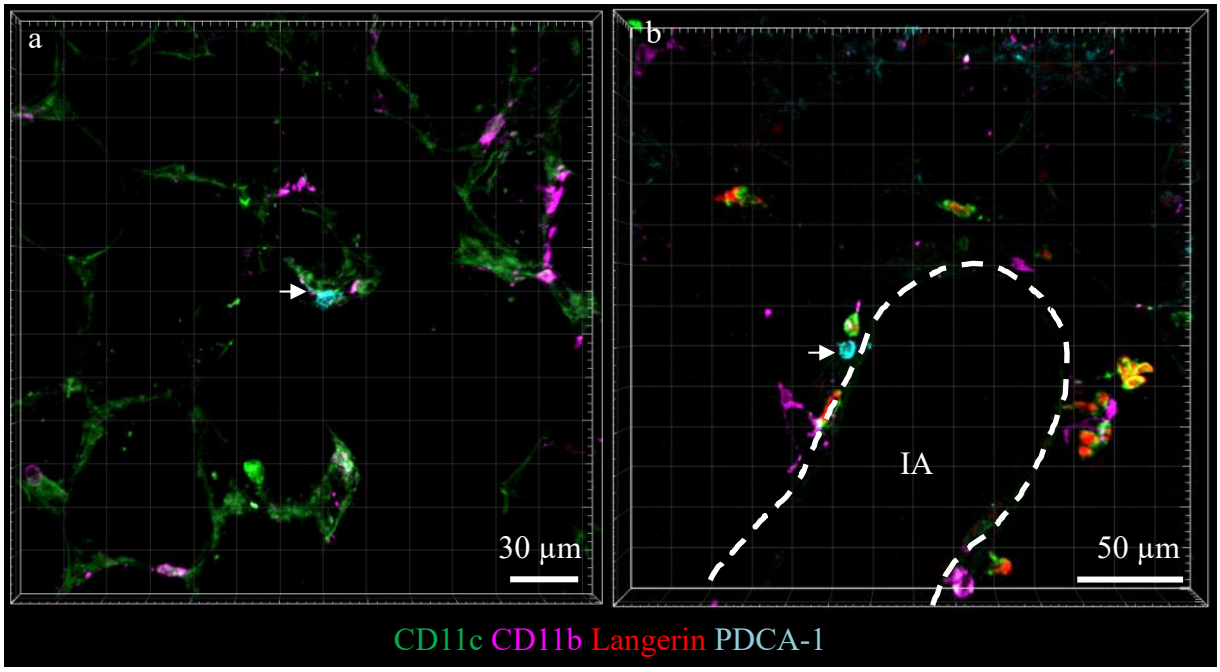

Figure 19: Plasmacytoid DCs are mainly located in the alveolar interstitium. PCLS from naïve and C57BL/6 mice (n= 2) were stained with CD11c (green), Langerin (red), CD11b (pink), and PDCA-1 (cyan). Plasmacytoid DCs were located in the alveolar interstitium (a) and sometimes close to vessels (b), but never around airways. Dashed white line indicates the border of an intra-acinar artery (IA).

5.5 Comparison of Naïve and HDM-treated Lung

The first part of this study has concentrated on steady-state conditions. Based on the knowledge concerning cell numbers and localization this part will focus on differences between steady-state and the early phase of allergic inflammation 24 h after the mice were treated with HDM.

5.5.1 Quantification of Dendritic Cells and Macrophages

Cell numbers and proportions were defined for steady-state so far. Since it is known that inflammatory cells are recruited rapidly to the site of inflammation, in the next step, numbers

of pulmonary DCs and macrophages and proportions were determined after allergen induction and compared to steady-state conditions.

5.5.1.1 Conventional Dendritic Cells and Macrophages

Cell numbers were determined in mice that were treated with a single dose of house dust mite extract 24 h after allergen challenge. Analysis was performed as described and is based on counting an average of 785 cells per animal (min 696, max 833). Quantification of DCs and macrophages in HDM stimulated lungs caused some difficulties, on the one hand there were more cells in the lung (fig. 23) and on the other hand the cells were not equally distributed. In addition, there was an increasing autofluorescence especially at regions with high cell density. As a result, numbers calculated for HDM-treated mice were the same as or even lower than in naïve mice with a high variation (data shown in the appendix). Although, calculation of absolute numbers did not work in a proper way for HDM-treated mice, the proportions of interstitial phagocytes were considerably stable.

The comparison of the proportions of cDCs and macrophages in naïve and HDM-treated mice showed a significant increase in $CD11b^+$ DCs while IMLCs significantly decreased (fig. 20). Proportion of $CD103^+$ cDCs stayed unaffected compared to naïve mice. This effect was observed in BALB/c and C57BL/6 mice. No statistical analysis was done in BALB/c mice due to a low sample size. $CD11b^+$ DCs significantly increased in the inflamed lung and their proportion is up to 62.6± 1.38% in C57BL/6 (n= 4) mice. In BALB/c mice the proportion of $CD11b^+$ DCs is up to 70.6% (fig. 21). Again, no statistical analysis could be performed in BALB/c mice due to low sample number (n= 2).

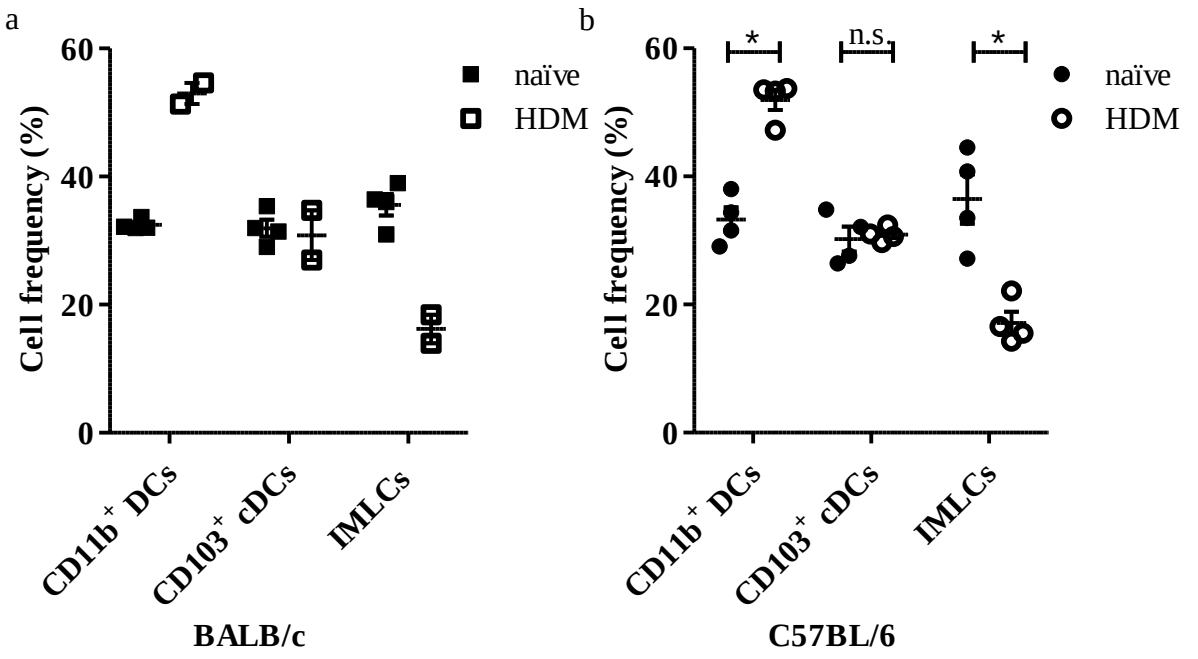

Figure 20: Proportions of DCs and IMLCs change after antigen administration. HDM-treated BALB/c (a, n= 2) and C57BL/6 (b, n= 4) mice were sacrificed 24 h after allergen administration. PCLS of those mice were stained for CD11c, MHCII, CD11b, and Langerin. DCs and IMLCs were counted, the proportions were determined, and compared to naïve mice (C57BL/6 n= 4, BALB/c n= 4). Depicted are mean and SEM; $p \leq 0.05$ (*) statistical test: Mann-Whitney U-test.

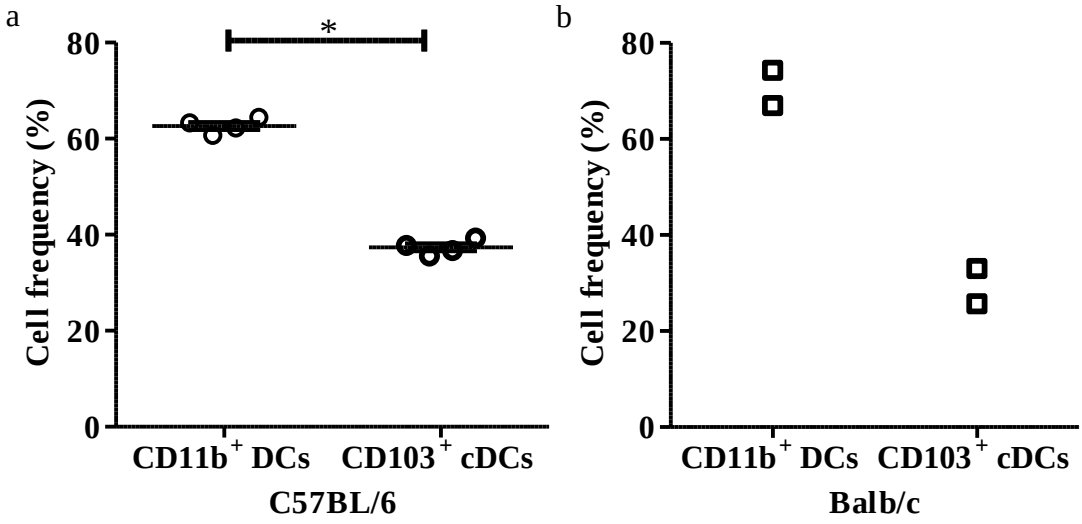

Figure 21: Frequencies of CD11b$^+$ DCs and CD103$^+$ cDCs after antigen challenge. HDM treated C57BL/6 (a, n= 4) and BALB/c (b, n= 2) mice were sacrificed 24 h after allergen administration. PCLS of those mice were stained for CD11c, MHCII, CD11b, and Langerin. CD11b$^+$ DCs and CD103$^+$ cDCs were counted and the proportion were determined. Depicted are mean and SEM; $p < 0.05$ (*), statistical test: Mann-Whitney U-test

5.5.1.2 CD11b$^+$ Monocyte-Derived Dendritic Cells

Proportion of CD11b$^+$ moDCs was also determined in HDM-treated C57BL/6 mice (n= 3). Analysis was performed as described for naïve mice and is based on the counting of 406 cells. As shown in above, in naïve mice CD11b$^+$ moDCs constituted 51.5± 6.2% from the total CD11b$^+$ DC population, indicating that CD11b$^+$ DCs consist of a heterogeneous population at steady-state. The percentage of CD11b$^+$ moDCs raised up to 81.2± 1.9% in HDM-treated mice (fig. 22). Due to the small sample size in the HDM group no statistical analysis was possible.

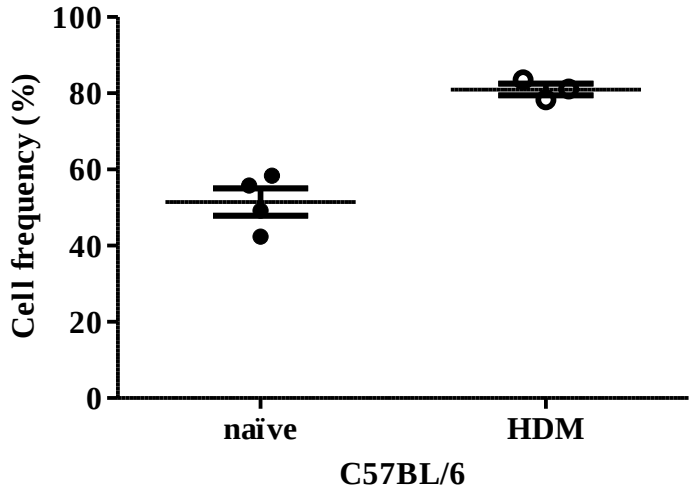

Figure 22: HDM administration caused a rise of CD11b$^+$ moDCs. HDM-treated C57BL/6 mice (n= 3) were sacrificed 24 h after allergen administration and stained for CD11c, MHCII, CD11b, and CD64. CD11b$^+$ cDCs and CD11b$^+$ moDCs were counted, the proportion of CD64$^+$ moDCs was determined, and compared to the steady-state. Depicted are mean and SEM. Due to low sample numbers no statistical analysis was performed.

5.5.2 Localization

The localization of pulmonary phagocytes has been examined under steady-state conditions in this study. Due to antigen uptake and cell activation under inflammatory conditions it is likely that some changes regarding localization occur, especially since quantification has already shown differences in relative cell numbers.

5.5.2.1 Localization of Conventional Dendritic Cells and Macrophages

The localization of DCs and macrophages was determined in inflamed lungs as described above for the steady-state in C57BL/6 (n= 4) and BALB/c (n= 2) mice. Treatment with HDM has led

to more background signals compared to the naïve lung. This background was even higher in regions with many cells like airways and blood vessels. Cell identification around airways was also impeded due to the high autofluorescence of the epithelium.

Localization of DCs and macrophages did not change in the inflamed lung. It was obvious that there were less IMLCs situated around airways, but that was due to the decrease in total cell numbers. Both DC populations, $CD11b^+$ DCs and $CD103^+$ cDCs, were located around airways and blood vessels but as reported above not in the alveolar interstitium. AMs did not change their location either (fig. 23).

Although there were no changes regarding localization in general (fig. 23 a- c), some differences were observed. First, phagocytes, in particular DCs, were not distributed equally anymore, but occasionally formed accumulations around airways or blood vessels (fig. 23 a and c). Second, there was an influx of small $CD11b^+$ cells, mainly in the alveolar region but also close to airways (fig. 23 a- c). Due to their expression of CD11b, those cells might be neutrophils or eosinophils that were recruited to the site of inflammation. No differences were observed between the strains.

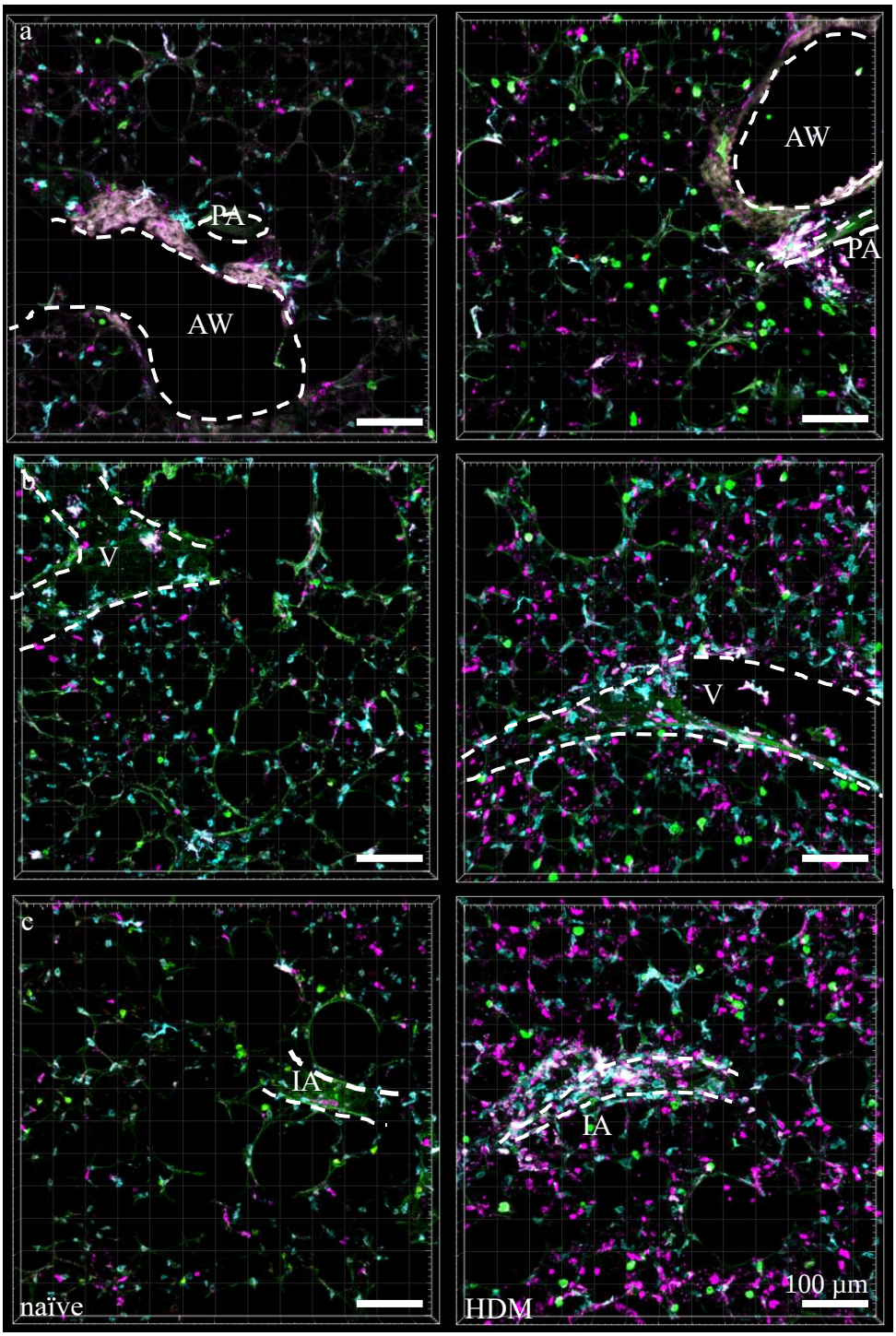

Figure 23: HDM treatment causes an influx of cells to the lung that accumulate around airways and vessels. BALB/c (n= 2) and C57BL/6 (n= 4) mice were treated with HDM and sacrificed after 24 h. PCLS were stained with CD11c (green), MHCII (cyan), CD11b (pink), and Langerin (red). Conventional DCs and IMLCs were localized in the interstitium around airways and pulmonary arteries (a), around intra-acinar arteries (b), veins (c), while AMs were located in the alveolar lumen (a- c). Dashed white line indicates borders of airways and vessels. No difference was observed between the strains. AW-airway, PA- pulmonary artery, V- vein, IA- intra-acinar artery.

5.5.2.2 Cells with Monocytic Origin

In inflamed lungs the number of $CD11b^+$ moDCs showed a strong increase compared to the naïve lung (fig. 22). This increase appearing not only in $CD11b^+$ moDCs, but also in classical monocytes, was most striking around airways, where those cells form a dense network (fig. 24). No considerable increase of monocytic cells was observed around blood vessels or in the alveolar interstitium.

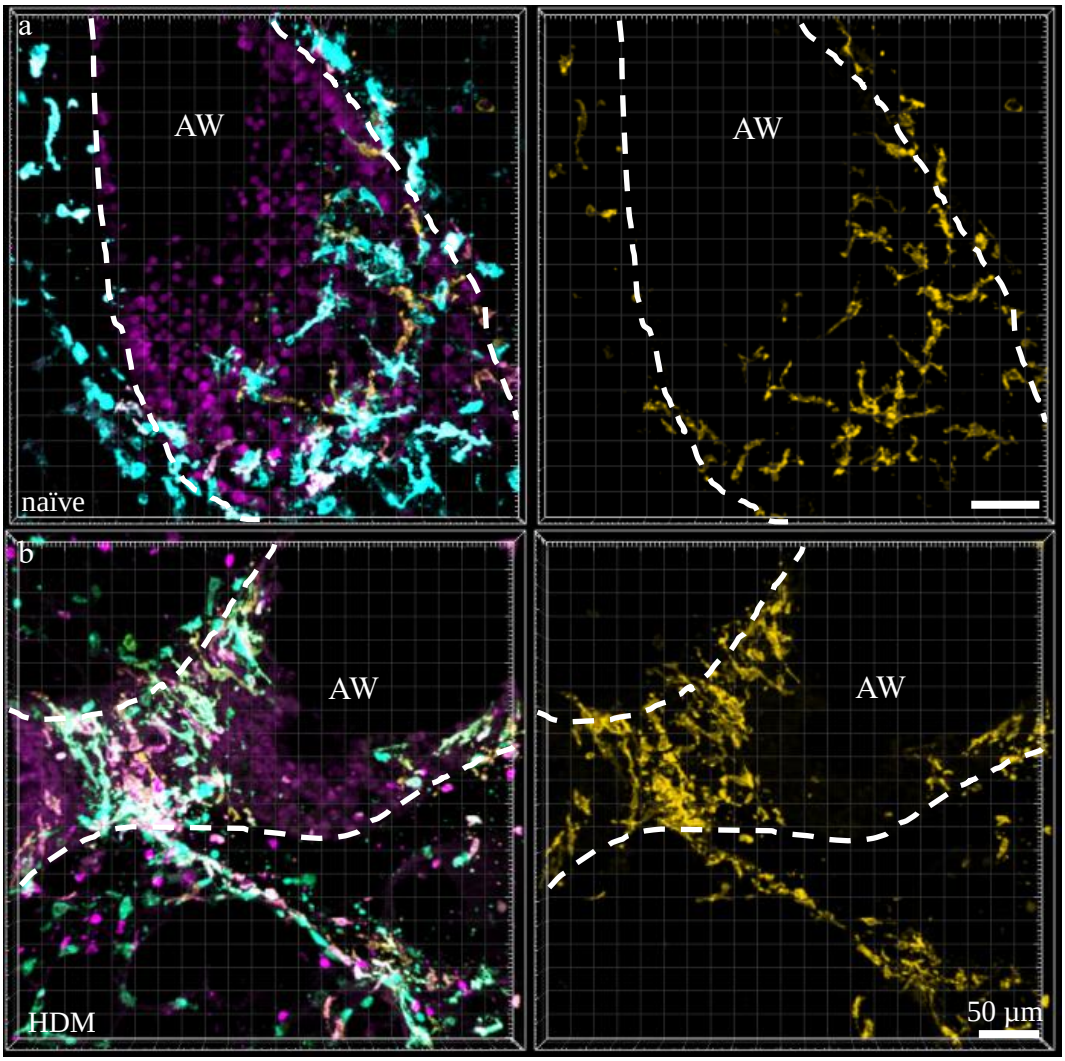

Figure 24: Cells with monocytic origin accumulate around airways in HDM-treated mice. C57BL/6 mice (n= 3) were treated with HDM and sacrificed after 24 h. PCLS were stained with CD11c (green), MHCII (cyan), CD11b (pink), and CD64 (yellow). Shown are airway at steady-state (a) and under inflammatory condition (b) and the increasing number of cells with monocytic background. Dashed white lines indicate borders of airways. AW- airway.

5.6 CD103$^+$ cDCs are in Specific Contact to the Newly Described IMLC Population Around Airways and Blood Vessels at Steady-State

As mentioned, knowing cell localization inside the tissue is important for the examination of possible cell interactions of pulmonary phagocytes by analyzing cell contacts. This part of the study will deal with cell contacts between CD103$^+$ cDCs and the former mostly unrecognized IMLCs populations, based on qualitative localization analyses as well as quantitative analyses.

5.6.1 CD103$^+$ Conventional DCs are in Contact to IMLCs Around Airways

While studying the localization of cDCs and macrophages it turned out that CD103$^+$ cDCs were often in direct contact to IMLCs (fig. 25). These contacts were observed around airways (fig. 25 a) and blood vessels (fig. 25 b and c) in naïve C57BL/6 and BALB/c mice.

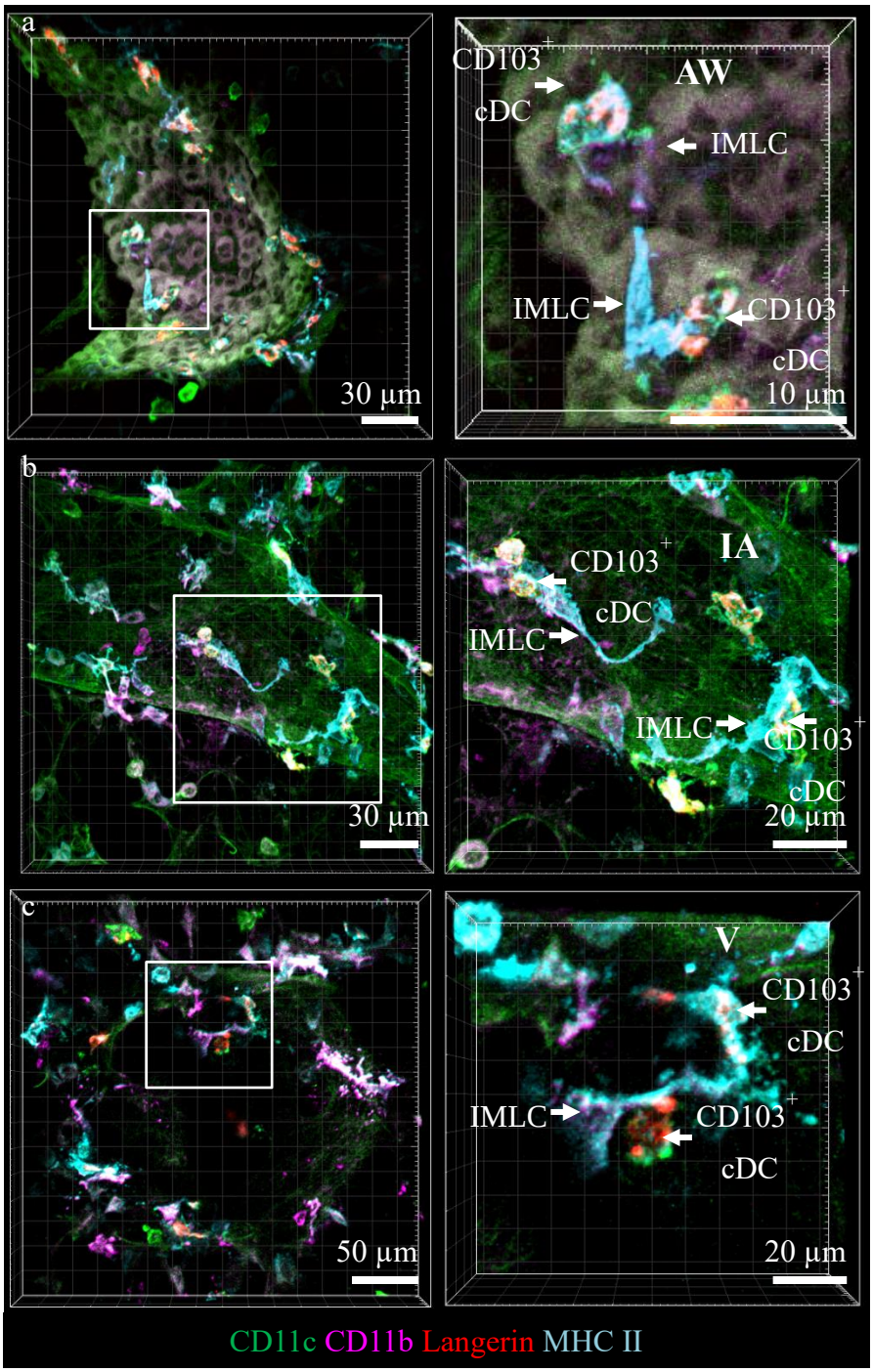

Figure 25: CD103$^+$ cDCs are in contact to IMLCs around airways and blood vessels. PCLS from naïve BALB/c (n= 4) and C57BL/6 (n= 4) mice were stained with CD11c (green), MHCII (cyan), CD11b (pink), and Langerin (red). CD103$^+$ cDCs and IMLCs were often found in close contact to each other at the airway epithelium (a) and around blood vessels (b, c). No difference was observed between the strains. Right column shows bigger magnifications of regions of interest highlighted with a white box on the left.AW- airway, V- vein, IA- intra-acinar artery.

5.6.2 Contacts Between CD103$^+$ conventional DCs and IMLCs are Specific

To determine if the contacts between CD103$^+$ cDCs and IMLCs were specific another quantification was performed. For analysis, an average amount of 158 (min 114, max 189) CD103$^+$ cDCs in C57BL/6 mice and 124 (min 79, max 170) CD103$^+$ cDCs in BALB/c mice was counted. Further in average 122 (min 68, max 179) and 89 (min 60, max 110) blood vessel adjacent IMLCs were counted in C57BL/6 and BALB/c mice respectively. For airway adjacent IMLCs averaged numbers were 55 (min 32, max 100) in C57BL/6 and 50 (min 29, max 89) in BALB/c mice.

First, cell contacts between IMLCs and different cell types, including CD11b$^+$ DCs, CD103$^+$ cDCs, AMs and, any other cells, were examined. For the analysis, IMLCs were differentiated into IMLCs located either at airways or at blood vessels. It turned out that about 41.01± 13.12% to 55.63± 7.07% (C57BL/6 and BALB/c respectively) of IMLCs were in specific contact with CD103$^+$ cDCs around airways (fig. 26 a). Cell contacts at blood vessels were less frequent (21.44± 11.48% C57BL/6 and 22.94± 3.57% BALB/c) but also very specific (fig. 26 b). Only few IMLCs were in contact to any other cell types and the majority showed no cell contacts (fig. 26 a and b). In addition, 40.18± 7.61% (C57BL/6) to 52.49± 6.49% (BALB/c) of CD103$^+$ cDCs were in contact to airway IMLCs. As for the contact rate of IMLCs less contacts were observed around vessels compared to the airways (20.54± 2.25% C57BL/6; 29.32± 2.97% BALB/c) (fig. 26 c and d). Interestingly, there was a tendency towards higher contact rates in BALB/c mice compared to C57BL/6.

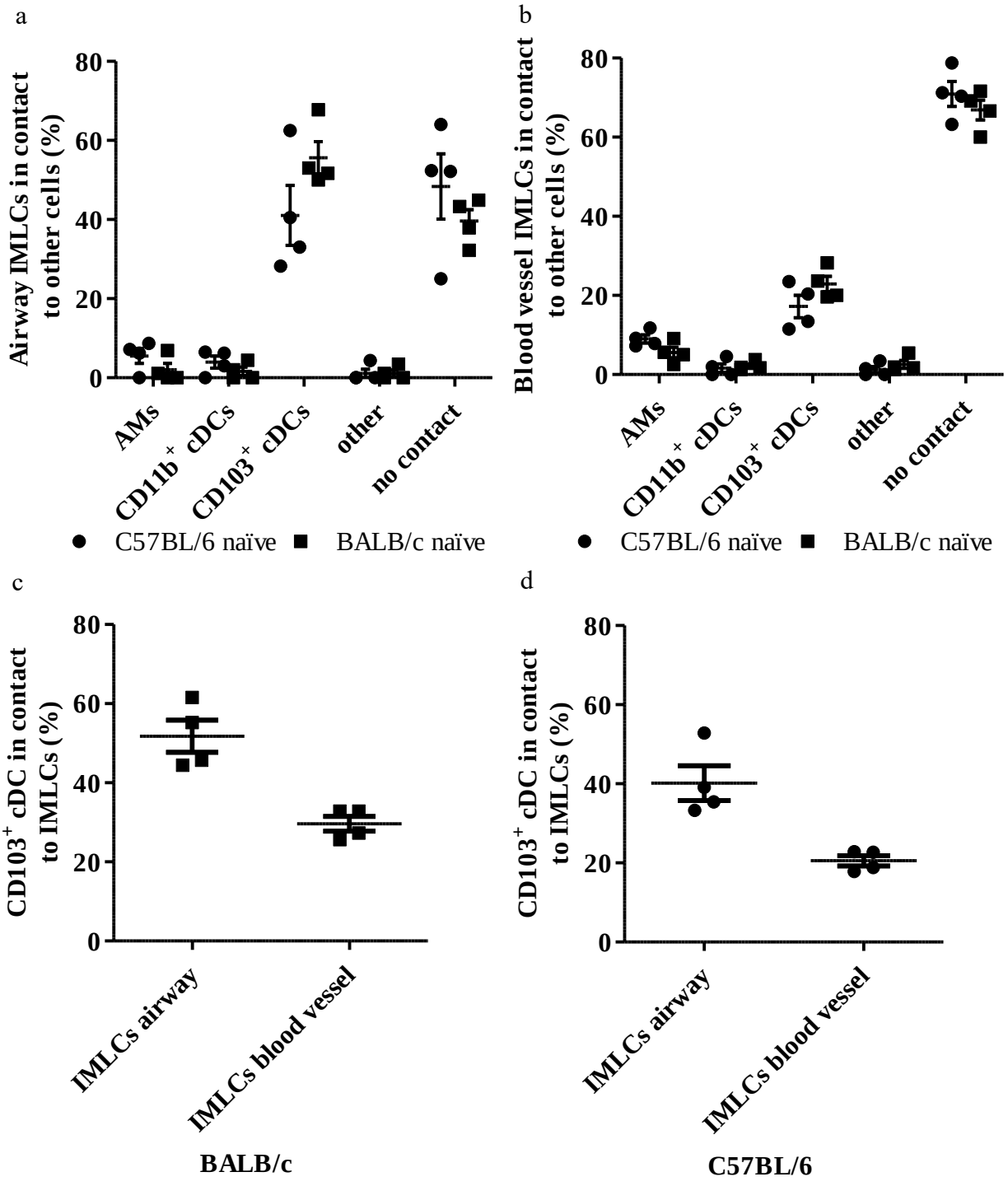

Figure 26: CD103$^+$ cDCs and IMLCs are in specific contact around airways and blood vessels. PCLS from naïve BALB/c (n= 4) and C57BL/6 (n= 4) mice were stained with CD11c, MHCII, CD11b, and Langerin. CD103$^+$ cDCs and IMLCs were counted around airways and blood vessels and cell contacts from IMLCs to other cells (a and b) and from CD103$^+$ cDCs to IMLCs (c and d) were determined. Depicted are mean with SEM.

5.6.3 The Contact Rate between IMLCs and CD103$^+$ Conventional DCs Decrease after HDM Treatment

Contact rates were also determined after the induction of an allergic inflammation. Quantification has already shown that proportion and absolute numbers of IMLCs in the lung decreased. Furthermore, in the context of a related cell identification-based study that showed a high efficiency of IMLCs in antigen-uptake during the initial hours after antigen challenge (unpublished data, Johann Berger). Indeed, there were only few remaining contacts between IMLCs and CD103$^+$ cDCs (fig. 27 a) at airways (18.05± 20.73% C57BL/6, 11.54% BALB/c) and blood vessels (12.59± 1.99% C57BL/6, 11.54% BALB/c). Accordingly, only about 10% of CD103$^+$ cDCs showed contacts to IMLCs (7.12± 4.7% C57BL/6, 9.81% BALB/c), while the contact rate around vessels was even lower (6.42%± 1.52% C57BL/6, 5.66% BALB/c) (fig. 26 7 and c). The direct comparison of contact rates between naïve and inflamed lungs of C57BL/6 mice showed a clear trend towards lower numbers in HDM-treated animals around airways (fig. 27 a). For IMLCs around blood vessels almost no changes in contact rate were observed (fig. 27 b). Interestingly, the trend for lower contact rates in treated animals was even stronger for airway IMLCs and for IMLCs situated around blood vessels in BALB/c mice. Due to the low sample number no statistical analysis was possible (fig. 27 a and b). Comparison of the contact rate between CD103$^+$ cDCs and IMLCs revealed that there was a significant decrease in contacted IMLCs at airways and blood vessels (fig. 27 c) in C57BL/6 mice. The same trend was observed for BALB/c mice, but due to low sample number no statistical was performed (fig. 27 c).

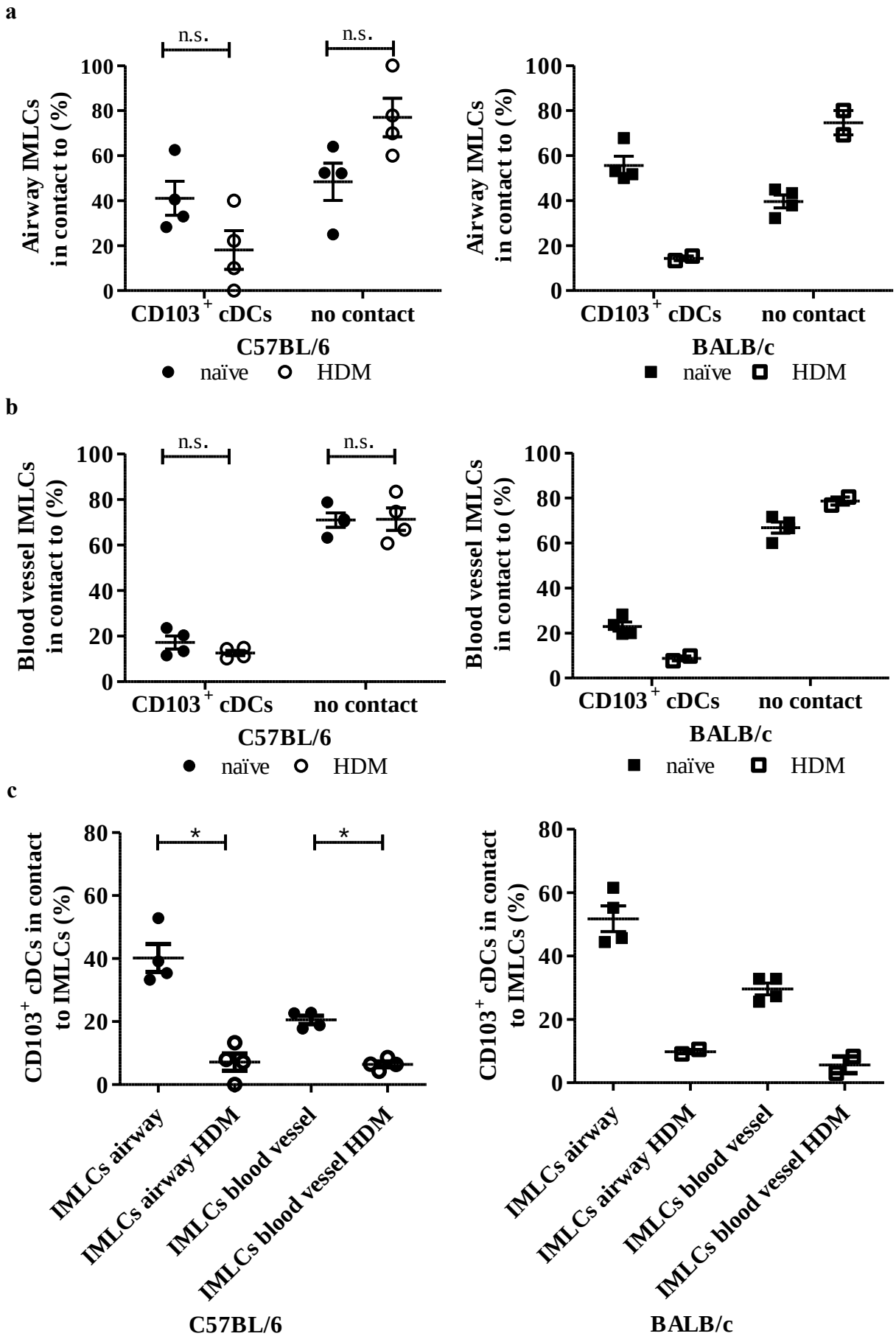
a
n.s.
n.s.
Airway IMLCs in contact to (%)
100
80
60
40
20
0
CD103+ cDCs
no contact
C57BL/6
naïve
HDM
BALB/c
b
Blood vessel IMLCs in contact to (%)
c
CD103+ cDCs in contact to IMLCs (%)
*
IMLCs airway
IMLCs airway HDM
IMLCs blood vessel
IMLCs blood vessel HDM

Figure 27: Comparison of contact rates between CD103$^+$ cDCs and IMLCs in naïve and HDM-treated mice are reduced in inflamed lungs. HDM-treated BALB/c (n= 4) and C57BL/6 (n= 2) mice were sacrificed 24h after treatment. PCLS of naïve and HDM-treated mice were stained with CD11c, MHCII, CD11b, and Langerin. Contact rates of IMLCs to CD103$^+$ cDCs around airways were compared between naïve and HDM-treated C57BL/6 and BALB/c mice (a). The same analysis was performed for contact rates of IMLCs to CD103$^+$ cDCs around blood vessels in naïve and HDM-treated C57BL/6 and BALB/c mice (b). Contact rates from CD103$^+$ cDCs contacting IMLCs were compared in naïve and HDM-treated C57BL/6 and BALB/c (c) mice. Depicted are mean and SEM; $p \leq 0.05$ (*), statistical test: Mann-Whitney U-test.

5.7 Migratory Potential of Pulmonary Phagocytes

It is known that DCs, which have taken up antigen, migrate towards the lung draining lymph nodes in a CCR7 depending manner. But until now, it is unclear where in the lung DCs get activated and there are contradictory findings regarding steady-state turnover of DCs [145]. Further, a related project has shown that IMLCs are very efficient in antigen uptake, even more prominent than DCs, in the first hours after antigen challenge (Berger, unpublished data). Their ability to take up large amounts of antigen raises the question, if they possess a migratory potential like DCs.

5.7.1 Distribution of Lymph Vessels

Knowing the distribution of LVs is important, as well, to understand the structure of the lung and the localization of immune cells. As published [110], CD90.2 is a reliable marker to identify LVs in the murine lung. Costaining of α-SMA and CD90.2 confirmed published data and showed that LVs either run with airways or veins (fig. 28 a and c). LVs can also be located between airway and pulmonary artery (fig. 28 b), but there are no LVs running with intra-acinar arteries (fig. 28 d). Besides LVs that can be easily identified based on their morphology CD90.2 is also expressed by different immune cells, e.g. innate lymphoid cells [154], T cells [155], or natural killer (NK) cells [156, 157] that are distributed over the lung tissue (fig. 28 a-d).

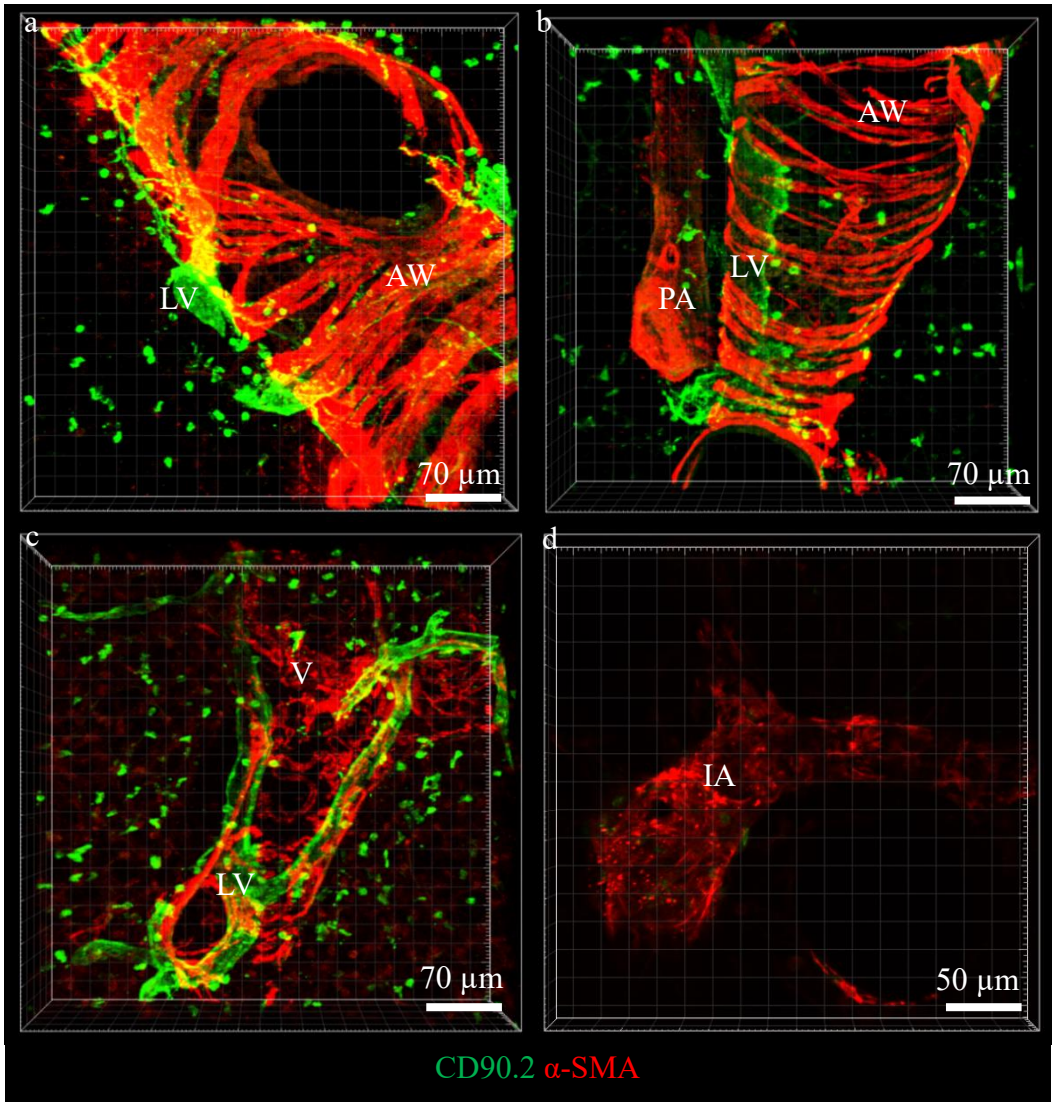

Figure 28: Lymph vessels are located around airways and veins in the murine lung. PCLS from naïve C57BL/6 mice (n= 6) were stained with CD90.2 (green), and α-SMA (red) to visualize lymph vessels around airways (a), between airway and pulmonary artery (b), and veins (c). No lymph vessels are running with intra-acinar arteries (d). Roundish green cells represent T cells, NK cells or natural killer cells. AW-airway, PA- pulmonary artery, V- vein, IA- intra-acinar artery, LV- lymph vessel.

5.7.2 CCL21 is Expressed by Pulmonary Lymph Vessels

It was shown in the skin [158, 159] that $CCR7^+$ DCs follow a CCL19 and CCL21 gradient towards the lymph nodes. A similar mechanism was suggested for the lung, but until now the exact localization of CCL21 inside the tissue is unknown. Therefore, as a first step, the localization of CCL21 was determined. Costaining of α-SMA, the lymph vessel marker CD90.2, and CCL21 revealed that CCL21 expression is limited to LVs (fig. 29). Expression of CCL21 was not ubiquitous distributed over the LVs but restricted to a spot-like pattern indicating endothelial cells as the source of CCL21 expression (fig. 29 a). CCL21 was detected

at all LVs around airways and also around veins independent from their size (fig. 29 b and c), but no CCL21 gradient inside the tissue could be detected.

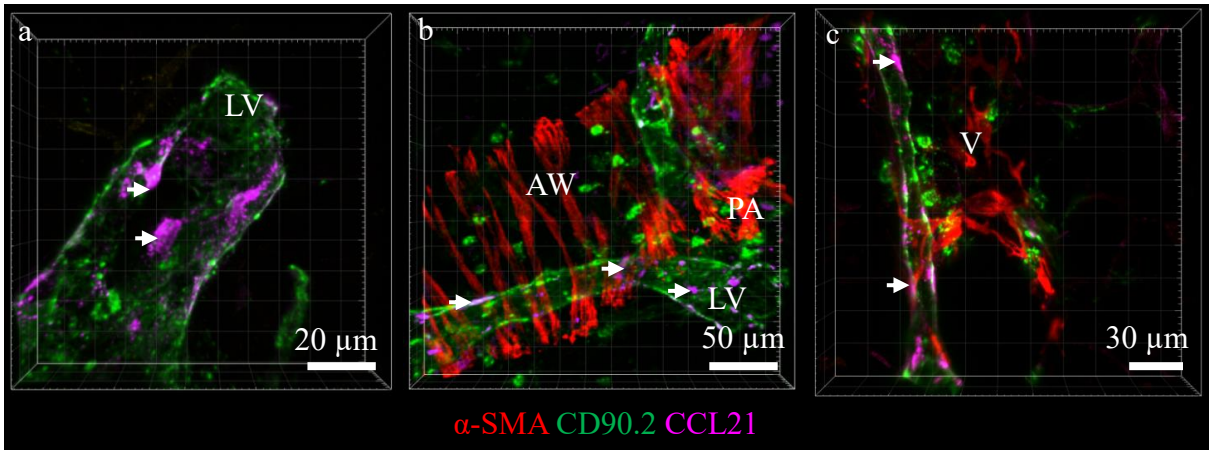

Figure 29: Lymph vessel endothelial cells are the source of CCL21. PCLS from naïve C57BL/6 mice (n= 6) were stained with CD90.2 (green), α-SMA (red), and CCL21 (pink) to determine the source of CCL21 in the lung tissue. CCL21 is expressed by endothelial cells (a) of LVs around airways (b) and veins (c). Endothelial cells are indicated by arrows. AW- airway, PA- pulmonary artery, V- vein, LV- lymph vessel.

5.7.3 Identification of CCR7 Expressing Cells in the Naïve Lung

Next, the aim was to determine, if there were any CCR7 expressing cells in the naïve lung. An adapted panel for the identification of DCs and macrophages, including CD11c, MHCII, CD11b, and CCR7, was used. It turned out that under steady-state conditions parts of the $CD11b^+$ DC and $CD103^+$ cDC populations were $CCR7^+$ (fig. 29 a and b), while IMLCs and AMs did not express CCR7 (fig. 30 c and d). Further, there was another $CCR7^+$ cell population that did neither express CD11c, MHCII, nor CD11b (fig. 30 e). Those cells were smaller and more roundish compared to DCs. A costaining of CCR7 and CD90.2 revealed that those $CCR7^+$ cells were also $CD90.2^+$ (fig. 30 f), indicating that these cells might be naïve T-cells [160]. $CCR7^+CD90.2^+$ cells were located around airways and vessels, but they were also found in the alveolar interstitium. However, approximately half of the $CD90.2^+$ cells did not express CCR7. Neither $CCR7^+$ AMs nor IMLCs were detected in the naïve lung (fig. 30). Further, repetition of this staining after HDM treatment showed no macrophages that were $CCR7^+$ suggesting that antigen bearing AMs and IMLCs have no migratory potential.

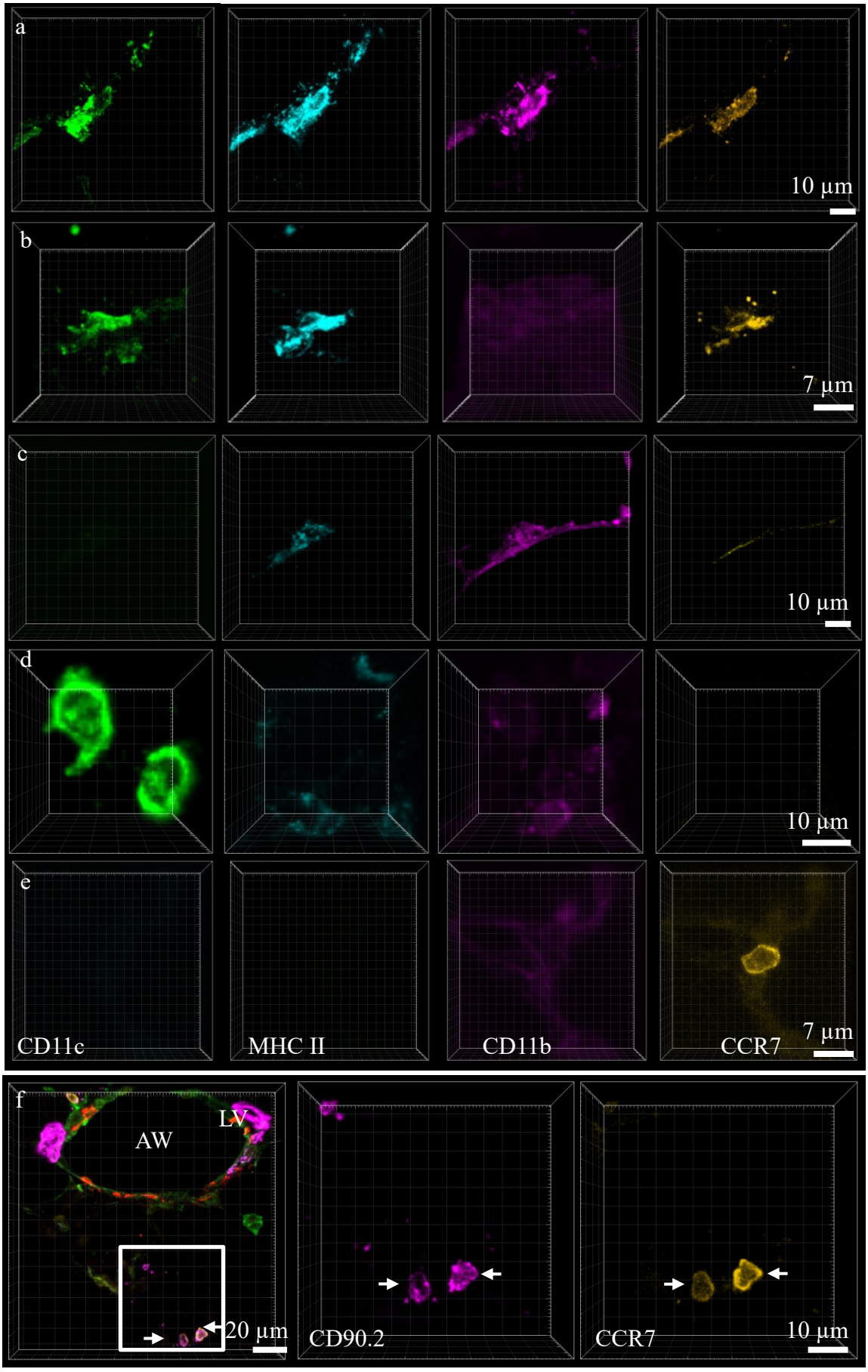
a
10 µm
b
7 µm
c
10 µm
d
10 µm
e
CD11c
MHC II
CD11b
CCR7
7 µm
f
AW
LV
20 µm
CD90.2
CCR7
10 µm

Figure 30: CCR7 expression is restricted to DCs and a subpopulation of CD90.2$^+$ cells. PCLS from naïve C57BL/6 mice (n= 4) were stained with CD11c (green), MHCII (cyan), CD11b (pink), and CCR7 (yellow) to identify CCR7-expressing DCs in the lunge tissue (a-b). IMLCs (c) and AMs (d) are negative for CCR7, while there is an additional CCR7 single positive population (e). PCLS were from naïve C57BL/6 mice (n= 4) stained with CD11c (green), CCR7 (yellow), CD90.2 (pink), and α-SMA (red) to identify CCR7 single positive cells as CD90.2 expressing cells (e and f, arrows). Single stainings in f show a bigger magnification from the box highlighted in the overview image on the left. AW- airway, LV- lymph vessel.

5.7.4 Localization of CCR7$^+$ Dendritic Cells

The presented data suggest that there must be some kind of steady-state turnover in the lung, because there are CCR7$^+$ DCs in the lung of untreated mice. In the next step activated DCs were localized based on their CCR7 expression. The localization of activated DCs also allows conclusions about the sites of activation. To localize CD11c$^+$CCR7$^+$ DCs, they were costained with LVs (CD90.2) and airways and vessels (α-SMA). CCR7 expressing DCs were found around airways, veins and, interestingly, also around intra-acinar arteries in the absence of any CCL21 expressing lymph vessel (fig. 31 a-c). Further, CCR7$^+$ DCs were often located inside of LVs around airways and veins (fig. 31 a and b). Although CCR7$^+$ DCs were often found inside of LVs, there were only a few rare cases observed, where DCs are caught entering a lymph vessel (fig. 31 d) in HDM-treated mice. Although this case was not observed in naïve mice it is likely that this was due to the low number of CCR7$^+$ DCs at steady-state.

Identification of CCR7$^+$ DCs showed that activated DCs were rare at steady-state, but both, CD11b$^+$ DCs and CD103$^+$ cDCs, are able to express CCR7 in the naïve and the HDM-treated lung. To get an overview about the expression of CRR7 a quantification essay was performed. At least 100 DCs per mouse were counted randomly and checked for their CCR7 expression. At steady-state an average of 9.42± 5.34% of the total DC population expressed CCR7 (fig. 32 a). This proportion increased significantly up to an average of 33.39± 11.14% in HDM-treated mice. Further, the proportion of CD11b$^+$ DC and CD103$^+$ cDCs out of the CCR7$^+$ DC population was determined. Because there were only low numbers of CCR7$^+$ cDCs there was a high variation at steady-state regarding the proportion of CCR7$^+$CD11b$^+$ DCs$^+$ to CCR7$^+$CD103$^+$ cDCs. This variation was mainly due to one animal with very high CCR7$^+$ DC numbers (fig. 32 a). There was a tendency towards a higher number of CD11b$^+$ DCs at steady-state (66.73± 23.48%) while the proportion of CD103$^+$ cDCs was higher (58.24± 6.66%) in the inflamed lung (fig. 32 b).

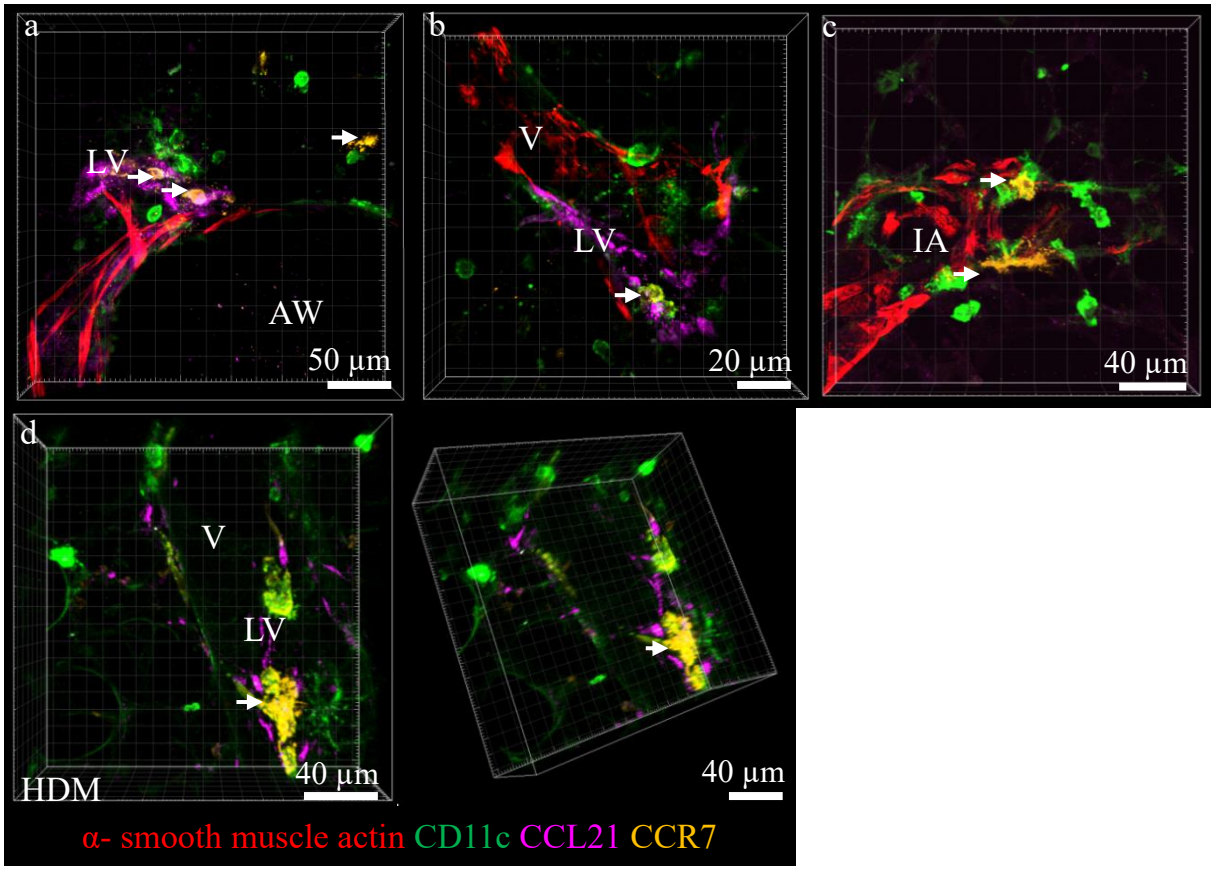

Figure 31: CRR7$^+$ DCs are located around airways, veins, intra-acinar arteries, and inside LVs. PCLS from naïve and HDM-treated C57BL/6 mice (n= 5) sacrificed 24 h after administration were stained with CD11c (green), α-SMA (red), CCL21 (pink), and CCR7 (yellow) to localize CCR7-expressing DCs in the lunge tissue. CCR7$^+$ DCs (arrows) are localized at airways (a), veins (b), and intra-acinar arteries (c) in and outside of LVs. A CCR7$^+$ DC was observed entering a LV (arrow) (d). For a better view a second perspective was added (d, right image). AW- airway, V- vein, IA- intra-acinar artery, LV- lymph vessel.

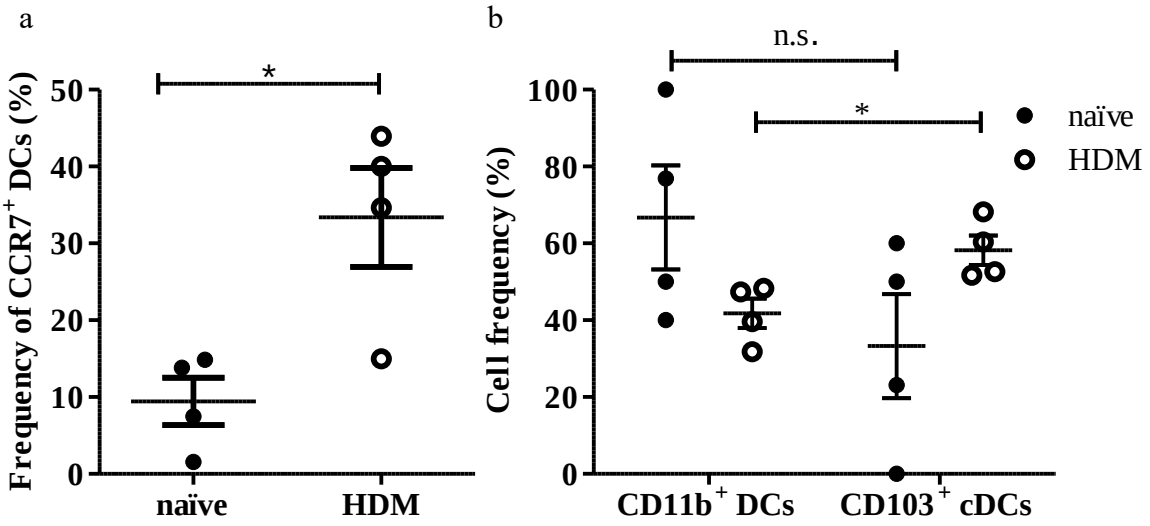

Figure 32: Proportion of CCR7$^+$ DCs increased after HDM stimulation. HDM-treated mice were sacrificed 24 h after allergen administration. DCs were stained on PCLS from naïve C57BL/6 (n= 4) and HDM-treated (n= 4) mice and at least 100 DCs per mouse were screened for their CCR7 expression (a). CCR7$^+$ DCs were separated into CD11b$^+$ and CD103$^+$ DCs to determine their frequency (b). Depicted are mean and SEM; p≤ 0.05 (*), statistical test: Mann-Whitney U-test.

5.7.5 Accumulation of CCR7$^+$ Cells Inside of Lymph Vessels in the Inflamed Lung

As mentioned, CCR7$^+$ DCs were also detected inside of LVs. While there were only few cells observed inside of LVs under steady-state conditions (fig. 33 a) there was a higher number in inflamed lungs. Actually, there were conspicuous clusters of CCR7$^+$ DCs inside of LVs linked to airways after HDM challenge (fig. 33 b-e). To determine the frequency of such clusters, LVs around airways were imaged randomly and cell cluster with equal or more than 5 cells were counted. Since accumulations were quite numerous (fig. 33 b), more than one cluster inside a vessel was set as 1 because quantification was based on the numbers of lymph vessel harboring accumulations and not on the total number of accumulations. Even small clusters were rather uncommon at steady-state and mainly single cells were counted inside the vessels. Unlike several clusters in the same LVs were observed in HDM-treated lungs. In contrast, the percentage of vessels with clusters rose from 7.04± 0.4% at steady-state to 43.27± 6.41% in the inflamed lung (fig. 33 c). Presentation of single channels of a large cluster (fig. 33 d) and changed perspective (fig. 33 e) shows that this cluster of cells is inside the lymph vessel.

The presence of numerous clusters of CCR7$^+$ DCs inside of lymph vessels indicate a disturbed cell transportation within the lymph flow at the airways. Another suggestion is that these

clusters do not appear as malfunction but because DCs are actively accumulating for a functional reason.

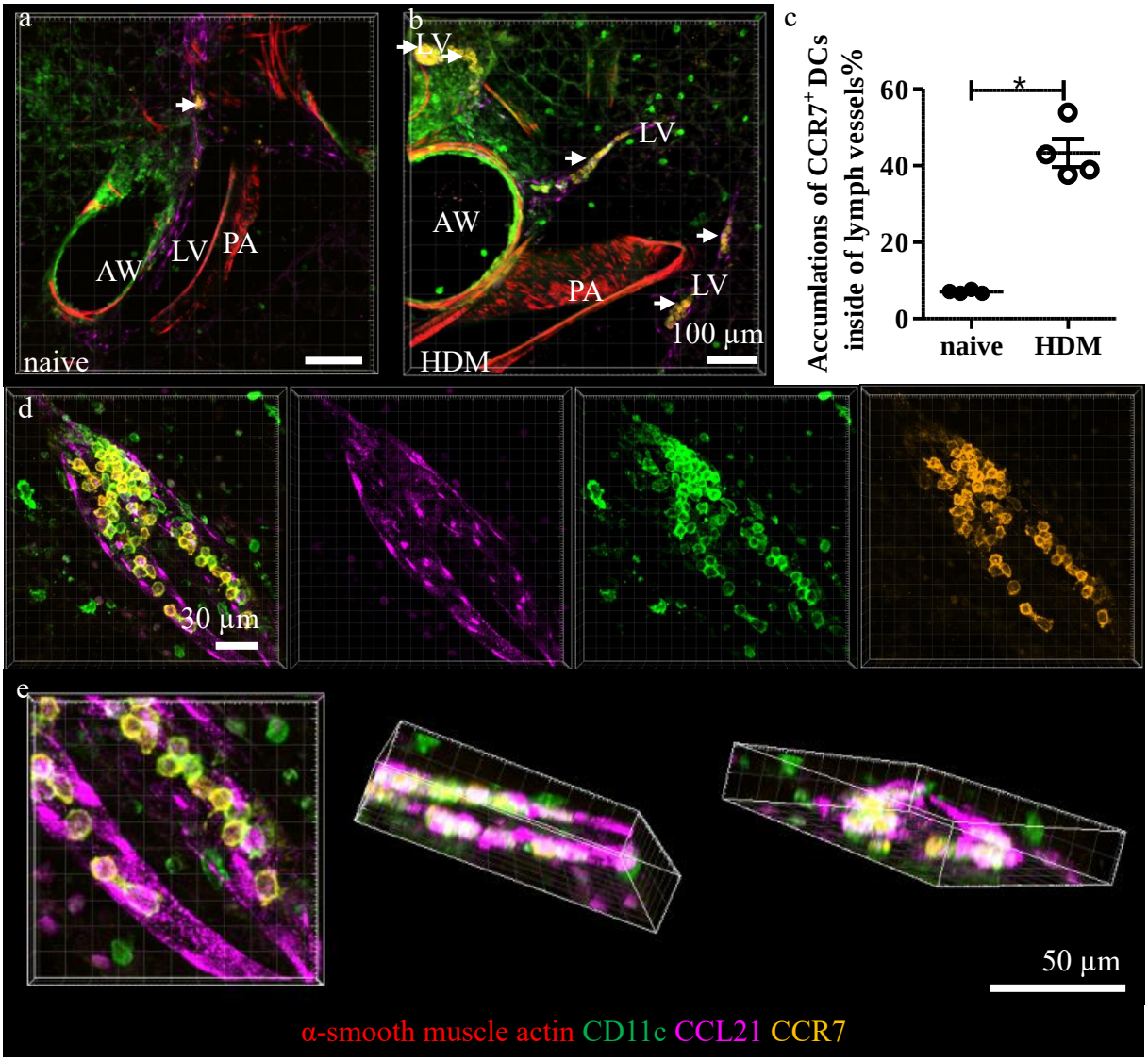

Figure 33: CCR7⁺ DCs are accumulating in lymph vessels around airways after HDM treatment. HDM-treated mice were sacrificed 24 h after allergen administration. PCLS from naïve C57BL/6 (n= 5) and treated (n= 4) mice were stained with CD11c (green), α-SMA (red), CD90.2 (pink), and CCR7 (yellow). Lymph vessels were screened for cell accumulations (≥ 5 cells) and the ratio of lymph vessels that harbors accumulations was determined (a-c). Analysis of single channels (d) and 3D reconstructions that allow a lateral view (e) are shown to prove that accumulations are inside of vessels. Depicted are mean and SEM; p≤ 0.05 (*), statistical test: Mann-Whitney U-test. AW- airway, PA- pulmonary artery, LV- lymph vessel.

5.7.6 CCR7$^+$ DCs are Contacted by CD90.2$^+$ Cells

To prove the hypothesis that there might be interactions inside the LVs, a costaining with CD90.2 was done in naïve and in HDM-treated mice. In those individuals, CCR7$^+$ DCs were imaged inside of LVs and accumulations were analyzed for potential interactions. In naïve mice direct cell contacts between CCR7$^+$ DCs and CD90.2$^+$CCR7$^-$ cells were observed. (fig. 34 a). No contacts were found yet inside of LVs, but due to the low cell numbers it is possible that within a more extensive screening they might be found.

In contrast, contacts between CD90.2$^+$ cells and CCR7$^+$ DCs occurred frequently inside of LVs of HDM-treated animals. Cell contacts were observed with single CCR7$^+$ DCs (fig. 34 b), as well as inside of cell accumulations (fig. 34 c and d). Within those accumulations determination of cell contacts was difficult but by analysis of the single layers at the z-axis it became apparent that there were clear contacts between CCR7$^+$ DCs and CD90.2$^+$CCR7$^-$ cells were observed.

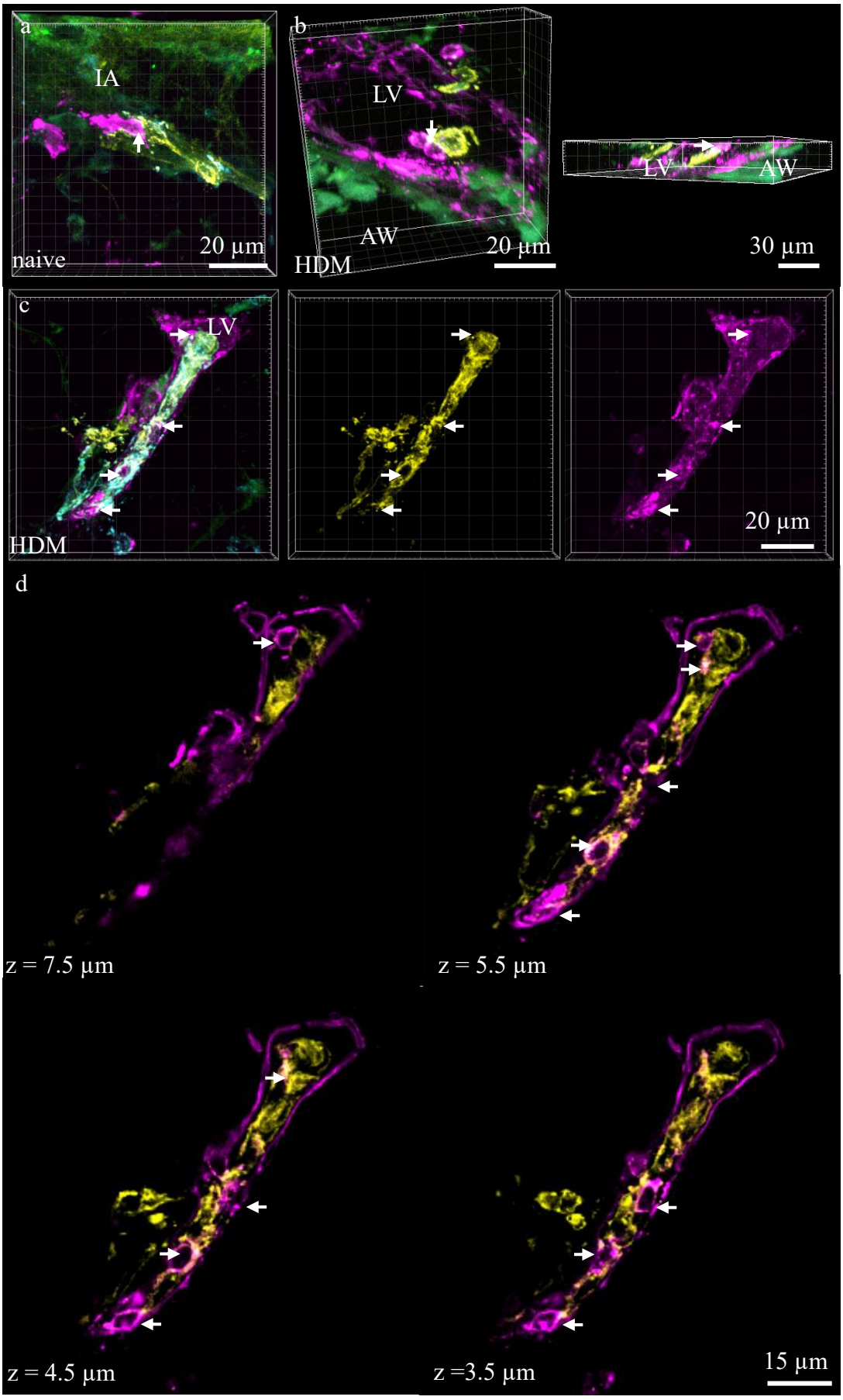
a
IA
20 µm
naive
b
LV
AW
20 µm
HDM
LV
AW
30 µm
c
LV
HDM
20 µm
d
z = 7.5 µm
z = 5.5 µm
z = 4.5 µm
z =3.5 µm
15 µm

Figure 34: CCR7 expressing DCs are in contact to CD90.2$^+$ cells inside and outside LVs. HDM-treated mice were sacrificed 24 h after allergen administration. PCLS from naïve C57BL/6 (n= 4) and treated (n= 3) mice were stained with CD11c (green), MHCII (cyan), CD90.2 (pink), and CCR7 (yellow). Arrows indicate cell contacts between CCR7$^+$ DCs and CD90.2$^+$ cells at steady-state at an intra-acinar artery (a), and inside a LV after HDM treatment (b) Cell contacts were also observed in DC accumulations inside of LVs (c) including single focal planes (d). AW- airway, LV- lymph vessel., IA- intra-acinar artery.

6 Discussion

For the first time this study provides a comprehensive overview regarding the localization of different subtypes of DCs and macrophages in C57BL/6 and BALB/c mice. Such an overview is important since cell localization already provides hints regarding possible cell functions. In addition, the observation of cell contacts is only possible by staining of different cell populations simultaneously. Using a four-color panel for IHC the visualization of $CD103^+$ cDCs, $CD11b^+$ DCs, AMs, and IMLCs at the same time was possible. The inclusion of CD64, a typical monocyte marker [161], further provided data regarding a monocytic-lineage for a subpopulation of $CD11b^+$ DCs and IMLCs in steady-state with increasing frequency of $CD64^+CD11b^+$ moDCs after HDM treatment. Further, these populations were quantified by a microscopy-based approach, because until now there is no study available dealing with total numbers for DCs, AMs, and IMLCs. The comparison of data derived by flow cytometry or microscopy showed major differences concerning the ratio of $CD103^+$ cDCs to $CD11b^+$ DCs under steady-state conditions. Additionally, there was a big discrepancy regarding the frequency of resident moDCs based on CD64 expression which was resolved by the usage of C5aR1/CD88. Localization analyses identified airways, the connective tissue between airway and pulmonary artery, as well as intra-acinar arteries and veins as regions where DCs and IMLCs are located. The combination of localization and quantification also allowed to discover a specific cell contact between $CD103^+$ cDCs and newly defined IMLCs around airways and blood vessels which decreases after allergen challenge. Since a related study in the working group has observed that IMLCs are very efficient early antigen uptakers (Johann Berger, unpublished data), this contact might be important for the onset of a regulatory immune response as it was shown for similar populations in the gut [1]. Although, IMLCs take up considerable amounts of antigen they did not show any migratory potential at steady-state or after HDM treatment based on CCR7. Nevertheless, this study provides strong hints for steady-state turnover of DCs in the lung since about 10% of total DCs expressed CCR7 at steady-state with increasing prevalence after stimulation with HDM. Interestingly, airway adjacent LVs harbored large accumulations of DCs in HDM-treated mice which were not found under steady-state conditions. This finding indicates that activated DCs interact with T cells or ILCs in the lung and inside of pulmonary LVs which might lead to the induction of an immune response without the need of a lymph node. The induction of an inflammatory immune response without the need of lymph nodes was described for $CCR7^{-/-}$ mice [142], while intrapulmonary interactions of DC and T cells also have been reported before [115].

6.1 Identification, Quantification, and Localization of Pulmonary Phagocytes

6.1.1 Identification

The detection of pulmonary phagocytes inside the lung tissue is sometimes difficult due to high autofluorescence of the tissue and especially the airway epithelium under naïve and especially HDM-induced asthmatic conditions. Further, influx of immune cells and cell accumulations around airways [115] impeded with cell identification. Using three-dimensional confocal laser scanning microscopy enabled me to overcome these problems by the possibility to analyze different focal planes. The combination of CD11c, CD11b, Langerin and MHCII allows the reliable identification of AMs, $CD103^+$ cDCs, $CD11b^+$ DCs, and IMLCs. An adaption of the panel used to identify DCs and macrophages excluding Langerin and including CD64 allowed the discrimination between $CD11b^+$ cDCs and $CD11b^+$ moDCs. Further, inclusion of this marker shed light on the monocytic origin of the newly defined IMLC population and enables the identification of monocytes itself. Based on this adapted four-color panel six populations of pulmonary phagocytes can be identified simultaneously making it a useful tool for further analyses.

Until now publications showing immunohistochemistry for DCs have focused on single subsets [70, 115, 117] and, therefore, there is a need for a comprehensive overview. Regarding IMs the literature is inconsistent and no uniform definition is existing [2, 106, 107, 135]. Despite this inconsistency there is a congruency resulting in a $CD11c^-CD11b^+MHCII^+$ phenotype [66]. Although $CD11c^+$ IMs have been reported [67, 162], any $CD11c^+$ IM was found in this study. This is explained by the fact, that in this experimental setup $CD11b^+$ IMLCs would phenotypically match $CD11b^+$ DCs. In addition, in these studies IMs were defined from a gate with a broad range of expression of CD11c including $CD11c^+$, $CD11c^{int}$ and $CD11c^-$ cells. Based on these strategies it is not clear to which extent IMs express CD11c [67, 162]. Further, cells with a marker profile matching the IM phenotype were not found in the alveolar interstitium as it was described before [2] and therefore called IM-like cells. However, those IMs described by Bedoret [2] were identified to interact with DCs in an anti-inflammatory manner. They seem to be identical with the IMLCs that I observed to interact with $CD103^+$ cDCs. In addition, it was previously shown in the gut that a similar interaction has led to a tolerogenic immune response [1].

Originally it was thought that at steady-state there were only three populations of DCs ($CD11b^+$ cDCs, $CD103^+$ cDCs, and pDCs) and that DCs with monocytic origin will only be recruited to the lung under inflammatory conditions [51]. However, in the last years an increasing number of publications presented evidences for resident $CD11b^+$ moDCs in the steady-state, suggesting that the population, which was supposed to be $CD11b^+$ cDCs, in fact consists of two populations from different lineages. These populations, depending on the study, were only distinguishable by the addition of markers like C5aR1 [52] or lineage tracing [68], but clear evidence is still lacking. CD64 is a typical marker to detect cells with monocytic origin [161] and was described to be a suitable marker to define moDCs [51]. Nevertheless, Plantinga *et al.* [51] detected only very small amounts of resident moDCs in their control mice. In contrast to this finding, which has also been reproduced in this study, about half of the $CD11b^+$ DC population was identified to express CD64 by IHC using the same antibody clone. This indicates a general problem regarding the surface staining of CD64 for flow cytometry. Comparison of C5aR1/CD88 and CD64 showed that both markers stained the same cells including monocytes, AMs, IMLCs, and resident moDCs at steady-state. In fact, using C5aR1 to distinguish between $CD11b^+$ cDCs and moDCs reflects the data obtained by IHC based on CD64 as discriminative marker. Further, it agrees with the data of Nakano *et al.* [52] regarding the presence of a mixed $CD11b^+$ DC population at steady-state and the usefulness of C5aR1 as suitable marker to define different lineages inside the population. Unfortunately, the gating strategy presented by the group of Donald Cook [52] did only work for C57BL/6 but not for BALB/c mice. This problem was resolved by the reliable identification of $CD11b^+$ moDCs in both strains using IHC in this study.

A former study presenting a C5aR1-GFP mouse also showed C5aR1 expression for $CD64^+$ moDCs. In addition, this study showed a mixed $CD64^-CD11b^+$ cDC population regarding their expression of C5aR1 in approximately a 1:1 ratio [153]. Compared to the data by Nakano *et al.* [52] and this study it is likely, that the moDCs population is highly underrepresented in the study by the Köhl group [153] dependent on insufficient detection of CD64 in those cells. Flow based analyses of $CD64^+$ moDCs are dependent on cell isolation and suitable gating strategies while cell labeling in IHC shows all cells that express the selected markers at the same time in their natural environment. Because no gating is necessary any cell can be lost during the gating process that is based on positive and negative selection. In addition, based on the reported inconsistency regarding cell frequencies in flow cytometry it has been suggested that there is an alteration of surface marker expression during the isolation process resulting in varying results between flow cytometry and microscopy [163]. For example, the

strategy presented by Nakano *et al.* [52] did not work properly for BALB/c mice because they showed a slight difference in their CD24 expression compared to C57BL/6. This is a non-existing problem for immunohistochemistry on tissue sections because no preselection is necessary due to the simultaneous examination of all relevant markers. This was also demonstrated by the successful and unambiguous identification and quantification of $CD11b^+$ cDCs and $CD11b^+$ resident moDCs in both C57BL/6 and BALB/c mice.

6.1.2 Quantification

Reliable identification of pulmonary phagocytes enabled this study to perform a quantification assay and compare cell frequencies between naïve and HDM-treated mice and C57BL/6 and BALB/c mice. For cell quantification, a method based on several extrapolation steps was established for this study. DCs and macrophages were counted on a specified area of the lung and the numbers were extrapolated to the absolute numbers for the whole lung. Quantification assays based on microscopy are very time consuming and need a good strategy to ensure representative results. Thus, flow cytometry is regarded as the faster and more reliable technique to gain quantitative data. However, comparison of quantification data derived by IHC or flow cytometry has shown that numbers of $CD8^+$ memory T cells were highly underestimated in non-lymphoid organs using flow cytometry [152] questioning the suitability of flow cytometry based approaches for the determination of total cell numbers. The best way to quantify cells using a microscopy based approach is automated stereology [152, 163], which includes automated imaging of randomly selected areas on the slice and software for cell counting. Ideally an automated tool for stereological imaging and cell counting would have been used in this study. Since the suitable equipment was not available an alternative stereology-like approach was designed. At steady-state this approach allowed the generation of reproducible data regarding absolute and relative cell numbers, which were additionally comparable to published quantification data [67, 70, 71]. The accuracy of this method was supported by low standard deviations. However, compared to an automated stereology approach this assay only works in an adequate way for cells that are equally distributed in the tissue. After HDM treatment cells were not distributed equally anymore but irregularly accumulated around airways [115] and blood vessels. Due to this inhomogeneous distribution, total cell numbers were underestimated (supplementary fig. 1). This became apparent during the counting process, since in the HDM-treated mice there were images with high cell numbers and others with very low cell numbers. High cell density on a small area also constitutes the

problem that it was difficult to identify single cells resulting in the underestimation of cells in these accumulations. The problem of inhomogeneous cell distribution and the possible underestimation of cells in accumulations can be overcome by automated stereology because a higher number of regions of interests can be analyzed which will diminish the effects of inhomogeneous cell distribution. It was not possible to increase the sample size in this study since collection of image data took a full working day (20-30 min per image). The continuation on the next day was not advisable since it cannot be excluded to image same areas again. In addition to the time that was needed for data collection, one or two additional days were required for cell counting. Nevertheless, since the different subsets did not change their distribution pattern besides the formation of cell clusters cell data regarding cell frequencies were still reliable resulting in small standard deviations. Taken together, automated stereology would be the most reliable technique to quantify pulmonary phagocytes, but the assay established in this study allows the determination of cell frequencies in naïve and HDM-treated mice. Although there is no proof for the accuracy of the total numbers presented in this study, based on small standard deviations presented frequencies can be considered as true.

6.1.3 Localization

Reliable identification is also a fundamental requirement for cell localization. Combination of identification, quantification, and localization allows the investigation of cell interactions. For the analysis of cell localization, autofluorescence is a useful tool for navigation inside the lung, since airways and blood vessels show specific autofluorescence patterns. For a long time $CD103^+$ cDCs were postulated as intraepithelial cells sampling antigen from the airway lumen [101, 112, 113, 164]. However, more recent studies have questioned this assumption since none or only few intraepithelial DCs were identified [114, 115]. In contrast, active sampling of the alveolar lumen has been shown in an OVA-mediated model of allergic asthma *in vivo* using intravital lung imaging [115]. In this study neither any intraepithelial DC nor a DC sampling the airway lumen has been identified in naïve and HDM-treated mice. In fact, $CD103^+$ cDCs and $CD11b^+$ DCs were located in exactly the same regions, including airways and blood vessels. In contrast to earlier reports [62, 115, 116], no $CD11b^+$ DCs, including cDCs and moDCs, were identified in the alveolar interstitium. This difference might be explained by the fact, that the alveolar interstitium contains many small blood vessels that can be easily overlooked and in addition the distribution of blood vessels was not taken into account in those studies. Therefore, it is likely that $CD11b^+$ DC described for the alveolar interstitium represent cells located around

vessels. Likewise, the distribution of $CD103^+$ cDCs around pulmonary arteries was described before [70]. A separate analysis in this thesis based on CD64 revealed, that there is no difference concerning cell localization between $CD11b^+$ cDCs and $CD11b^+$ moDCs at steady-state and in the HDM-treated lung. In contrast to the other DC populations, pDCs were not found in the airway adjacent regions but in the alveolar interstitium as described before [70, 118]. Although it is generally accepted that AMs are situated in the alveolar lumen [62, 119, 120], there is an argument whether there are also tissue-resident AMs present in the lung because not all AMs are removable by BAL [119]. The findings of this study support another hypothesis, describing a separation of AMs into alveolus-adherent and alveolus-non-adherent AMs [55].

In principle cell localization was not altered during early inflammation, but an accumulation of DCs close to the airways [115, 165] and around vessels was observed while AMs were not affected. Combined with the data of another study from this lab showing antigen uptake around airways and, in addition, also around blood vessels (Berger unpublished), this study identified interstitial antigen-uptaking cells (IMLCs, $CD11b^+$ DCs, $CD103^+$ cDCs) located at all sites were antigen uptake has been observed.

6.2 Comparison of Microscopy and Flow Cytometry

Nowadays, flow cytometry has become a popular technique to define different cell subsets in immunologic assays. Often flow cytometry is used to observe differences in the frequency of cell populations after stimulation with a certain substance like HDM in a model of allergic asthma. Once a subset is well defined, cells can be sorted and used for functional studies *in vitro* or *in vivo* via adoptive transfer. In contrast, it is more difficult to collect functional data by microscopy for several reasons. Firstly, many organs are difficult to image *in vivo* or *ex vivo*. Secondly, data generation takes much longer. However, *in vivo* lung imaging has been established in recent years [115, 149]. Nevertheless, microscopy-based analyses are necessary to observe cells in their natural environment and shed light on their localization inside the tissue. Further, they are crucial for the detection of possible cell interactions at steady-state and under inflammatory conditions, as shown in this study for $CD103^+$ cDCs and IMLCs. The observation of cell contacts and potentially resulting interactions is difficult using flow cytometry. For the analysis of cells that are in physical contact to other cells the Image Stream® technology is necessary because conventional flow cytometry alone does not represent an adequate method for the analysis of cell doublets. Image Stream® combines the advantages of flow cytometry (speed, sensitivity, and phenotyping abilities) with the detailed imaging. Nevertheless, most cell

contacts will be cleaved during the cell isolation progress which complicates the analysis. Further, for a long time most studies dealing with allergic asthma were concentrating only on $CD11c^+$ subsets and overlooked $CD11c^-CD11b^+MHCII^+$ macrophages which is almost impossible using IHC since no population can be gated out.

As mentioned in the introduction both techniques have their advantages and disadvantages and for best results there is the need to combine both techniques in the same study. A former study already pointed out that flow cytometry is a useful method for the characterization of cells in a multifactorial approach while immunohistochemistry is more adequate for quantification since no isolation is needed. Further they indicated, that surface markers might be altered by the isolation process [163]. Recently it has been pointed out that there are substantial differences regarding the accuracy of flow cytometry compared to microscopy concerning the quantification of $CD8^+$ memory T cells in non-lymphatic organs [152]. A stereological approach detects and quantifies cells in their natural environment while cell isolation for flow cytometry is based on strong mechanical disruption of the tissue to get a single cell solution. The study focusing on $CD8^+$ memory T cells pointed out, that it is more difficult to isolate immune cells from non-lymphoid organs compared to lymph node or spleen which might be due to larger amounts of connective tissue in non-lymphoid organs. However, the mechanical stimuli or enzymes for tissue digestion during cell isolation might also cause changes to proteins on the cell surface as suggested before [163]. In addition, regarding pulmonary DCs big discrepancies have been reported for the frequency of $CD103^+$ cDCs in different flow cytometry based studies (reviewed in [66]). Since most of the studies were using the same antibody clones and similar gating strategies for cell identification an explanation for different results was presumed based on different isolation protocols and especially different enzymes. However, it is unlikely that the usage of different enzymes is responsible, since the studies of Nakano *et al*. [52, 98] and Plantinga *et al*. [51] resulted in different ratios of $CD103^+$ cDCs:$CD11b^+$ DCs, but were based on tissue digestion by Liberase TM (Roche, containing Collagenase I+II) and DNAse I. In addition, also other studies using Collagenase D (Invitrogen) [67, 70] or Collagenase IV (Roche) [68] in combination with DNAse I also resulted in different frequencies regarding $CD103^+$ cDCs. Since the hypothesis that these differences are caused by the used enzymes for digestion was disproved another, so far unknown, factor during cell isolation, staining, or analysis must cause the differences in marker expression. Similar to the differences described regarding the frequencies of $CD103^+$ cDCs, $CD11b^+$ resident moDCs represent an additional population which seems to be underrepresented by flow cytometry at least by the

usage of CD64 [51] compared to C5aR1 as discriminative marker [52]. However, comparison of both markers using IHC revealed that both markers specifically stain for the same cells.
Taken together, the comparison of different studies focusing on DC ratios resulted in different frequencies although the same reagents were used and there must be another reason causing these considerable differences which needs to be uncovered to allow a better comparability between studies from different groups. Taken together flow cytometry is a useful method to characterize different cell subsets since many markers can be used at the same time. However, flow cytometry is not the method of choice for the determination of total cell numbers and frequencies since cell isolation especially from non-lymphoid organs involves some problems. A stereological approach based on microscopy is more time-consuming compared to flow based quantification, but results in more accurate results. Further, only microscopy allows the observation and quantification of cell contacts and interactions.

6.3 Lung-Resident Monocytes, IMLCs, and Monocyte-Derived DCs

As described above, interstitial macrophages are a population of rather poor defined cells. Recently, many studies were published, that examined IMs, but there is no consensus about their definition. Based on the accordance regarding some markers, that have been published [2, 65, 97, 135], IMs in this study were characterized as $CD11c^{-}CD11b^{+}MHCII^{+}$ cells which were renamed to IMLCs due to striking differences regarding the reported localization of IMs [2]. Further characterization using the additional markers CD64 and C5aR1 revealed that IMLCs rise from a monocytic background. The successful combination of identification, localization, and quantification, enabled me to discover a specific cell contact between IMLCs and $CD103^{+}$ cDCs around airways and to a lesser extend also around blood vessels at steady-state. Those contacts were significantly decreased 24 h after antigen encounter. An uptake study based on the cell identification and localization data of this study using the same marker panels (Berger, unpublished) revealed that IMLCs were the main antigen uptaking cells in the first hours after antigen encounter to the lung. A similar contact for a $CD103^{+}$ DC and a $CX3CR1^{+}$ monocyte-derived macrophage population was recently described in the gut. It was shown that the $CX3CR1^{+}$ macrophage took up large amounts of antigen and transferred membrane particles with MHCII-bound peptides via Cx43 channels to the $CD103^{+}$ DC. This interaction facilitates $CD103^{+}$ DCs to induce a regulatory T cell response towards oral antigen resulting in oral tolerance [1]. It is therefore conceivable, that a similar mechanism is also

present in the lung. Preliminary data showed low Cx43 expression in $CD103^+$ cDCs and AMs but not in IMLCs (data not shown). AMs have been reported before to communicate via gap junctional proteins with the alveolar epithelium [55] indicating that Cx43 possesses an important role for the communication between immune cells and between immune cells and the epithelium. An indication for the presence of a similar interaction between IMLC and $CD103^+$ cDCs was provided by a study performing a coculture of pulmonary DCs with IMs. This experiment resulted in the repression of the inflammatory response, compared to single DC culture or DC:AM coculture, based on IL-10 that was secreted by IMs [2]. Further examinations are needed to investigate the suggested interaction between IMLCs and $CD103^+$ cDCs. For the determination of this potential interaction as a first step the isolation of IMLCs and both cDC populations will be necessary to determine, if a coculture of IMLCs with $CD103^+$ cDCs or $CD11b^+$ cDCs results in the secretion of IL-10 after stimulation. In a second step, imaging of lung slices *ex vivo* or intravital lung imaging can be used to observe cell contacts in their natural environment. Since it was shown that IMLCs are rapid antigen uptakers (Berger, unpublished) the administration of labeled antigen on lung slices *ex vivo* could shed light on the possibility of antigen transfer between IMLCs and $CD103^+$ cDCs.

Based on the lack of CCR7 expression IMLCs represent a non-migratory subset. Data from a related project within the IRTG1911 also showed no $CD11c^-CD11b^+MHCII^+$ cells in the lung draining lymph nodes up to 72 h after antigen encounter (Ender, unpublished). This is in accordance with the hypothesis that IMLCs act as antigen uptaking cells, which transfer parts of the processed antigen to $CD103^+$ cDCs, as it was shown in the gut [1]. Accordingly, $CD103^+$ cDCs were shown to migrate in a CCR7-dependent manner towards the lung draining lymph nodes, where they induce tolerance as described before [142, 143]. In this scenario, there is no need for a migratory activity by IMLCs. However, there is no final proof for IMLCs as non-migratory population available at the moment. On the other hand, the changes in IMLC and $CD11b^+$ DC frequencies after HDM stimulation indicate, that IMLCs might act as precursors for $CD11b^+$ inflammatory moDCs, because an influx of non-migratory $C5aR1^+CD64^+CD11b^+$ moDCs was shown under inflammatory conditions in this and also in other studies [51, 52, 73]. On first sight these findings seem to be contradictory because on the one hand an anti-inflammatory role was suggested for IMLCs and moDCs clearly act proinflammatory [51, 52]. Nevertheless, it can be hypothesized that IMLCs have different functions and act depending on the received stimulus. Based on their activation they can either act tolerogenic or promote inflammation.

However, a proper way to define IMs is urgently needed since it has also been shown that $CD11b^+Ly6C^+MHCII^-$ circulating blood monocytes enter non-inflamed tissues where they upregulate $MHCII^+$ [97]. Phenotypically these cells are very similar to IMs and IMLCs since these tissue monocytes were also able to ingest antigen and transport it to the draining lymph nodes. The same study indicates that tissue monocytes still resemble blood monocytes rather than macrophages or DCs although they share common characteristics. It is feasible, that $MHCII^+$ tissue monocytes already received a stimulus resulting in MHCII expression probably induced by the ingestion of antigen while $MHCII^-$ tissue monocytes are more immature. It therefore, remains unclear whether the cells defined as IMLCs here are bona fide macrophages or represent tissue monocytes. Regarding the similarities and confusions between tissue-resident monocytes and IMs or IMLCs it is likely that tissue-resident monocytes and IMs/ IMLCs are the same cell population that were differently characterized based on different staining and gating approaches. Lineage tracing revealed that $CD11b^+$ cDCs and moDCs rise from different origins [90, 92, 166], while the origin of IMs is still under debate since no uniform definition is available. Data presented here indicates that IMLCs might act as a lung-resident $CD11b^+$ moDC precursor. It was described that moDCs, that are recruited to the lung under inflammatory conditions, show a $Ly6C^+$ phenotype, although also a loss of Ly6C expression during the maturation progress from monocyte to moDCs was reported [51, 52]. Unfortunately, my study failed to shed light on the expression of Ly6C on IMLCs using currently available antibodies for IHC or to clarify, if there is a difference in Ly6C expression between resident and inflammatory moDCs. However, the presence of Ly6C on IMLCs would be an additional hint suggesting their role as a precursor. To analyze the relationship of IMLCs, $CD11b^+$ cDCs, and $CD11b^+$ resident moDCs a RNA-based gene expression analysis for this populations was planned. Comparison of histological data with established panels for flow cytometry to detect DCs [153] and macrophages (Dunkel, unpublished) by cooperating projects revealed, that those panels can be used for cell sorting with slight adaptions for the sequencing approach. Unfortunately, technical problems inhibited the isolation of IMLCs, because the staining did not work properly at the cooperating facility at the Cincinnati Children's Hospital Medical Center compared to the staining that has been established in Lübeck. Nevertheless, suitable conditions for the isolation of $CD11b^+$ cDCs and $CD11b^+$ resident moDCs were established in Cincinnati based on their different expression of C5aR1. The establishment and optimization of suitable conditions for cell sorting will allow us to purify DC and macrophage subpopulations and to analyze their ontogenetic background by RNA sequencing in a follow up study.

Analysis of the mRNA level of CCR7 in different pulmonary DC populations also identified moDCs as non-migrating population [73]. Functional data propose a proinflammatory role for $CD11b^+$ DCs in allergic asthma [51, 53, 54, 85, 124]. However, most studies are dealing with the total $CD11b^+$ DC population and only few studies focus on the $CD11b^+$ cDC and moDC subsets. Those studies showed that $CD11b^+$ cDCs are more efficient in driving an inflammatory Th2/Th17 response compared to moDCs [51, 52]. This is congruent with the assumption that moDCs mature from IMLCs in a proinflammatory environment inducing a positive loop of lung-resident moDCs acting proinflammatory, which results in the recruitment of inflammatory moDCs to the lung. This might be linked to the fact that, although moDCs represent the largest DC population in the inflamed lung, only few moDCs were found in the lymph node due to their limited migratory properties [51, 73]. Whereas moDCs were shown to be very efficient producers of proinflammatory cytokines like IL-6 and TNF-α [52]. Studies using $C5aR1^{-/-}$ mice showed exacerbated asthma features in those animals. Further it was shown that C5aR1-mediated signaling is active in moDCs [130, 167, 168]. Taken together this indicates that C5aR1 has a regulatory function in moDCs, which is abrogated in $C5aR1^{-/-}$ animals, resulting in exacerbated asthma features which are caused by $C5aR1^{-/-}$ DCs promoting the production of proinflammatory cytokines by T cells in the effector phase.[167]. In contrast, dysfunction of C5 [169, 170] or the C5ar1 [167, 171, 172] resulted in an increased asthma phenotype, suggesting an anti-inflammatory role for C5aR1, indicating a dual role for C5a or C5aR1.

This study revealed a significant higher number of $CD64^+C5aR1^+$ resident moDCs in the lungs of naïve BALB/c mice compared to C57BL/6 mice. Due to their higher susceptibility to allergic asthma BALB/c mice are the most common strain used for asthma research. However, until now there is no explanation for this difference and potentially the numbers of resident moDCs or a different regulation of C5aR1 on these cells might have an influence on the asthma prevalence of different mouse strains. Based on this observation the analysis of the functional influence of C5aR1 on these cells might be a promising approach to unravel the differences regarding asthma susceptibility between BALB/c and C57BL/6 strains.

6.4 Migration

Migration of activated DCs to the draining lymph nodes in a CCR7 dependent manner is believed to be crucial for the induction of an immune response while it has been shown, that an inflammatory response towards inhaled allergen can be established in the absence of $CCR7^{-/-}$ [137, 142, 160]. This study showed the expression of the CCR7 ligand CCL21 on all pulmonary lymph vessels, that are running with airways, veins, or in the connective tissue between pulmonary artery and airway. The staining pattern indicates that CCL21 is secreted by lymphatic endothelial cells. Although previously described for the skin [173-176], a CCL21 gradient was not identified by immunohistochemistry in the lung, but CCL21 secreted to the tissue might be washed out during sample preparation and its presence is therefore not excluded by this finding. In this study, CCR7 expression in the lung is restricted to DCs and a $CD90.2^{+}CCR7^{+}$ positive population which might represent naïve or memory T cells [160, 177]. Those CCR7 expressing DCs were situated around airways, veins, pulmonary arteries, and partly inside of lymph vessels. Interestingly $CCR7^{+}$ DCs were also found around intra-acinar arteries in the absence of any lymph vessels.

The presence of steady-state migration is still highly debated [51, 145], but the presence of CCR7 expressing DCs in the steady-state clearly indicates the presence of such a mechanism. Activated $CCR7^{+}$ DCs were found on all lung compartments where antigen uptake has been reported including airways as well as blood vessels (Berger, unpublished) except for the alveolar space [115]. However, since the study reporting antigen uptake from the alveolar lumen did not consider any blood vessels it is likely that they described uptake around blood vessels, especially because no DCs were found apart from blood vessels in the alveolar region in this study in naïve and HDM-treated lungs. Interestingly, the same study showed accumulations of antigen harboring $CD11b^{+}$ DCs close to airways where they interacted with T cells in the effector phase of an OVA-mediated asthma model. These accumulations might represent the accumulations inside of airways adjacent lymph vessels observed in this study after HDM-treatment, since cell contacts to $CD90.2^{+}$ cells, probably T cells, were shown. Cell contacts between $CCR7^{+}$ DCs and $CD90.2^{+}$ cells were also present outside of lymph vessels. Studies using $CCR7^{-/-}$ showed an exacerbated asthmatic phenotype compared to control animals, because $CD103^{+}$ DCs were not able to migrate to the lymph node to induce a regulatory response [142, 143]. These observations indicate that there might be a lymph node independent mechanism for the induction of an inflammatory immune response in the lung.

Stimulation with HDM induced a significant increase in the amount migratory DCs, while $CD103^+$ cDCs and $CD11b^+$ DCs showed similar frequencies of $CCR7^+$ cells. Due to low cell numbers the quantification assay is based on a small sample size resulting in a high variation especially for naïve mice regarding the CCR7 expression in $CD11b^+$ DCs or $CD103^+$ cDCs. With one exception [175] previous studies dealing with $CCR7^+$ DCs were using CCR7-GFP mice [74] or $CCR7^{-/-}$ mice to examine the consequences of the absence of migratory DCs [142, 143]. Reporter mice for CCR7 were not available in this study and an antibody-based approach for flow cytometry was unsuccessful since staining for CCR7 did not work. Therefore, data presented in this study presents a first guideline with respect to frequencies of $CCR7^+$ DC subsets, but need to be repeated with alternative techniques. However, considering what is known about accuracies of quantificational assays a stereological approach based on IHC might be the most useful approach.

No migratory potential based on CCR7 was found for IMLCs, since neither at steady-state nor after HDM stimulation any CCR7 expressing IMLCs were detected. This is in accordance with the hypothesis that IMLCs might be lung-resident moDCs precursors as moDCs were reported to show only limited migratory potential [51, 73]. However, no migratory potential was also described in a functional study using $CD11b^+Gr1^+F4/80^+$ myeloid cells which resemble IMs based on their marker profile [106, 107]. Nevertheless, since IMLCs phenotypically are also similar to tissue monocytes, which are reported to migrate to the lymph nodes in a CCR7 independent way [97] analysis of other markers might be useful.

6.5 Conclusion

This study presents a detailed overview about the steady-state lung including identification, localization and quantification of up to six pulmonary subsets simultaneously using a four-color panel for IHC. Further, a comparison with conditions during early inflammation 24 h after HDM administration was given. Localization and quantification analyzes uncovered a specific cell contact between an IM-like cell population and $CD103^+$ cDCs, which was abrogated after antigen encounter. Based on a similar cell contact reported in the gut [1] resulting in the induction of tolerance, it is likely that a similar mechanism is also present in the lung. As a first hint a former study has already shown the secretion of IL-10 by IMs that suppressed the inflammatory response induced by DCs [2].

Characterization of this IMLCs in the lung revealed that these cells share many characteristics with tissue-resident monocytes [97]. In addition, IMLCs might also be linked to moDCs based

on their similar morphology, localization, and marker profile. This once again points out how important a universal strategy for DC, macrophage, and monocyte classification is needed. Recently, different groups suggested new strategies based on ontology or function [65, 178] but so far none of them was generally accepted. For a long time studies were only focusing on DC subsets, but since the different phagocyte populations are very similar and there is a high plasticity especially for monocytes focusing on a single subset does not represent the overall mechanism.

Data from this study combined with data from the literature also indicate an ambivalent role for IMLCs in a way that depending on the stimuli present in the tissue one the one hand they might interact with $CD103^+$ cDCs resulting in the induction of tolerance, while on the other hand they might be tissue-resident precursors for inflammatory moDCs based on their marker profile and changing frequencies after HDM stimulation. Further, as suggested before [66] the combination of flow cytometry and IHC is needed for the successful investigation of the pathogenesis of allergic asthma, since it was shown here, that the expression or at least the detection of surface markers can be altered during cell isolation for flow cytometry. A conceivable strategy might be the characterization of localization, quantification, and possible cell contacts by IHC, while basing on these findings flow cytometry can be used for further characterizations in combination with RNA sequencing and functional analysis using sorted cells.

7 Literature

1. Mazzini, E., et al., *Oral tolerance can be established via gap junction transfer of fed antigens from CX3CR1(+) macrophages to CD103(+) dendritic cells.* Immunity, 2014. **40**(2): p. 248-61.

2. Bedoret, D., et al., *Lung interstitial macrophages alter dendritic cell functions to prevent airway allergy in mice.* J Clin Invest, 2009. **119**(12): p. 3723-38.

3. Kopf, M., C. Schneider, and S.P. Nobs, *The development and function of lung-resident macrophages and dendritic cells.* Nat Immunol, 2015. **16**(1): p. 36-44.

4. Weibel, E.R., *What makes a good lung?* Swiss Med Wkly, 2009. **139**(27-28): p. 375-86.

5. Revoir, W.H. and C.-T. Bien, *Respiratory Protection Handbook.* CRC Press, 1997.

6. Hariri, B.M. and N.A. Cohen, *New insights into upper airway innate immunity.* Am J Rhinol Allergy, 2016. **30**(5): p. 319-23.

7. Knight DA, H.S., *The airway epithelium: structural and functional properties in health and disease.* Respirology, 2003. **8**(4): p. 432-46.

8. Gras, D., et al., *Bronchial epithelium as a target for innovative treatments in asthma.* Pharmacol Ther, 2013. **140**(3): p. 290-305.

9. Gohy, S.T., et al., *Chronic inflammatory airway diseases: the central role of the epithelium revisited.* Clin Exp Allergy, 2016. **46**(4): p. 529-42.

10. Horsfield, K. and G. Cumming, *Morphology of the bronchial tree in man.* J Appl Physiol, 1968. **24**(3): p. 373-83.

11. Murray, J.F., *The structure and function of the lung.* Int J Tuberc Lung Dis, 2010. **14**(4): p. 391-6.

12. Murray, J.F., *The normal lung: the basis for diagnosis and treatment of pulmonary disease.* 2nd ed. 1985, Philadelphia, PA, USA Saunder W B.

13. Lippert, H., *Kapitel 3 Brusteingeweide. In: Lippert H. (Hrsg.) Lehrbuch Anatomie 6. Aufl.* Elsevier GmbH, München, 2003: p. 203-275.

14. Tillmann, B.N., Schumacher, U., *Kapitel 9 Organe der Atmung. In Zilles, K., Tillmann, B.N. (Hrsg.) Anatomie. 1. Auflage.* Springer Medizin Verlag, Heidelberg, 2010: p. 393-422.

15. Netter, F.H., *Sektion I Anatomie und Embryologie. In: Netter F.H. Farbatlanten der Medizin Band 4: Atmungsorgane*, ed. P. Endres. 1982, Stuttgart, Georg Thieme Verlag: Peter Endres. 23-24.

16. Alfven, T., et al., *Allergic diseases and atopic sensitization in children related to farming and anthroposophic lifestyle--the PARSIFAL study.* Allergy, 2006. **61**(4): p. 414-21.

17. Eder, W., M.J. Ege, and E. von Mutius, *The asthma epidemic.* N Engl J Med, 2006. **355**(21): p. 2226-35.

18. Moorman, J.E., et al., *National surveillance of asthma: United States, 2001-2010.* Vital Health Stat 3, 2012(35): p. 1-58.

19. Cookson, W., *The immunogenetics of asthma and eczema: a new focus on the epithelium.* Nat Rev Immunol, 2004. **4**(12): p. 978-88.

20. Wills-Karp, M. and M. Chiaramonte, *Interleukin-13 in asthma.* Curr Opin Pulm Med, 2003. **9**(1): p. 21-7.

21. Robinson, D.S., et al., *Predominant TH2-like bronchoalveolar T-lymphocyte population in atopic asthma.* N Engl J Med, 1992. **326**(5): p. 298-304.

22. Wills-Karp, M., et al., *Interleukin-13: central mediator of allergic asthma.* Science, 1998. **282**(5397): p. 2258-61.

23. Plopper, C. and D.M. Hyde, *Epithelial cells of bronchioles. In: Parent RA, editor. Treatise on pulmonary toxicology: comparative biology of the normal lung.* Boca Raton (FL): CRC Press, 1992: p. 85-92.

24. Mariassy, A.T., *Epithelial cell of trachea bronchi. In: Parent RA, editor. Treatise on pulmonary toxicology: comparative biology of the normal lung.* Boca Raton (FL): CRC Press, 1992: p. 63-76.

25. McBride, J.T., *Architecture of the tracheobronchial tree. In: Parent RA, editor. Treatise on pulmonary toxicology: comparative biology of the normal lung.* Boca Raton (FL): CRC Press, 1992: p. 49-61.

26. Tyler, W.S. and M.D. Julian, *Gross and subgross anatomy of lungs, pleura, connective tissue septa, distal airways, and structural units. In: Parent RA, editor. Treatise on pulmonary toxicology: comparative biology of the normal lung.* boca Raton (FL): CRC Press, 1992: p. 37-48.

27. Hyde, D.M., Q. Hamid, and C.G. Irvin, *Anatomy, pathology, and physiology of the tracheobronchial tree: emphasis on the distal airways.* J Allergy Clin Immunol, 2009. **124**(6 Suppl): p. S72-7.

28. Martin, R.A., et al., *Aligning mouse models of asthma to human endotypes of disease.* Respirology, 2014. **19**(6): p. 823-33.

29. Bates, J.H., M. Rincon, and C.G. Irvin, *Animal models of asthma.* Am J Physiol Lung Cell Mol Physiol, 2009. **297**(3): p. L401-10.

30. Shinagawa, K. and M. Kojima, *Mouse model of airway remodeling: strain differences.* Am J Respir Crit Care Med, 2003. **168**(8): p. 959-67.

31. Tumes, D.J., et al., *Strain-dependent resistance to allergen-induced lung pathophysiology in mice correlates with rate of apoptosis of lung-derived eosinophils.* J Leukoc Biol, 2007. **81**(6): p. 1362-73.

32. Kodama, M., et al., *Strain-specific phenotypes of airway inflammation and bronchial hyperresponsiveness induced by epicutaneous allergen sensitization in BALB/c and C57BL/6 mice.* Int Arch Allergy Immunol, 2010. **152 Suppl 1**: p. 67-74.

33. Perros, F., B.N. Lambrecht, and H. Hammad, *TLR4 signalling in pulmonary stromal cells is critical for inflammation and immunity in the airways.* Respir Res, 2011. **12**: p. 125.

34. Tan, A.M., et al., *TLR4 signaling in stromal cells is critical for the initiation of allergic Th2 responses to inhaled antigen.* J Immunol, 2010. **184**(7): p. 3535-44.

35. Lambrecht, B.N. and H. Hammad, *The airway epithelium in asthma.* Nat Med, 2012. **18**(5): p. 684-92.

36. Lambrecht, B.N. and H. Hammad, *Allergens and the airway epithelium response: gateway to allergic sensitization.* J Allergy Clin Immunol, 2014. **134**(3): p. 499-507.

37. Lambrecht, B.N. and H. Hammad, *The immunology of asthma.* Nat Immunol, 2015. **16**(1): p. 45-56.

38. Pichavant, M., et al., *Asthmatic bronchial epithelium activated by the proteolytic allergen Der p 1 increases selective dendritic cell recruitment.* J Allergy Clin Immunol, 2005. **115**(4): p. 771-8.

39. Adam, E., et al., *The house dust mite allergen Der p 1, unlike Der p 3, stimulates the expression of interleukin-8 in human airway epithelial cells via a proteinase-activated receptor-2-independent mechanism.* J Biol Chem, 2006. **281**(11): p. 6910-23.

40. Page, K., et al., *Mucosal sensitization to German cockroach involves protease-activated receptor-2.* Respir Res, 2010. **11**: p. 62.

41. Lambrecht, B.N. and H. Hammad, *Asthma: the importance of dysregulated barrier immunity.* Eur J Immunol, 2013. **43**(12): p. 3125-37.

42. Steinman, R.M., *Linking innate to adaptive immunity through dendritic cells.* Novartis Found Symp, 2006. **279**: p. 101-9; discussion 109-13, 216-9.

43. Perros, F., et al., *Blockade of CCR4 in a humanized model of asthma reveals a critical role for DC-derived CCL17 and CCL22 in attracting Th2 cells and inducing airway inflammation.* Allergy, 2009. **64**(7): p. 995-1002.

44. Chesné, J., et al., *Prime role of IL-17A in neutrophilia and airway smooth muscle contraction in a house dust mite-induced allergic asthma model.* J Allergy Clin Immunol, 2015. **135**(6): p. 1643-1643.e3.

45. Cook, P.C. and A.S. MacDonald, *Dendritic cells in lung immunopathology.* Semin Immunopathol, 2016. **38**(4): p. 449-60.

46. Kudo, M., et al., *IL-17A produced by alphabeta T cells drives airway hyper-responsiveness in mice and enhances mouse and human airway smooth muscle contraction.* Nat Med, 2012. **18**(4): p. 547-54.

47. Grunig, G., et al., *Requirement for IL-13 independently of IL-4 in experimental asthma.* Science, 1998. **282**(5397): p. 2261-3.

48. Kuperman, D.A., et al., *Direct effects of interleukin-13 on epithelial cells cause airway hyperreactivity and mucus overproduction in asthma.* Nat Med, 2002. **8**(8): p. 885-9.

49. Khare, A., et al., *Cutting Edge: Dual Function of PPARgamma in CD11c+ Cells Ensures Immune Tolerance in the Airways.* J Immunol, 2015. **195**(2): p. 431-5.

50. Khare, A., et al., *Cutting edge: inhaled antigen upregulates retinaldehyde dehydrogenase in lung CD103+ but not plasmacytoid dendritic cells to induce Foxp3 de novo in CD4+ T cells and promote airway tolerance.* J Immunol, 2013. **191**(1): p. 25-9.

51. Plantinga, M., et al., *Conventional and monocyte-derived CD11b(+) dendritic cells initiate and maintain T helper 2 cell-mediated immunity to house dust mite allergen.* Immunity, 2013. **38**(2): p. 322-35.

52. Nakano, H., et al., *Complement receptor C5aR1/CD88 and dipeptidyl peptidase-4/CD26 define distinct hematopoietic lineages of dendritic cells.* J Immunol, 2015. **194**(8): p. 3808-19.

53. Furuhashi, K., et al., *Mouse lung CD103+ and CD11bhigh dendritic cells preferentially induce distinct CD4+ T-cell responses.* Am J Respir Cell Mol Biol, 2012. **46**(2): p. 165-72.

54. Norimoto, A., et al., *Dectin-2 promotes house dust mite-induced T helper type 2 and type 17 cell differentiation and allergic airway inflammation in mice.* Am J Respir Cell Mol Biol, 2014. **51**(2): p. 201-9.

55. Westphalen, A.C. and A.B. Rosenkrantz, *Prostate imaging reporting and data system (PI-RADS): reflections on early experience with a standardized interpretation scheme for multiparametric prostate MRI.* AJR Am J Roentgenol, 2014. **202**(1): p. 121-3.

56. Zaslona, Z., et al., *Resident alveolar macrophages suppress, whereas recruited monocytes promote, allergic lung inflammation in murine models of asthma.* J Immunol, 2014. **193**(8): p. 4245-53.

57. Song, C., et al., *IL-17-producing alveolar macrophages mediate allergic lung inflammation related to asthma.* J Immunol, 2008. **181**(9): p. 6117-24.

58. Peters-Golden, M., *The alveolar macrophage: the forgotten cell in asthma.* Am J Respir Cell Mol Biol, 2004. **31**(1): p. 3-7.

59. Masten, B.J. and M.F. Lipscomb, *Comparison of lung dendritic cells and B cells in stimulating naive antigen-specific T cells.* J Immunol, 1999. **162**(3): p. 1310-7.

60. Masten, B.J., *Initiation of lung immunity: the afferent limb and the role of dendritic cells.* Semin Respir Crit Care Med, 2004. **25**(1): p. 11-20.

61. Sertl, K., et al., *Dendritic cells with antigen-presenting capability reside in airway epithelium, lung parenchyma, and visceral pleura.* J Exp Med, 1986. **163**(2): p. 436-51.

62. von Garnier, C., et al., *Anatomical location determines the distribution and function of dendritic cells and other APCs in the respiratory tract.* J Immunol, 2005. **175**(3): p. 1609-18.

63. Steinman, R.M., *The dendritic cell system and its role in immunogenicity.* Annu Rev Immunol, 1991. **9**: p. 271-96.

64. Ginhoux, F. and S. Jung, *Monocytes and macrophages: developmental pathways and tissue homeostasis.* Nat Rev Immunol, 2014. **14**(6): p. 392-404.

65. Guilliams, M., et al., *Dendritic cells, monocytes and macrophages: a unified nomenclature based on ontogeny.* Nat Rev Immunol, 2014. **14**(8): p. 571-8.

66. Hoffmann, F., et al., *Origin, Localization, and Immunoregulatory Properties of Pulmonary Phagocytes in Allergic Asthma.* Front Immunol, 2016. **7**: p. 107.

67. Misharin, A.V., et al., *Flow cytometric analysis of macrophages and dendritic cell subsets in the mouse lung.* Am J Respir Cell Mol Biol, 2013. **49**(4): p. 503-10.

68. Schraml, B.U., et al., *Genetic tracing via DNGR-1 expression history defines dendritic cells as a hematopoietic lineage.* Cell, 2013. **154**(4): p. 843-58.

69. Desch, A.N., et al., *CD103+ pulmonary dendritic cells preferentially acquire and present apoptotic cell-associated antigen.* J Exp Med, 2011. **208**(9): p. 1789-97.

70. Sung, S.S., et al., *A major lung CD103 (alphaE)-beta7 integrin-positive epithelial dendritic cell population expressing Langerin and tight junction proteins.* J Immunol, 2006. **176**(4): p. 2161-72.

71. Hackstein, H., et al., *Heterogeneity of respiratory dendritic cell subsets and lymphocyte populations in inbred mouse strains.* Respir Res, 2012. **13**: p. 94.

72. Liu, K., et al., *In vivo analysis of dendritic cell development and homeostasis.* Science, 2009. **324**(5925): p. 392-7.

73. Moran, T.P., et al., *Inhaled house dust programs pulmonary dendritic cells to promote type 2 T-cell responses by an indirect mechanism.* Am J Physiol Lung Cell Mol Physiol, 2015. **309**(10): p. L1208-18.

74. Nakano, H., et al., *Migratory properties of pulmonary dendritic cells are determined by their developmental lineage.* Mucosal Immunol, 2013. **6**(4): p. 678-91.

75. Naik, S.H., et al., *Development of plasmacytoid and conventional dendritic cell subtypes from single precursor cells derived in vitro and in vivo.* Nat Immunol, 2007. **8**(11): p. 1217-26.

76. Fogg, D.K., et al., *A clonogenic bone marrow progenitor specific for macrophages and dendritic cells.* Science, 2006. **311**(5757): p. 83-7.

77. Hettinger, J., et al., *Origin of monocytes and macrophages in a committed progenitor.* Nat Immunol, 2013. **14**(8): p. 821-30.

78. Sathe, P., et al., *Lymphoid tissue and plasmacytoid dendritic cells and macrophages do not share a common macrophage-dendritic cell-restricted progenitor.* Immunity, 2014. **41**(1): p. 104-15.

79. Onai, N., et al., *A clonogenic progenitor with prominent plasmacytoid dendritic cell developmental potential.* Immunity, 2013. **38**(5): p. 943-57.

80. Tsitoura, D.C., et al., *Intranasal exposure to protein antigen induces immunological tolerance mediated by functionally disabled CD4+ T cells.* J Immunol, 1999. **163**(5): p. 2592-600.

81. Gilliet, M., et al., *The development of murine plasmacytoid dendritic cell precursors is differentially regulated by FLT3-ligand and granulocyte/macrophage colony-stimulating factor.* J Exp Med, 2002. **195**(7): p. 953-8.

82. Edelson, B.T., et al., *Peripheral CD103+ dendritic cells form a unified subset developmentally related to CD8alpha+ conventional dendritic cells.* J Exp Med, 2010. **207**(4): p. 823-36.

83. Hildner, K., et al., *Batf3 deficiency reveals a critical role for CD8alpha+ dendritic cells in cytotoxic T cell immunity.* Science, 2008. **322**(5904): p. 1097-100.

84. Ginhoux, F., et al., *The origin and development of nonlymphoid tissue CD103+ DCs.* J Exp Med, 2009. **206**(13): p. 3115-30.

85. Schlitzer, A., et al., *IRF4 transcription factor-dependent CD11b+ dendritic cells in human and mouse control mucosal IL-17 cytokine responses.* Immunity, 2013. **38**(5): p. 970-83.

86. Schlitzer, A., et al., *Identification of cDC1- and cDC2-committed DC progenitors reveals early lineage priming at the common DC progenitor stage in the bone marrow.* Nat Immunol, 2015. **16**(7): p. 718-28.

87. Varol, C., et al., *Monocytes give rise to mucosal, but not splenic, conventional dendritic cells.* J Exp Med, 2007. **204**(1): p. 171-80.

88. Lin, K.L., et al., *CCR2+ monocyte-derived dendritic cells and exudate macrophages produce influenza-induced pulmonary immune pathology and mortality.* J Immunol, 2008. **180**(4): p. 2562-72.

89. Idoyaga, J. and R.M. Steinman, *SnapShot: Dendritic Cells.* Cell, 2011. **146**(4): p. 660-660 e2.

90. Satpathy, A.T., et al., *Re(de)fining the dendritic cell lineage.* Nat Immunol, 2012. **13**(12): p. 1145-54.

91. Waskow, C., et al., *The receptor tyrosine kinase Flt3 is required for dendritic cell development in peripheral lymphoid tissues.* Nat Immunol, 2008. **9**(6): p. 676-83.

92. Schraml, B.U. and C. Reis e Sousa, *Defining dendritic cells.* Curr Opin Immunol, 2015. **32**: p. 13-20.

93. Yona, S., et al., *Fate mapping reveals origins and dynamics of monocytes and tissue macrophages under homeostasis.* Immunity, 2013. **38**(1): p. 79-91.

94. Bain, C.C., et al., *Resident and pro-inflammatory macrophages in the colon represent alternative context-dependent fates of the same Ly6Chi monocyte precursors.* Mucosal Immunol, 2013. **6**(3): p. 498-510.

95. Sunderkotter, C., et al., *Subpopulations of mouse blood monocytes differ in maturation stage and inflammatory response.* J Immunol, 2004. **172**(7): p. 4410-7.

96. Gautier, E.L., et al., *Gene-expression profiles and transcriptional regulatory pathways that underlie the identity and diversity of mouse tissue macrophages.* Nat Immunol, 2012. **13**(11): p. 1118-28.

97. Jakubzick, C., et al., *Minimal differentiation of classical monocytes as they survey steady-state tissues and transport antigen to lymph nodes.* Immunity, 2013. **39**(3): p. 599-610.

98. Nakano, H., et al., *Pulmonary CD103(+) dendritic cells prime Th2 responses to inhaled allergens.* Mucosal Immunol, 2012. **5**(1): p. 53-65.

99. Osterholzer, J.J., et al., *CCR2 and CCR6, but not endothelial selectins, mediate the accumulation of immature dendritic cells within the lungs of mice in response to particulate antigen.* J Immunol, 2005. **175**(2): p. 874-83.

100. Burgdorf, S., et al., *Distinct pathways of antigen uptake and intracellular routing in CD4 and CD8 T cell activation.* Science, 2007. **316**(5824): p. 612-6.

101. GeurtsvanKessel, C.H. and B.N. Lambrecht, *Division of labor between dendritic cell subsets of the lung.* Mucosal Immunol, 2008. **1**(6): p. 442-50.

102. Robays, L.J., et al., *Chemokine receptor CCR2 but not CCR5 or CCR6 mediates the increase in pulmonary dendritic cells during allergic airway inflammation.* J Immunol, 2007. **178**(8): p. 5305-11.

103. Guilliams, M., et al., *Alveolar macrophages develop from fetal monocytes that differentiate into long-lived cells in the first week of life via GM-CSF*. J Exp Med, 2013. **210**(10): p. 1977-92.

104. Landsman, L. and S. Jung, *Lung macrophages serve as obligatory intermediate between blood monocytes and alveolar macrophages.* J Immunol, 2007. **179**(6): p. 3488-94.

105. Lagranderie, M., et al., *Dendritic cells recruited to the lung shortly after intranasal delivery of Mycobacterium bovis BCG drive the primary immune response towards a type 1 cytokine production.* Immunology, 2003. **108**(3): p. 352-64.

106. Arora, M., et al., *LPS-induced CD11b+Gr1(int)F4/80+ regulatory myeloid cells suppress allergen-induced airway inflammation.* Int Immunopharmacol, 2011. **11**(7): p. 827-32.

107. Arora, M., et al., *TLR4/MyD88-induced CD11b+Gr-1 int F4/80+ non-migratory myeloid cells suppress Th2 effector function in the lung.* Mucosal Immunol, 2010. **3**(6): p. 578-93.

108. Merad, M., et al., *The dendritic cell lineage: ontogeny and function of dendritic cells and their subsets in the steady state and the inflamed setting.* Annu Rev Immunol, 2013. **31**: p. 563-604.

109. Winter, D.R. and I. Amit, *DCs are ready to commit.* Nat Immunol, 2015. **16**(7): p. 683-5.

110. Kretschmer, S., et al., *Visualization of intrapulmonary lymph vessels in healthy and inflamed murine lung using CD90/Thy-1 as a marker.* PLoS One, 2013. **8**(2): p. e55201.

111. Suda, T., et al., *Dendritic cell precursors are enriched in the vascular compartment of the lung.* Am J Respir Cell Mol Biol, 1998. **19**(5): p. 728-37.

112. Holt, P.G., et al., *Origin and steady-state turnover of class II MHC-bearing dendritic cells in the epithelium of the conducting airways.* J Immunol, 1994. **153**(1): p. 256-61.

113. Jahnsen, F.L., et al., *Accelerated antigen sampling and transport by airway mucosal dendritic cells following inhalation of a bacterial stimulus.* J Immunol, 2006. **177**(9): p. 5861-7.

114. Veres, T.Z., et al., *Spatiotemporal and functional behavior of airway dendritic cells visualized by two-photon microscopy.* Am J Pathol, 2011. **179**(2): p. 603-9.

115. Thornton, E.E., et al., *Spatiotemporally separated antigen uptake by alveolar dendritic cells and airway presentation to T cells in the lung.* J Exp Med, 2012. **209**(6): p. 1183-99.

116. Cleret, A., et al., *Lung dendritic cells rapidly mediate anthrax spore entry through the pulmonary route.* J Immunol, 2007. **178**(12): p. 7994-8001.

117. Wikstrom, M.E. and P.A. Stumbles, *Mouse respiratory tract dendritic cell subsets and the immunological fate of inhaled antigens.* Immunol Cell Biol, 2007. **85**(3): p. 182-8.

118. de Heer, H.J., et al., *Essential role of lung plasmacytoid dendritic cells in preventing asthmatic reactions to harmless inhaled antigen.* J Exp Med, 2004. **200**(1): p. 89-98.

119. Soroosh, P., et al., *Lung-resident tissue macrophages generate Foxp3+ regulatory T cells and promote airway tolerance.* J Exp Med, 2013. **210**(4): p. 775-88.

120. Martin, T.R. and C.W. Frevert, *Innate immunity in the lungs.* Proc Am Thorac Soc, 2005. **2**(5): p. 403-11.

121. Ho, A.W., et al., *Lung CD103+ dendritic cells efficiently transport influenza virus to the lymph node and load viral antigen onto MHC class I for presentation to CD8 T cells.* J Immunol, 2011. **187**(11): p. 6011-21.

122. del Rio, M.L., et al., *CD103- and CD103+ bronchial lymph node dendritic cells are specialized in presenting and cross-presenting innocuous antigen to CD4+ and CD8+ T cells.* J Immunol, 2007. **178**(11): p. 6861-6.

123. Beaty, S.R., C.E. Rose, Jr., and S.S. Sung, *Diverse and potent chemokine production by lung CD11bhigh dendritic cells in homeostasis and in allergic lung inflammation.* J Immunol, 2007. **178**(3): p. 1882-95.

124. Raymond, M., et al., *Selective control of SIRP-alpha-positive airway dendritic cell trafficking through CD47 is critical for the development of T(H)2-mediated allergic inflammation.* J Allergy Clin Immunol, 2009. **124**(6): p. 1333-42 e1.

125. Chen, K., et al., *Signal relay by CC chemokine receptor 2 (CCR2) and formylpeptide receptor 2 (Fpr2) in the recruitment of monocyte-derived dendritic cells in allergic airway inflammation.* J Biol Chem, 2013. **288**(23): p. 16262-73.

126. Poulin, L.F., et al., *DNGR-1 is a specific and universal marker of mouse and human Batf3-dependent dendritic cells in lymphoid and nonlymphoid tissues.* Blood, 2012. **119**(25): p. 6052-62.

127. Sancho, D., et al., *Tumor therapy in mice via antigen targeting to a novel, DC-restricted C-type lectin.* J Clin Invest, 2008. **118**(6): p. 2098-110.

128. Lewkowich, I.P., et al., *Allergen uptake, activation, and IL-23 production by pulmonary myeloid DCs drives airway hyperresponsiveness in asthma-susceptible mice.* PLoS One, 2008. **3**(12): p. e3879.

129. Regamey, N., et al., *Airway epithelial IL-15 transforms monocytes into dendritic cells.* Am J Respir Cell Mol Biol, 2007. **37**(1): p. 75-84.

130. Lewkowich, I.P., et al., *CD4+CD25+ T cells protect against experimentally induced asthma and alter pulmonary dendritic cell phenotype and function.* J Exp Med, 2005. **202**(11): p. 1549-61.

131. Oriss, T.B., et al., *Dynamics of dendritic cell phenotype and interactions with CD4+ T cells in airway inflammation and tolerance.* J Immunol, 2005. **174**(2): p. 854-63.

132. Takagi, H., et al., *Plasmacytoid dendritic cells are crucial for the initiation of inflammation and T cell immunity in vivo.* Immunity, 2011. **35**(6): p. 958-71.

133. Lombardi, V., et al., *CD8alpha(+)beta(-) and CD8alpha(+)beta(+) plasmacytoid dendritic cells induce Foxp3(+) regulatory T cells and prevent the induction of airway hyper-reactivity.* Mucosal Immunol, 2012. **5**(4): p. 432-43.

134. Stafford, J.L., N.F. Neumann, and M. Belosevic, *Macrophage-mediated innate host defense against protozoan parasites.* Crit Rev Microbiol, 2002. **28**(3): p. 187-248.

135. Hussell, T. and T.J. Bell, *Alveolar macrophages: plasticity in a tissue-specific context.* Nat Rev Immunol, 2014. **14**(2): p. 81-93.

136. Mathie, S.A., et al., *Alveolar macrophages are sentinels of murine pulmonary homeostasis following inhaled antigen challenge.* Allergy, 2015. **70**(1): p. 80-9.

137. Forster, R., A.C. Davalos-Misslitz, and A. Rot, *CCR7 and its ligands: balancing immunity and tolerance.* Nat Rev Immunol, 2008. **8**(5): p. 362-71.

138. Holgate, S.T., *Innate and adaptive immune responses in asthma.* Nat Med, 2012. **18**(5): p. 673-83.

139. Forster, R., et al., *CCR7 coordinates the primary immune response by establishing functional microenvironments in secondary lymphoid organs.* Cell, 1999. **99**(1): p. 23-33.

140. Ohl, L., et al., *CCR7 governs skin dendritic cell migration under inflammatory and steady-state conditions.* Immunity, 2004. **21**(2): p. 279-88.

141. Braun, A., et al., *Afferent lymph-derived T cells and DCs use different chemokine receptor CCR7-dependent routes for entry into the lymph node and intranodal migration.* Nat Immunol, 2011. **12**(9): p. 879-87.

142. Hintzen, G., et al., *Induction of tolerance to innocuous inhaled antigen relies on a CCR7-dependent dendritic cell-mediated antigen transport to the bronchial lymph node.* J Immunol, 2006. **177**(10): p. 7346-54.

143. Kawakami, M., et al., *The role of CCR7 in allergic airway inflammation induced by house dust mite exposure.* Cell Immunol, 2012. **275**(1-2): p. 24-32.

144. Kocks, J.R., et al., *Regulatory T cells interfere with the development of bronchus-associated lymphoid tissue.* J Exp Med, 2007. **204**(4): p. 723-34.

145. Jakubzick, C., et al., *Lymph-migrating, tissue-derived dendritic cells are minor constituents within steady-state lymph nodes.* J Exp Med, 2008. **205**(12): p. 2839-50.

146. Saeki, H., et al., *Cutting edge: secondary lymphoid-tissue chemokine (SLC) and CC chemokine receptor 7 (CCR7) participate in the emigration pathway of mature dendritic cells from the skin to regional lymph nodes.* J Immunol, 1999. **162**(5): p. 2472-5.

147. Yu, Y.R., et al., *A Protocol for the Comprehensive Flow Cytometric Analysis of Immune Cells in Normal and Inflamed Murine Non-Lymphoid Tissues.* PLoS One, 2016. **11**(3): p. e0150606.

148. Verschoor, C.P., et al., *An Introduction to Automated Flow Cytometry Gating Tools and Their Implementation.* Front Immunol, 2015. **6**: p. 380.

149. Looney, M.R., et al., *Stabilized imaging of immune surveillance in the mouse lung.* Nat Methods, 2011. **8**(1): p. 91-6.

150. Beavis, A.J. and K.J. Pennline, *Detection of cell-surface antigens using antibody-conjugated fluorospheres (ACF): application for six-color immunofluorescence.* Biotechniques, 1996. **21**(3): p. 498-503.

151. Eissing, N., et al., *Easy performance of 6-color confocal immunofluorescence with 4-laser line microscopes.* Immunol Lett, 2014. **161**(1): p. 1-5.

152. Steinert, E.M., et al., *Quantifying Memory CD8 T Cells Reveals Regionalization of Immunosurveillance.* Cell, 2015. **161**(4): p. 737-49.

153. Karsten, C.M., et al., *Monitoring and cell-specific deletion of C5aR1 using a novel floxed GFP-C5aR1 reporter knock-in mouse.* J Immunol, 2015. **194**(4): p. 1841-55.

154. Engelbertsen, D., et al., *Expansion of CD25+ Innate Lymphoid Cells Reduces Atherosclerosis.* Arterioscler Thromb Vasc Biol, 2015. **35**(12): p. 2526-35.

155. Stohlman, S.A., et al., *CD4 T cells contribute to virus control and pathology following central nervous system infection with neurotropic mouse hepatitis virus.* J Virol, 2008. **82**(5): p. 2130-9.

156. Kupz, A., et al., *Contribution of Thy1+ NK cells to protective IFN-gamma production during Salmonella typhimurium infections.* Proc Natl Acad Sci U S A, 2013. **110**(6): p. 2252-7.

157. Gillard, G.O., et al., *Thy1+ NK [corrected] cells from vaccinia virus-primed mice confer protection against vaccinia virus challenge in the absence of adaptive lymphocytes.* PLoS Pathog, 2011. **7**(8): p. e1002141.

158. Bryce, S.A., et al., *ACKR4 on Stromal Cells Scavenges CCL19 To Enable CCR7-Dependent Trafficking of APCs from Inflamed Skin to Lymph Nodes.* J Immunol, 2016. **196**(8): p. 3341-53.

159. Teijeira, A., A. Rouzaut, and I. Melero, *Initial afferent lymphatic vessels controlling outbound leukocyte traffic from skin to lymph nodes.* Front Immunol, 2013. **4**: p. 433.

160. Moschovakis, G.L., et al., *Deficient CCR7 signaling promotes TH2 polarization and B-cell activation in vivo.* Eur J Immunol, 2012. **42**(1): p. 48-57.

161. Ingersoll, M.A., et al., *Comparison of gene expression profiles between human and mouse monocyte subsets.* Blood, 2010. **115**(3): p. e10-9.

162. Zaynagetdinov, R., et al., *Identification of myeloid cell subsets in murine lungs using flow cytometry.* Am J Respir Cell Mol Biol, 2013. **49**(2): p. 180-9.

163. Ballesteros, I., et al., *Stereological and flow cytometry characterization of leukocyte subpopulations in models of transient or permanent cerebral ischemia.* J Vis Exp, 2014(94).

164. Lambrecht, B.N. and H. Hammad, *Biology of lung dendritic cells at the origin of asthma.* Immunity, 2009. **31**(3): p. 412-24.

165. Sen, D., et al., *Tracking the Spatial and Functional Gradient of Monocyte-To-Macrophage Differentiation in Inflamed Lung.* PLoS One, 2016. **11**(10): p. e0165064.

166. Satpathy, A.T., et al., *Zbtb46 expression distinguishes classical dendritic cells and their committed progenitors from other immune lineages.* J Exp Med, 2012. **209**(6): p. 1135-52.

167. Kohl, J., et al., *A regulatory role for the C5a anaphylatoxin in type 2 immunity in asthma.* J Clin Invest, 2006. **116**(3): p. 783-96.

168. McKinley, L., et al., *Allergens induce enhanced bronchoconstriction and leukotriene production in C5 deficient mice.* Respir Res, 2006. **7**: p. 129.

169. Karp, C.L., et al., *Identification of complement factor 5 as a susceptibility locus for experimental allergic asthma.* Nat Immunol, 2000. **1**(3): p. 221-6.

170. Drouin, S.M., et al., *A protective role for the fifth complement component (c5) in allergic airway disease.* Am J Respir Crit Care Med, 2006. **173**(8): p. 852-7.

171. Zhang, X., et al., *A protective role for C5a in the development of allergic asthma associated with altered levels of B7-H1 and B7-DC on plasmacytoid dendritic cells.* J Immunol, 2009. **182**(8): p. 5123-30.

172. Lajoie, S., et al., *Complement-mediated regulation of the IL-17A axis is a central genetic determinant of the severity of experimental allergic asthma.* Nat Immunol, 2010. **11**(10): p. 928-35.

173. Russo, E., et al., *Intralymphatic CCL21 Promotes Tissue Egress of Dendritic Cells through Afferent Lymphatic Vessels.* Cell Rep, 2016. **14**(7): p. 1723-34.

174. Haessler, U., et al., *Dendritic cell chemotaxis in 3D under defined chemokine gradients reveals differential response to ligands CCL21 and CCL19.* Proc Natl Acad Sci U S A, 2011. **108**(14): p. 5614-9.

175. Clatworthy, M.R., et al., *Immune complexes stimulate CCR7-dependent dendritic cell migration to lymph nodes.* Nat Med, 2014. **20**(12): p. 1458-63.

176. Tal, O., et al., *DC mobilization from the skin requires docking to immobilized CCL21 on lymphatic endothelium and intralymphatic crawling.* J Exp Med, 2011. **208**(10): p. 2141-53.

177. Sallusto, F., et al., *Pillars article: two subsets of memory T lymphocytes with distinct homing potentials and effector functions. Nature. 1999. 401: 708-712.* J Immunol, 2014. **192**(3): p. 840-4.

178. Ginhoux, F. and M. Guilliams, *Tissue-Resident Macrophage Ontogeny and Homeostasis.* Immunity, 2016. **44**(3): p. 439-49.

8 List of Tables

9 List of Figures

10 Appendix

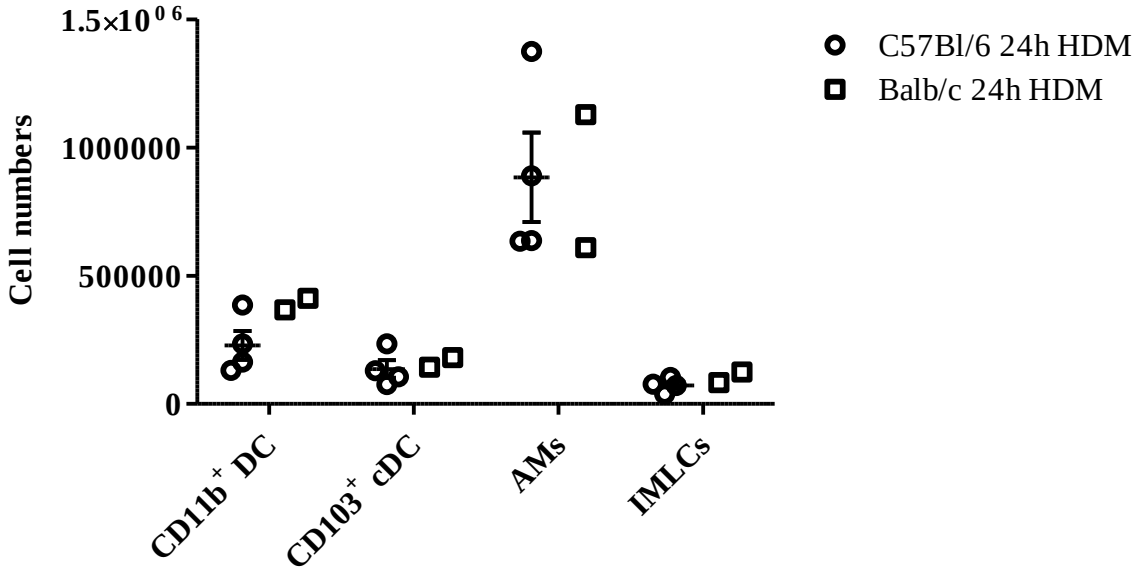

Supplementary Figure 1: Total cell numbers for DCs and macrophages obtained from HDM-treated BALB/c and C57BL/6 mice. PCLS from HDM-treated BALB/c (n= 2) and C57BL/6 (n= 4) mice were stained for CD11c, MHCII, CD11b, and Langerin. DCs and macrophages were counted and extrapolated to absolute numbers. Depicted are mean and SEM.

1. Measured weight for left, right, and total lung

Mouse	Left Lung (g)	Right Lung (g)	Lung total (g)
1	0.40	0.70	1.10
2	0.41	0.73	1.14
3	0.52	1.02	1.54
4	0.50	0.88	1.37
5	0.53	0.99	1.51
6	0.54	0.86	1.40
mean	0.48	0.86	1.34

2. Relative weight of left and right lung

Mouse	Left Lung %	Right Lung %
1	36.60	63.46
2	36.60	63.88
3	33.50	66.23
4	36.13	63.87
5	34.77	65.23
6	38.57	61.43
mean	35.99	64.01

3. Mice used for quantification essays

C57BL/6 1	M1191	BALB/c 1	M1162
C57BL/6 2	M1192	BALB/c 2	M1155
C57BL/6 3	M1134	BALB/c 3	M1156
C57BL/6 4	M1135	BALB/c 4	M1157
C57BL/6 5	M1409	BALB/c 5	M1154
C57BL/6 6	M1410	BALB/c 6	M1407
C57BL/6 7	M1151	BALB/c 7	M1425
C57BL/6 8	M1152	BALB/c 8	M1426
C57BL/6 9	M1360		
C57BL/6 HDM 1	M1251	BALB/c HDM 1	M1286
C57BL/6 HDM 2	M1271	BALB/c HDM 2	M1287
C57BL/6 HDM 3	M1272	BALB/c HDM 3	M1477
C57BL/6 HDM 4	M1273		
C57BL/6 HDM 5	M1476		

4. Counted cell numbers for calculation of absolute and relative population sizes

Mouse	CD11b$^+$ DC	CD103$^+$ cDC	IM vessel	IM airway	AM	pDC	Σ
C57BL/6 1	0	0	0	0	0	7	7
C57BL/6 2	0	0	0	0	0	9	9
C57BL/6 6	0	0	0	0	0	6	6
C57BL/6 1	216	189	179	100	603	0	1287
C57BL/6 2	264	175	152	46	503	0	1140
C57BL/6 3	154	141	68	42	464	0	869
C57BL/6 4	122	114	87	32	517	0	872
C57BL/6 7	92	86	32	53	256	0	519
C57BL/6 8	168	134	65	504	882	0	1753
C57BL/6 HDM 1	107	62	27	4	521	0	721
C57BL/6 HDM 2	123	68	28	10	467	0	696
C57BL/6 HDM 3	153	93	36	5	546	0	833
C57BL/6 HDM 4	145	94	59	9	565	0	872
BALB/c 1	116	105	110	31	490	0	852
BALB/c 2	174	170	107	90	405	0	946
BALB/c 3	79	79	60	29	238	0	485
BALB/c 4	138	145	78	49	299	0	709
BALB/c HDM 1	266	92	39	15	393	0	805
BALB/c HDM 2	160	79	41	13	492	0	785

5. Parameters for cDC and macrophage quantification

Mouse	Slice [g]	Left Lung [g]	Images	ROI [mm²]	Thicknes Slice [µm]	Thickness Slice [µm]	Area [mm²]	Factor Lung
C57BL/6 1	0.027	0.50	20	0.636	40	179.0	90.4	2.79
C57BL/6 2	0.032	0.53	18	0.636	40	171.2	94.5	2.79
C57BL/6 3	0.019	0.40	12	0.636	40	122.7	85.0	2.79
C57BL/6 4	0.027	0.43	12	0.636	40	170.0	89.0	2.79
C57BL/6 HDM 1	0.026	0.37	15	0.636	40	139.0	84.3	2.79
C57BL/6 HDM 2	0.028	0.42	13	0.636	40	179.7	83.9	2.79
C57BL/6 HDM 3	0.027	0.49	14	0.636	40	181.6	97.6	2.79
C57BL/6 HDM 4	0.03	0.43	17	0.636	40	206.5	59.1	2.79
BALB/c 1	0.013	0.37	16	0.636	40	183.8	75.2	2.79
BALB/c 2	0.016	0.58	17	0.636	40	165.6	77.6	2.79
BALB/c 3	0.042	0.61	13	0.636	40	200.4	111.9	2.79
BALB/c 4	0.025	0.62	16	0.636	40	191.6	112.5	2.79
BALB/c HDM 1	0.032	0.50	14	0.636	40	175.4	72.0	2.79
BALB/c HDM 2	0.023	0.49	15	0.636	40	188.2	77.9	2.79

6. Parameters for pDC quantification

Mouse	Slice [g]	Left Lung [g]	Images	ROI [mm²]	Thickness Slice [µm]	Thickness Slice [µm]	Area [mm²]	Factor Lung
C57BL/6 1	0.038	0.5	9	0.636	40	170.6	118.33	2.79
C57BL/6 2	0.032	0.525	11	0.636	40	176	119.25	2.79
C57BL/6 6	0.037	0.58	10	0.636	40	205	135	2.79

7. Calculated cell numbers

Maus	CD11b$^+$ DC	CD103$^+$ cDC	IM vessel	IM airway	AM	pDC
C57BL/6 1	0	0	0	0	0	35624
C57BL/6 2	0	0	0	0	0	48501
C57BL/6 6	0	0	0	0	0	25962
C57BL/6 1	557144	487501	461707	257937	1555361	0
C57BL/6 2	670182	444249	385862	116774	1276899	0
C57BL/6 3	484819	443893	214076	132223	1460754	0
C57BL/6 4	412065	385044	293850	108083	1746209	0
C57BL/6 HDM 1	204849	118698	51691	7658	997443	0
C57BL/6 HDM 2	368166	203539	83810	29932	1397832	0
C57BL/6 HDM 3	605449	368018	142459	19786	2160623	0
C57BL/6 HDM 4	256856	166514	104514	15943	1000853	0
BALB/c 1	490994	444434	465597	131214	2074025	0
BALB/c 2	821082	802206	504918	424698	1911139	0
BALB/c 3	340850	340850	258874	125122	1026865	0
BALB/c 4	781210	820836	441553	277386	1692621	0
BALB/c HDM 1	648196	224188	95036	36552	957673	0
BALB/c HDM 2	576773	284782	147798	46863	1773576	0

8. Frequencies of tissue-resident phagocytes

Mouse	CD11b$^+$ DCs	CD103$^+$ cDCs	IM vessel	IM airway
C57BL/6 1	29.09	26.42	27.99	16.51
C57BL/6 2	31.58	27.63	26.17	14.62
C57BL/6 3	38.02	34.81	16.79	10.37
C57BL/6 4	34.37	32.11	24.51	9.01
C57BL/6 HDM 1	53.50	31.00	13.50	2.00
C57BL/6 HDM 2	53.71	29.69	12.23	4.37
C57BL/6 HDM 3	53.31	32.40	12.54	1.74
C57BL/6 HDM 4	47.23	30.62	19.22	2.93
BALB/c 1	32.04	29.01	30.39	8.56
BALB/c 2	32.16	31.42	19.78	16.64
BALB/c 3	31.98	31.98	24.29	11.74
BALB/c 4	33.66	35.37	19.02	11.95
BALB/c HDM 1	58.31	39.47	13.65	2.23
BALB/c HDM 2	54.61	26.96	13.99	4.44

9. Freqeuncies of $CD11b^+$:$CD103^+$ DCs

Mouse	$CD11b^+$ DC	$CD103^+$ cDC
C57BL/6 1	53	47
C57BL/6 2	60	40
C57BL/6 3	52.2	47.8
C57BL/6 4	51.69	48.31
C57BL/6 HDM 1	63.31	36.69
C57BL/6 HDM 2	64.4	35.6
C57BL/6 HDM 3	62.2	37.8
C57BL/6 HDM 4	60.67	39.33
BALB/c 1	52.49	47.51
BALB/c 2	50.58	49.42
BALB/c 3	50	50
BALB/c 4	48.76	51.24
BALB/c HDM 1	74,3	25,7
BALB/c HDM 2	66,95	33,05

10. Contact rate of airways adjacent IMLCs (relative)

Mouse	AM	$CD11b^+$ DC	$CD103^+$ cDC	other	no contact
C57BL/6 1	0.00	3.00	33.00	0.00	64.00
C57BL/6 2	8.70	6.52	28.26	4.35	52.17
C57BL/6 3	7.14	0.00	40.48	0.00	52.38
C57BL/6 4	6.25	6.25	62.50	0.00	25.00
C57BL/6 HDM 1	0.00	0.00	0.00	0.00	100.00
C57BL/6 HDM 2	0.00	20.00	10.00	0.00	70.00
C57BL/6 HDM 3	0.00	0.00	40.00	0.00	60.00
C57BL/6 HDM 4	0.00	0.00	22.22	0.00	77.78
BALB/c 1	0.00	0.00	67.74	0.00	32.26
BALB/c 2	1.11	4.44	50.00	1.11	43.33
BALB/c 3	6.90	0.00	51.72	3.45	37.93
BALB/c 4	0.00	2.04	53.06	0.00	44.90
BALB/c HDM 1	0.00	6.67	13.33	0.00	80.00
BALB/c HDM 2	4.88	0.00	9.76	4.88	80.49

11. Contact rate of blood vessel adjacent IMLCs (relative)

Mouse	AM	CD11b^{+} DC	CD103^{+} cDC	other	no contact
C57BL/6 1	7.82	0.00	13.41	0.00	78.77
C57BL/6 2	7.24	1.97	20.39	0.00	70.39
C57BL/6 3	11.76	0.00	23.53	1.47	63.24
C57BL/6 4	9.20	4.60	11.49	3.45	71.26
C57BL/6 HDM 1	14.81	3.70	14.81	0.00	66.67
C57BL/6 HDM 2	10.71	10.71	14.29	3.57	60.71
C57BL/6 HDM 3	2.78	0.00	11.11	2.78	83.33
C57BL/6 HDM 4	5.08	3.39	10.17	6.78	74.58
BALB/c 1	9.09	1.82	23.64	5.45	60.00
BALB/c 2	5.61	3.74	19.63	1.87	69.16
BALB/c 3	5.00	1.67	20.00	1.67	71.67
BALB/c 4	2.56	1.28	28.21	1.28	66.67
BALB/c HDM 1	10.26	2.56	7.69	2.56	76.92
BALB/c HDM 2	0.00	7.69	15.38	7.69	69.23

12. Contact rate of CD103+ cDCs to IMLCs

Mouse	Airway IMLCs		Blood vessel IMLCs	
	Contact	no Contact	Contact	no Contact
C57BL/6 1	52.86	47.14	22.69	77.31
C57BL/6 2	35.42	64.58	22.83	77.17
C57BL/6 3	33.33	67.67	18.82	81.18
C57BL/6 4	39.13	60.87	17.81	82.19
C57BL/6 HDM 1	000	100.00	6.45	93.55
C57BL/6 HDM 2	7.17	92.86	4.26	95.74
C57BL/6 HDM 3	13.33	86.67	6.41	93.59
C57BL/6 HDM 4	8.00	92.00	8.57	91.43
BALB/c 1	55.26	44.74	32.81	67.19
BALB/c 2	61.54	38.46	31.58	68.42
BALB/c 3	45.71	54.29	27.27	72.73
BALB/c 4	44.44	55.56	25.61	74.39
BALB/c HDM 1	9.09	90.91	2.99	97.01
BALB/c HDM 2	10.53	89.47	8.33	91.67

13. Frequency of monocyte-derived CD11b+ DCs based on CD64

Mouse	Absolute			Relative	
	$CD11b^+$ DCs	**$CD64^+$ moDC**	**$CD64^-$ cDC**	**$CD64^+$ moDC**	**$CD64^-$ cDC**
C57BL/6 1	70	36	34	49.22	50.78
C57BL/6 2	41	23	18	55.77	44.23
C57BL/6 7	83	58	25	58.39	41.61
C57BL/6 8	24	13	11	42.41	57.59
C57BL/6 HDM 3	144	115	29	78.79	21.21
C57BL/6 HDM 4	114	92	22	81.12	18.88
C57BL/6 HDM 5	148	122	26	83.57	16.43
BALB/c 1	78	48	30	59.64	40.36
BALB/c 6	80	47	33	58.76	41.24
BALB/c 7	89	62	27	68.9	31.1
BALB/c 8	77	48	29	61.31	38.69

14. $CCR7^+$ DCs

Mouse	Absolute			Relative	
	$CCR7^+$ DC	**$CD11b^+$**	**$CD103^+$**	**$CD11b^+$**	**$CD103^+$**
C57BL/6 1	13	10	3	76.92	23.08
C57BL/6 2	2	2	0	100	0
C57BL/6 5	15	6	9	40	60
C57BL/6 7	16	8	8	50	50
C57BL/6 HDM 1	19	9	10	47.37	52.63
C57BL/6 HDM 3	48	19	29	39.58	60.42
C57BL/6 HDM 4	58	28	30	48.28	51.72
C57BL/6 HDM 5	44	14	30	31.82	68.18

15. Quantification table for accumulations in airways adjacent lymph vessels

Mice	LV	Accumulation	LVs with Accumulations (%)
C57BL/6 2	15	1	6.67
C57BL/6 3	14	1	7.14
C57BL/6 6	13	1	7.69
C57BL/6 7	15	1	6.67
C57BL/6 HDM 1	18	7	38.89
C57BL/6 HDM 2	14	6	42.86
C57BL/6 HDM 3	24	9	37.50
C57BL/6 HDM 4	13	7	53.85

Acknowledgement

At the end, I want to thank everybody who supported me during my time as PhD student.

First and foremost, I want to thank my doctoral supervisor Prof. Dr. König from the Institute of Anatomy, who initiated this project. During my time as PhD student he has always supported me with a lot of patience and encouragement. Even during busy periods, he always took some time for lively discussions.

Thanks to Prof. Dr. Frank Petersen who agreed to act as second reviewer for my thesis.

I also want to thank Prof. Dr. Köhl for his efforts to build up a graduate school including an exchange to the Cincinnati Children's Hospital in the United States of America. In addition, I want to thank him for his support during regular meetings and discussions.

Some big thanks are due to my dear colleagues from the AG König Kathy, Sarah, Karina, Inken, and Mario for their support and funny times in the lab. My special thanks are also to Johann whose findings have also supported my study. Further, I want to thank the other PhD students from the Institute of Anatomy and the IRTG1911.

During my time in Cincinnati I stayed at the Lewkowich lab and was kindly supervised by Ian. I want to thank him for this time and all of his suggestions during our regular video conferences. In addition, I want to thank the whole Lewkowich lab: Jacky, Sarah, Phoebe, Amnah, and Emily. I had a great time with you!

I acknowledge Prof. Dr. Christine Klein for the opportunity to use her confocal microscopy and Aleksandar Racovic for his technical support. For their support for cell sorting I want to thank Dr. Tillman Vollbrandt (CanaCore, Lübeck) and Monica DeLay, PhD and her team from the flow core in Cincinnati.

Last but not least I want to thank my family and my friends for their support, patience, and encouragement. My special thanks are to my dear Mathias who has always disburden and encouraged me in difficult times.

Curriculum Vitae

Publications and Congress Contributions

Publications

Kosulin K*, **Hoffmann F***, et al. Presence of adenovirus species C in infiltrating lymphocytes of human sarcoma. PloS One 2013; 8:e63646.

Hoffmann F*, Ender F*, et al. Origin, localization and immunoregulatoy properties of pulmonary phagocytes in allergic asthma. Front Immunol. 2016; 7: 107

Hoffmann F*, Berger J*, et al. A new antigen uptaking interstitial macrophage-like population interacts with CD103+ cDCs but shows no migratory potential. (working title, manuscript in preparation)

* denotes equal contributions

Poster Presentations

103. Jahrestagung der Deutschen Zoologischen Gesellschaft e.V. 2010, Hamburg

Hoffmann, F., Dobler, S.: Multiple W*olbachia* infections within the flea beetle genus *Altica* (Coleoptera, Chrysomelidae): Implications for exploring the impact of the parasite on the host.

Retreat Heinrich-Pette-Institut, 2012, Hamburg

Hoffmann, F., Kosulin, K., Ching, W., Clauditz, T., Dobner, T.: FISH technology to investigate modulated adenoviral replication and the presence of adenovirus in human tissue sections.

37. Symposium of the North German Immunologists, 2014, Research Center Borstel

Hoffmann, F., König, P.: Dendritic Cell and macrophage subtype localization in the lung of C57BL/6 and BALB/c mice.

International 5th Annual Cluster Symposium, 2015, Kiel

Hoffmann, F., Berger, J., Lewkowich I. P., König, P.: A new antigen-uptaking macrophage-like cell population contacts CD103+ conventional dendritic cells around airways

Uni im Dialog, 2015, Lübeck

Hoffmann, F., König, P.: Fresszellen in der Lunge: Eine unerwartete Begegnung

12th Spring School on Immunology 2015, Deutsche Gesellschaft für Immunologie e.V., Ettal

Hoffmann, F., Berger, J., Lewkowich I. P., Laumonnier, Y., König, P.: A new antigen-uptaking macrophage-like cell population contacts CD103+ conventional dendritic cells around airways

International Congress of Mucosal Immunology, 2015, Berlin

Hoffmann, F., Berger, J., Ender, F., Lewkowich I. P., Laumonnier, Y., König, P.: CD103+ Conventional Dendritic Cells Are in Contact to a Macrophage-Like Cell Population around the Airways

110. Jahrestagung der Anatomischen Gesellschaft, 2015, Würzburg

Hoffmann, F., Berger, J., Lewkowich I. P., Laumonnier, Y., König, P.:CD103+ conventional dendritic cells are in contact to a new antigen-uptaking interstitial macrophage-like cell population around the airways

Allergy meets Infection, 2015, Lübeck

Hoffmann, F., Berger, J., Lewkowich I. P., Laumonnier, Y., König, P.:CD103+ conventional dendritic cells are in contact to a new antigen-uptaking interstitial macrophage-like cell population around the airways

Annual Immunology Retreat, 2016, Greewood Village, Ohio, USA

Hoffmann, F., Berger, J., Lewkowich I. P., König, P.: A new interstitial macrophage-like population, that is interacting with CD103+ cDCs, is the main antigen uptaking cell subset but shows no migratory potential.

Talks

Presymposium International 5th Annual Cluster Symposium, 2015, Kiel

A new antigen-uptaking macrophage-like cell population contacts CD103+ conventional dendritic cells around airways

Allergy meets Infection, 2015, Lübeck

CD103+ conventional dendritic cells are in contact to a new antigen-uptaking interstitial macrophage-like cell population around the airways